

AD-A252 459



DTIC
S ELECTE D
JUN 9 1992
C

(2)

²³⁸U NEUTRON CAPTURE GAMMA CASCADE GENERATION
AND TRANSPORT
SIMULATION FOR CAPTURE TANK RESPONSE

By

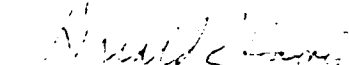
Thomas Jay Rosener

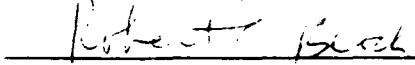
A Thesis Submitted to the Graduate
Faculty of Rensselaer Polytechnic Institute

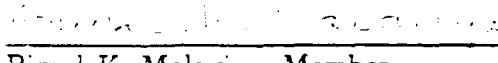
in Partial Fulfillment of the
Requirements for the Degree of
DOCTOR OF PHILOSOPHY

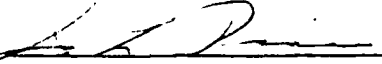
Major Subject: Nuclear Engineering and Science

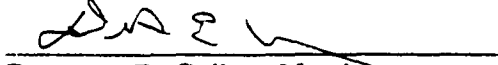
Approved by the
Examining Committee:


Donald R. Harris, Thesis Adviser


Robert C. Block, Member


Bimal K. Malaviya, Member


Ivor L. Preiss, Member


Dermott E. Cullen, Member

DISTRIBUTION STATEMENT A

Approved for public release;
Distribution Unlimited

Rensselaer Polytechnic Institute
Troy, New York

May 1992
(For Graduation August 1992)

92-15830


92 6 17 026

REPORT DOCUMENTATION PAGE			Form Approved OMB No. 0704-0188	
Public reporting burden for this collection of information is estimated to average 1 hour per response, including the time for reviewing instructions, searching existing data sources, gathering and maintaining the data needed, and completing and reviewing the collection of information. Send comments regarding this burden estimate or any other aspect of this collection of information, including suggestions for reducing this burden, to Washington Headquarters Services, Directorate for Information Operations and Reports, 1215 Jefferson Davis Highway, Suite 1204, Arlington, VA 22202-4302, and to the Office of Management and Budget, Paperwork Reduction Project (0704-0188), Washington, DC 20503.				
1. AGENCY USE ONLY (Leave blank)		2. REPORT DATE 7 May, 1992		3. REPORT TYPE AND DATES COVERED Final
4. TITLE AND SUBTITLE U-238 Neutron Capture Gamma Cascade (PhD Thesis) Generation and Transport Simulation for Capture Tank Response			5. FUNDING NUMBERS NA	
6. AUTHOR(S) Thomas J. Rosener				
7. PERFORMING ORGANIZATION NAME(S) AND ADDRESS(ES) U. S. Army Research done at Rensselaer Polytechnic Institute Troy, NY 12180			8. PERFORMING ORGANIZATION REPORT NUMBER NA	
9. SPONSORING/MONITORING AGENCY NAME(S) AND ADDRESS(ES) U.S. Army Student Detachment Ft. Benjamin Harrison, IN 46216-5820			10. SPONSORING/MONITORING AGENCY REPORT NUMBER NA	
11. SUPPLEMENTARY NOTES Thesis performed in PhD work.				
12a. DISTRIBUTION/AVAILABILITY STATEMENT Unlimited			12b. DISTRIBUTION CODE	
13. ABSTRACT (Maximum 200 words) A computer analysis has been performed to evaluate the energy dependent response of a capture tank to the gamma rays emitted in the cascades of the excited U-239 nucleus. This model determines the energies of the gamma-ray cascades, the order of emission of the gamma rays in a cascade, and the gamma-ray multiplicity of the cascades using Monte Carlo techniques. A capture tank responds to the combined effect of the various gamma rays emitted in the cascade. Examined is the energy deposition in a capture tank by the cascades generated in resonant (surface) capture and off-resonant (volumetric) capture, with and without internal conversion. Off-resonant capture deposits, on the average, less energy than resonant capture, due to self-shielding of the gamma rays in the capture sample. Internal conversion has negligible effect on the average cascade energy deposited in the capture tank.				
14. SUBJECT TERMS Gamma-ray cascades. Capture tank. U-238 neutron capture.			15. NUMBER OF PAGES 168	
			16. PRICE CODE	
17. SECURITY CLASSIFICATION OF REPORT Unclassified	18. SECURITY CLASSIFICATION OF THIS PAGE Unclassified	19. SECURITY CLASSIFICATION OF ABSTRACT Unclassified	20. LIMITATION OF ABSTRACT UL	

© Copyright 1992

by

Thomas Jay Rosener

All Rights Reserved

CONTENTS



LIST OF TABLES	iv
LIST OF FIGURES	v
ACKNOWLEDGEMENT	vi
ABSTRACT	vii
1. INTRODUCTION AND HISTORICAL REVIEW	1
1.1 Introduction	1
1.2 Objectives	3
1.3 Calculations of Booth et al.	3
1.4 Calculations of Takahashi	6
1.5 Calculations of Yamamuro et al.	9
1.6 Review of Primary Experimental Work	10
1.6.1 Campion et al.	11
1.6.2 John, et al.	13
2. ENERGY LEVELS OF THE NUCLEUS	15
2.1 Nuclear Levels	15
2.2 Bethe's Free Gas Model	18
2.3 Gilbert and Cameron Formulation	20
2.4 The Back-Shifted Fermi-Gas Model of Dilg et al.	22
2.5 Comparison of the Level Density Models	24
3. GAMMA TRANSITIONS	28
3.1 Energetics Of Gamma Decay	28
3.2 Level Width	30
3.3 Gamma Transitions	30
3.4 Selection Rules	32
3.5 Classification of Gamma-Rays	35
3.6 Internal Conversion and Internal Conversion Coefficients	35
3.7 Transition Probabilities	37

3.8	Yrast levels	37
3.9	Hindrance Factors	38
3.10	Angular Distribution of Gamma Rays	42
3.11	Expectations of the Single-Particle Model	44
4.	THE GAMINT CODE	50
4.1	Introduction to the GAMINT Code	50
4.2	Input to the GAMINT Code	50
4.3	Details of the GAMINT Code	59
4.4	Treatment of Internal Conversion	63
4.5	Transition Selection	67
4.6	Tallies Performed by the GAMINT Code	69
5.	RESULTS	71
5.1	Results of the GAMINT Code	71
5.2	Comparison to Published Results	86
6.	SIMULATION OF CAPTURE TANK RESPONSE USING MICROSHIELD	93
6.1	Introduction to the Microshield Program	93
6.2	Description of the Physical System	96
6.3	Microshield Model	96
6.4	Results of the Microshield Model	98
7.	DISCUSSION AND CONCLUSION	110
	LITERATURE CITED	113
	APPENDICES	116
	A. GAMINT SOURCE CODE	116
	APPENDICES	152
	B. SAMPLE OF REPRESENTATIVE CASCADES	152

LIST OF TABLES

Table 1.1	Branching ratios used in Takahashi's calculation	7
Table 1.2	Comparison of the calculated gamma yields from neutron capture in ^{238}U	8
Table 1.3	Resolved neutron capture gamma radiation from neutron capture in ^{238}U , from Campion et al.	13
Table 1.4	Neutron capture gamma radiation from neutron capture in ^{238}U , from John et al.	14
Table 2.1	Discrete energy levels in ^{239}U up to 0.950 MeV	16
Table 2.2	Spacing of nuclear energy levels of zero angular momentum in eV	19
Table 3.1	Classification of gamma rays	35
Table 4.1	Input variables to the GAMINT code	58
Table 4.2	Discrete energy levels in ^{239}U	60
Table 4.3	Transition probabilities (per second) for discrete level transitions	62
Table 6.1	Probability of transport of gammas of various energies from capture sample to capture tank for resonant capture	99
Table 6.2	Probability of transport of gammas of various energies from capture sample to capture tank for off-resonant capture . . .	100
Table 6.3	Energy Deposited in Tank by a Cascade	100

LIST OF FIGURES

Figure 1.1	Smoothed gamma ray spectrum due to neutron capture by ^{238}U	12
Figure 2.1	Level density versus energy for $J=1/2$	25
Figure 2.2	Level density versus energy for $J=3/2$	26
Figure 2.3	Level density versus energy for $J=5/2$	27
Figure 3.1	Half-life versus gamma-ray energy for different multipoles.	33
Figure 3.2	Histogram of the values of the hindrance factors for the E1 transitions in heavy nuclei.	40
Figure 3.3	Histogram of the values of the hindrance factors for the E2 transitions in heavy nuclei.	41
Figure 3.4	Angular distribution of second gammas relative to the first gamma ($l=1$).	45
Figure 3.5	Angular distribution of second gammas relative to the first gamma ($l=2$).	46
Figure 3.6	Angular distribution of second gammas relative to the first gamma ($l=3$).	47
Figure 3.7	Angular distribution of second gammas relative to the first gamma, with the multipole (l) randomly selected for 10,000 isotropic gammas.	48
Figure 4.1	Flowchart for the GAMINT code initialization.	51
Figure 4.2	Flowchart for the discrete level selection criteria.	52
Figure 4.3	Flowchart for the discrete level transition probabilities.	53
Figure 4.4	Flowchart for the continuum selection criteria.	54
Figure 4.5	Flowchart for the continuum level transitions.	55
Figure 4.6	Flowchart for the selection of the transition.	56
Figure 4.7	Flowchart for the tallies performed in the GAMINT code.	57

Figure 4.8	Internal conversion coefficients for K-shell conversion used in the GAMINT Code	64
Figure 4.9	Internal conversion coefficients for L-shell conversion used in the GAMINT Code	65
Figure 4.10	Internal conversion coefficients for M-shell conversion used in the GAMINT Code	66
Figure 5.1	Gamma-ray multiplicity versus transition energy.	73
Figure 5.2	Gamma-ray emission ratio	74
Figure 5.3	Fraction of total gamma-ray energy released per energy group.	75
Figure 5.4	Gamma-ray frequency versus energy presented by multipolarity	77
Figure 5.5	Gamma-ray frequency versus energy presented by gamma-ray order.	78
Figure 5.6	Gamma-ray energy for the first and second gamma rays	79
Figure 5.7	Gamma-ray energy for the first and third gamma rays	80
Figure 5.8	Gamma-ray energy for the first and fourth gamma rays	81
Figure 5.9	Gamma-ray energy for the first and fifth gamma rays	82
Figure 5.10	Gamma-ray energy for the first and last gamma rays	83
Figure 5.11	Gamma-ray spectrum for different excitation energies.	85
Figure 5.12	Angular distribution of second gamma relative to first gamma.	87
Figure 5.13	Angular distribution of third gamma relative to first gamma.	88
Figure 5.14	Angular distribution of fourth gamma relative to first gamma.	89
Figure 5.15	Angular distribution of fifth gamma relative to first gamma.	90
Figure 5.16	Comparison to published results.	91
Figure 6.1	Total gamma cascade energy deposited in capture tank for 100 representative cascades (resonant capture, no internal conversion)	102
Figure 6.2	Total gamma cascade energy deposited in capture tank for 100 representative cascades (off-resonant capture, no internal conversion)	103

Figure 6.3	Total gamma cascade energy deposited in capture tank for 100 representative cascades (resonant capture, internal conversion)	104
Figure 6.4	Total gamma cascade energy deposited in capture tank for 100 representative cascades (off-resonant capture, internal conversion)	105
Figure 6.5	Spectrum of cascade gamma energy deposited in capture tank (resonant capture)	106
Figure 6.6	Spectrum of cascade gamma energy deposited in capture tank (off-resonant capture)	107
Figure 6.7	Spectrum of cascade gamma energy deposited in capture tank (internal conversion)	108
Figure 6.8	Spectrum of cascade gamma energy deposited in capture tank (no internal conversion)	109

ACKNOWLEDGEMENT

The author wishes to express his sincere gratitude to his thesis advisor Professor Donald R. Harris. Over my five years of graduate studies, his guidance, encouragement, and advice has inspired me to complete the demanding requirements of this program. As an educator, he has instilled in me a great appreciation for the field of Nuclear Engineering.

I also wish to extend my appreciation to my doctoral committee members. Professor Robert C. Block, Head of the Nuclear Engineering and Engineering Department, Professor Bimal K. Malaviya, Executive Officer of the Nuclear Engineering and Engineering Department, Professor Ivor L. Preiss, Department of Chemistry, and Dr. Dermott E. Cullen, Lawrence Livermore Laboratory, all provided me their wisdom and insight, which made this thesis all the more enjoyable and enlightening to do.

I wish to thank the staff of the Rensselaer Computing Center for their technical support in using the computing facilities. I particularly thank Mrs. Harriet Borton for her assistance in using the typesetting program, LATEX, which was used in the preparation of this thesis.

I am also most thankful for the support my family provided during my degree program. My wife Annie, my daughter Teri, and my son Danny, provided me all of the love and encouragement I needed.

ABSTRACT

A computer analysis has been performed to evaluate the energy dependent response of a capture tank to the gamma-ray cascades emitted from excited ^{239}U . The GAMINT code was developed to simulate the decay of the ^{239}U nucleus, formed in the $^{238}\text{U}(n,\gamma)^{239}\text{U}$ reaction, in order to provide the source spectrum for the complete analysis of the capture tank efficiency. This model determines the energies of the gamma-ray cascades, the order of emission of the gamma rays in a cascade, and the gamma-ray multiplicities by Monte Carlo techniques. A gamma-ray emission spectrum for the excited ^{239}U nucleus is generated.

In the GAMINT code, known level data for ^{239}U is used below 1 MeV. A statistical approach based on the back-shifted Fermi gas model is used for the continuum level density. A single-particle model description for transition rates, with hindrance factors applied, is used to determine the gamma ray transition probabilities. Internal conversion probabilities are determined and the inclusion of this competing process suppresses the low energy portion of the gamma spectrum.

A capture tank responds to the combined effect of the gamma rays of various energies from a cascade, after being transported through the material between the sample and the capture tank. Examined is the energy deposition, in a capture tank, by the cascades generated from resonant and off-resonant capture in a ^{238}U sample. Internal conversion has a negligible effect on the average cascade energy deposited in the tank. Off-resonant (volumetric) capture deposits, on the average, less energy than resonant (surface) capture in the capture tank as a result of self-shielding of the gamma rays in the capture sample.

CHAPTER 1

INTRODUCTION AND HISTORICAL REVIEW

1.1 Introduction

Gamma rays are produced in many nuclear reactions. In neutron capture reactions, a nucleus becomes excited by the addition of the captured neutron and then decays to the ground state by the emission of sequential gamma rays. This series of gamma rays is called a gamma cascade. In this work, the computer code GAMINT is developed to simulate the gamma cascades formed in the $^{238}\text{U}(n,\gamma)^{239}\text{U}$ reaction.

The study of the sequential emission of gamma rays may be performed experimentally. The current generation of experiments resolve the energies of one or two of the gamma rays in a cascade. The determination of the angular correlation between a gamma emitted in some preferred direction and the subsequent gamma ray is also limited to two gammas. Future experiments [1] will be able to simultaneously measure the energies of up to a half dozen gamma rays produced in the step by step deexcitation of a single excited nucleus. This ability to measure the multifold coincidence of gamma rays will not be available until 1994 and will not be without tremendous effort and expense.

Internal conversion is an additional decay process which competes with gamma decay. For low energy transitions in nuclei of high mass number, the internal conversion process dominates over the gamma emission process. It is therefore necessary to include internal conversion in the cascade model. This work, for the first time, includes internal conversion in a ^{239}U decay model.

Developing a computer code to simulate the decay of the excited ^{239}U nucleus allows one to study the character of the gammas emitted in the cascade, without the

expense of repeated experimental procedure. The computer model determines the energy, the multipolarity, order of emission of a gamma ray in a cascade, and the number of gamma rays emitted in a cascade. The angular distribution between the first gamma ray in a cascade and any subsequent gamma ray in the same cascade is also determined. In addition, the computer code generates the source spectrum for the $^{238}\text{U}(n,\gamma)^{239}\text{U}$ reaction. This spectrum is used in this work for the determination of the energy dependent efficiency for gamma-ray detection in neutron capture tank experiments. This is important so that the data collection efforts of future experiments may be improved and the results of past experiments may be verified.

The $^{238}\text{U}(n,\gamma)^{239}\text{U}$ reaction is of importance in the design of fast reactors, and therefore must be fully understood in order to optimize fuel development in future reactor programs utilizing fast reactor technology. Experiments have been performed at Rensselaer Polytechnic Institute [2] and recently elsewhere [3] [4] to study the $^{238}\text{U}(n,\gamma)^{239}\text{U}$ reaction, using a large capture tank. An analysis of the data collected in the Rensselaer experiments [5] by Harris et al. [6] examined the capture tank efficiencies for average s-wave and p-wave neutron capture. However, the capture tank responds to the combined effect of the gamma rays of various energies from a cascade. Therefore, the cascade structure has a profound effect on the response of the capture tank to individual cascades. Further analysis is necessary to address the efficiency of the capture tank for detecting gamma rays emitted in neutron capture experiments. This work, for the first time, analyzes the multiple gammas in the individual cascades of the $^{238}\text{U}(n,\gamma)^{239}\text{U}$ reaction, and the resulting energy deposition in the capture tank.

Previous work in gamma cascade modeling has been performed by Booth et al. [7], Takahashi [8], and Yamamuro et al. [9]. Experimental results are found in the work of Campion et al. [10] and John et al. [11]. This chapter summarizes the literature applicable to the gamma cascade model developed in this work.

1.2 Objectives

The objectives of this thesis are:

- To develop a computer simulation of the gamma-ray cascade process in the $^{238}\text{U}(n,\gamma)^{239}\text{U}$ reaction in order to provide the source cascades in a capture tank model.
- To transport the cascade gamma rays from the source to the capture tank, through the intervening material, using a point-kernel calculation code.
- To examine the energy deposition in the capture tank for the following specific cases:
 1. Resonant (surface) capture in the sample.
 2. Off-resonant (volume) capture in the sample.
 3. Cascades in which internal conversion is considered.
 4. Cascades in which internal conversion is not considered.

1.3 Calculations of Booth et al.

Booth et al [7] used a calculational technique based on the works of Yost et al. [12] [13], in which the capture gamma-ray yields for neutron capture in ^{238}U were calculated by a technique which incorporates existing experimental results. The emphasis of this work was on implementation of the calculation on ^{238}U and comparison on an absolute basis, the results with differential measurements of capture gamma-ray yields. An advantage of this calculation is that gamma-ray group boundaries may be altered and new results determined at a fraction of the cost and time associated with the experimental work. The calculational technique uses several nuclear models with the constraint of conservation of binding energy. Also employed is a simple integral gamma-ray yield measurement to obtain differential

yield data. These experiments were conducted at the Tower Shielding Facility at Oak Ridge National Laboratory. These experiments were used to fix certain parameters by requiring the model to predict the experimental results on an absolute basis.

In the generation of the neutron-energy-dependent capture gamma-ray yields, Booth assumed that the composite epithermal spectrum was dominated by the capture of s, p, and d-wave neutrons. The calculation of the gamma-ray spectrum corresponding to each of the possible capture states was accomplished by using the DUCAL code of Yost. In this code, the gamma-ray cascade process is described in terms of (1) parameters which define relative electric and magnetic multipole transition strengths and which incorporate the appropriate selection rules, (2) statistical assumptions regarding energy-level density and spin and parity distributions in the energy continuum, (3) known energy levels in the lower energy region, and (4) energy levels, gamma-ray transition probabilities, and/or estimates of spin and parity distributions generated with an appropriate nuclear model over the range of energies for which the nuclear model has been shown to agree better than the model using statistical assumptions.

The DUCAL code of Yost incorporates some parameters which are proportional to the matrix elements of the radiative transition process. In generating the spectrum calculations, Booth relied on the accuracy of the thermal-capture primary line intensities found in the literature in order to fit the parameters of the model. The measured thermal line intensities were reproduced within 10 percent. Based on this fact, Booth applied the parameters which described the thermal spectrum to compound nucleus capture states at higher energies.

The statistical description of the nuclear energy levels in the continuum region used in the DUCAL code is based on the Gilbert and Cameron [24] formulation.

which predicts an energy-dependent observable level spacing, $D(U)$ given by:

$$D(U) = \begin{cases} T \exp[-(U - E_0)/T], & E \leq E_x \\ 12\sqrt{2c} a^{\frac{3}{2}} t^3 \exp(-\sqrt{a}U), & E > E_x \end{cases}$$

where $U = E - \Delta$ and $E_x = 2.5 - 150/A$ - the pairing energy in MeV. The parameter Δ is the fictive ground state level. In Booth's calculations, the parameters relevant to the Gilbert and Cameron formulation shown above are determined in part from the ^{238}U resonance data as given in BNL-325 [14] as well as the known discrete ^{239}U energy levels.

The DUCAL code requires the energy, spin, and parity of the energy levels in order to determine the gamma-ray spectrum for a given capture state. The required properties are only known for the energy levels of ^{239}U up to about 1 MeV. A level scheme was compiled based on existing experimental data and the results of a nuclear model calculation suitable for deformed odd-A nuclei. In this composite level scheme, level properties from measurements and detailed in the Nuclear Data Tables [15] were used in the energy range $0.0 \leq E \leq 0.83$ MeV, and level properties from the nuclear model were used in the range $0.83 \leq E \leq 2.0$ MeV. Individual levels in the range $1.23 \leq E \leq 2.0$ MeV were weighted by the ratio of the density of levels as suggested by the Gilbert and Cameron formulation to that of the nuclear model. Thus the nuclear model was used only to predict the spin and parity distributions in the $1.23 \leq E \leq 2.0$ MeV range. The primary line intensities used in Booth's calculation were taken from BNL-325 [14].

In Booth's work, comparison of the calculated energy spectrum to experimentally determined spectrum was not done in the region below 3.0 MeV, because of relatively large errors in the experimental results. The measured discrete photon intensity at 4.06 MeV was about 11% below the intensity measured in experiments performed by Sheline et al. [16] as stated in Booth's paper. As an additional check on the calculated gamma-ray yields, the percent of the binding energy, which must

be conserved in the calculation, is given. This figure in Booth's calculation for the capture of thermal neutrons is given as 89.0%.

1.4 Calculations of Takahashi

In Takahashi's work [8], the gamma-ray production cross sections of $^{238}\text{U}(n,\gamma)$ reactions are evaluated for thermal and epithermal energies primarily using a statistical model for the gamma cascade process. Also in this work, the gamma-ray spectra is determined by using a model which takes into account the known discrete energy levels, and uses a statistical theory for the continuum energy levels. This is done using a modified version of the DUCAL code of Yost called DUCAL-AVT.

In the process of calculating the gamma cascade using discrete and continuous energy levels, an important consideration is the matching of the discrete level density to the continuous level density at the junction energy (E_c). In the Takahashi work, the formulation of Gilbert and Cameron is used to provide the level densities in the continuum. Since the discrete levels formed in the (n,γ) reaction are not all of the discrete levels described by Gilbert and Cameron's formula, and some of the discrete levels are not populated in the (n,γ) reaction, normalization of the discrete level density is carried out. In the DUCAL-AVT code, this normalization is carried out in such a way that the level density of the discrete levels matches the level density of the continuum at the junction energy.

The branching ratios for the transitions to and from the levels in the continuum region are determined using the formulation of Blatt and Weisskopf [17] with a hindrance factor used to adjust the calculated ratio. These values are shown in Table 1.1.

In Takahashi's work, the branching ratios are assumed to be independent of the initial excitation energy. The transition probabilities are determined by a code called NGAMMA. The branching ratios do not depend strongly on the energy of the

Table 1.1: Branching ratios used in Takahashi's calculation

Energy (MeV)	E1	M1	E2	M2
	Branching Ratio			
	8.0×10^{-1}	1.99×10^{-1}	1.0×10^{-1}	9.9×10^{-4}
	Transition Probabilities (sec^{-1})			
0.1	8.2×10^8	1.6×10^8	9.9×10^5	8.5×10^2
2.4	2.5×10^{13}	3.0×10^{12}	8.7×10^{12}	6.8×10^9
4.8	4.4×10^{14}	3.4×10^{12}	2.8×10^{12}	2.2×10^{11}

initial states; therefore, Takahashi assumes that the energy-independent branching ratios used in the DUCAL-AVT code are a good approximation.

Since the intensities of the primary transitions in the low energy discrete states were available to Takahashi in the Nuclear Data Tables [15], the transition probabilities for primary transitions to these states were calculated from these data. The values for the transition probabilities used in Takahashi's work are also found in Table 1.1. In Takahashi's work, he found that if he calculated the transition probability for the primary transitions in the discrete region, the intensities for those transitions were about four times smaller than the experimentally observed intensities. This is a result of the fact that the statistical model treats the probabilities of transition to discrete states in the same way as transition probabilities to continuous states, and does not take into account non-statistical capture processes. Therefore, Takahashi takes the transition probabilities to the discrete levels to be four times larger than the transition probabilities to the continuous states.

In Takahashi's work, his calculated spectrum is compared to the experimentally determined spectrum of John et al. [11]. The spectrum differs from the experimental results of John et al., specifically in the position of the maximum. The maximum of the experimental spectrum lies at 1.8 MeV, while that of the calculated spectrum lies around 1.2 MeV. Takahashi was unable to shift this peak by adjusting the parameters in the Gilbert and Cameron formulation.

Table 1.2: Comparison of the calculated gamma yields from neutron capture in ^{238}U

Energy (MeV)	Intensity (gamma rays per 100 captures)	
	Booth et al.	Takahashi
0.0 - 0.25	-	124.12
0.25 - 0.50	-	13.47
0.50 - 0.75	-	43.28
0.75 - 1.00	-	28.12
1.00 - 1.25	29.9	34.23
1.25 - 1.50	25.5	33.20
1.50 - 1.75	25.7	29.80
1.75 - 2.00	25.4	25.63
2.00 - 2.25	21.3	21.30
2.25 - 2.50	17.2	17.07
2.50 - 2.75	13.8	13.09
2.75 - 3.00	10.6	9.49
3.00 - 3.25	5.4	6.43
3.25 - 3.50	3.5	4.06
3.50 - 3.75	5.3	2.34
3.75 - 4.00	3.9	1.014
4.00 - 4.25	10.8	5.72
4.25 - 4.50	0.024	0.0514
4.50 - 4.75	0.43	0.203

An examination of the conservation of binding energy in the experimental and calculated spectrum is accomplished by analyzing the integral:

$$\int_{1 \text{ MeV}}^{E_B} I(E_\gamma) E_\gamma dE_\gamma. \quad (1.1)$$

The experimental data covers 95% of the binding energy (E_B) and Takahashi's calculation covers 80% of the binding energy, for this integrated region. Table 1.2 compares the calculated neutron capture yields for the work of Booth et al. and Takahashi.

1.5 Calculations of Yamamuro et al.

In Yamamuro's work [9], the capture cross sections and gamma-ray spectra for neutron induced reactions in ^{181}Ta and ^{197}Au were calculated using a low-lying level fitting method in which the constant temperature partial-level density formula and the spin-selected level cumulation were used. The calculation of the capture cross section and the gamma-ray spectra uses the Brink-Axel form to represent the giant resonance of photon absorption for the gamma-ray profile function.

The nuclear temperature is normally determined by fitting the cumulative low-lying levels with the function describing the the number of levels. The low-lying level cumulation for heavy nuclei is usually below the expected exponential increase as a function of energy as a result of levels missing from the experimental data. Therefore, the temperature cannot be uniquely determined from the cumulative plot for an element. More than one temperature may therefore be used in the calculation of the gamma-ray spectrum instead of the constant temperature model.

In Yamamuro's work, the statistical model called GNASH was used for the calculation of the gamma-ray spectrum for ^{181}Ta and ^{197}Au . This calculation was performed for incident neutron energies in the range of 10 keV to 4.5 MeV.

Since the average gamma-ray transition probabilities depend strongly on the nuclear level density, the level density $\rho(E, J)$ is an important quantity in the calculation of the gamma-ray spectrum. In the Yamamuro paper, the Fermi-gas model formula is used and is referred to as the partial level density formula, which is essentially the density of levels at energy E of each spin J , not of all observable spin.

$$\rho(E, J) = \frac{\exp\{2\sqrt{a(E - \Delta)}\}}{C_0(E - \Delta)^2} R(J, E), \quad (1.2)$$

where

$$C_0 = 24\sqrt{2}(0.146)^{\frac{3}{2}} aA.$$

and the spin term $R(J,E)$ is defined by the relationship

$$R(J,E) = (2J + 1) \exp \left\{ \frac{-(J + \frac{1}{2})^2}{2\sigma^2(E)} \right\},$$

where $\sigma(E)$ is defined as the spin cutoff factor, and is expressed by

$$\sigma^2(E) = 0.146 \{a(E - \Delta)\}^{\frac{1}{2}} A^{\frac{2}{3}}.$$

In Yamamuro's work, the constant temperature formula is used in the lower excitation energy region, and is joined to the Fermi gas level density formula at energy E_x . The constant temperature formula is:

$$\rho(E,J) = \rho(E_x) \exp \left\{ \frac{(E - E_x)}{T} \right\} R(J,E), \quad (1.3)$$

for $E < E_x$, and where $\rho(E_x)$ is the level density at energy E_x . In the constant temperature formula, the nuclear temperature is related to the level density parameter (a), the smooth joining energy (E_x), and the pairing correction (Δ), by the formula:

$$T = \frac{E_x - \Delta}{\sqrt{a(E_x - \Delta) - 2}}. \quad (1.4)$$

In the lower-lying energy region in which known levels exist, Yamamuro uses these known levels in the statistical-model calculations.

In the statistical-model code GNASH, which was used in Yamamuro's work to calculate the gamma-ray spectrum, transitions of the E1, E2, M1, and M2 type were permitted for the gamma rays. The Brink-Axel strength function was used for the E1 and M1 strength. The Weisskopf formulation was used for the E2 and M2. No higher multipolarities were considered.

1.6 Review of Primary Experimental Work

The primary literature on experimentally determined gamma-ray energy spectra for neutron capture in U^{238} can be attributed to the work of Campion et al. [10].

and John et al. [11]. The work of John et al. is used in the literature as a benchmark for the comparison of calculated spectra. These works are briefly summarized here in order to allow the reader to gain some insight into the methods used to collect the experimental data.

1.6.1 Campion et al.

In 1959, Campion et al. [10] examined the gamma spectrum resulting from the thermal neutron bombardment of uranium metal, depleted to 0.034% ^{235}U . Figure 1.1 [10] shows the smoothed gamma ray spectrum due to neutron capture by ^{238}U obtained by Campion. The gamma rays in the energy region between 0.14 MeV and 3.4 MeV were examined with a crystal spectrometer. The gamma rays in the 3.4 MeV to 4.2 MeV range were studied using a pair spectrometer with a resolution of about 1%. A survey was conducted at about 3% resolution for the gamma-energy range from 3.0 MeV to 7.7 MeV also with the pair spectrometer.

The absolute intensities for gamma rays above 3.4 MeV were determined by the use of a nickel comparison method attributed to Kinsey and Bartholomew [19]. The absolute intensities for the gamma rays in the 3.4 MeV and below region were determined by direct comparison to the gamma rays of known intensity emitted from ^{239}Np following the beta decay, which are in equilibrium with the (n,γ) reaction. Table 1.3 lists the energies and the absolute intensities of the resolved gamma-rays emitted in the thermal neutron capture in ^{238}U . Note that the intensity is reported on a number per single capture event basis.

In Campion's work, the energy radiated per capture in the thermal neutron capture in ^{238}U is found to be 4.3 MeV. No gamma rays were observed above 4.062 MeV. In this work, an attempt was made to find a gamma-ray in coincidence with the 4.062 MeV gamma ray. Two NaI(Tl) scintillation spectrometers were used to observe the spectrum from the bombardment of ^{238}U metal with thermal neutrons.

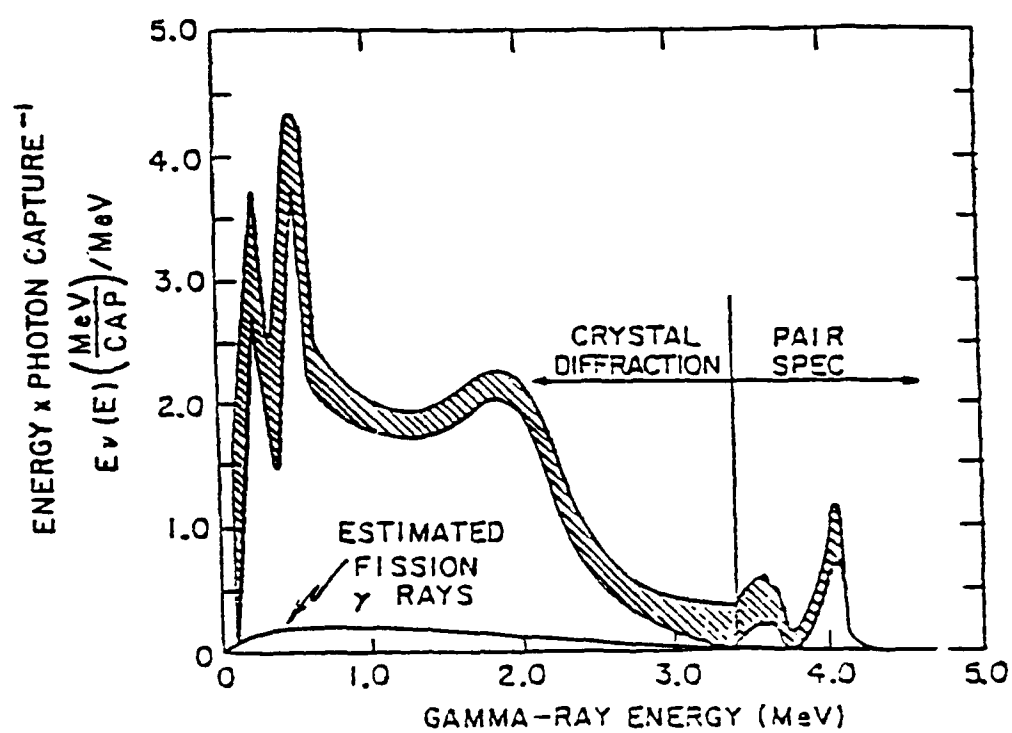


Figure 1.1: Smoothed gamma ray spectrum due to neutron capture by ^{238}U

Table 1.3: Resolved neutron capture gamma radiation from neutron capture in ^{238}U , from Campion et al.

Energy (MeV)	Intensity (gamma rays per capture)
0.5401 ± 0.004	0.09
0.5490 ± 0.004	0.09
0.5772 ± 0.004	0.09
0.5885 ± 0.004	0.05
0.6093 ± 0.004	0.06
0.6275 ± 0.004	0.09
0.6375 ± 0.004	0.03
3.576 ± 0.010	0.02
3.662 ± 0.018	0.02
4.062 ± 0.010	0.07

The resulting spectrum indicated that the 4.062 MeV gamma ray was not to the ground state.

1.6.2 John, et al.

In 1970, J. John, V.J. Orphan, and C.G. Hoot [20] reported experimental results on the epithermal-neutron capture gamma rays from shield materials, particularly ^{238}U . They measured the gamma rays from resonant capture in ^{238}U of neutrons up to 100 keV. An electron linear accelerator was used to produce a beam of pulsed neutrons from a cylindrical uranium target. The 6.0 inch diameter depleted uranium target was located at the end on a 16.0 meter flight tube. The neutrons incident on the target were moderated by a 1.0 inch thick slab of polyethylene. The gamma rays were detected using a Ge(LI)-NaI(Tl) spectrometer. This detector was operated simultaneously as a three-crystal pair spectrometer and an anti-Compton spectrometer.

Gamma-ray pulse-height spectra were generated from the data for 15 neutron energy groups. The gamma-ray intensities were determined from the experimentally

Table 1.4: Neutron capture gamma radiation from neutron capture in ^{238}U , from John et al.

Energy (MeV)	Intensity (gamma rays per 100 captures)
1.00	28.0
1.25	33.0
1.50	37.0
1.75	40.0
2.00	36.0
2.25	29.0
2.50	16.0
2.75	10.0
3.00	6.0
3.25	4.2
3.50	1.3
3.75	1.5
4.00	4.6
4.25	0.16
4.50	0.03
4.75	0.12

collected spectra. The intensities were reported in 0.25 MeV energy bins. No experimental data is given for below 1.0 MeV. The results for the lowest neutron energy capture ($5.6 \text{ eV} \leq E_n \leq 7.8 \text{ eV}$) is given in Table 1.4. Note that the intensity is reported on a number per one hundred capture events basis.

CHAPTER 2

ENERGY LEVELS OF THE NUCLEUS

2.1 Nuclear Levels

For a potential well of finite depth, the levels below the zero energy state are referred to as bound states. The energy levels above the zero energy state are referred to as virtual states. In the single particle shell model of the nucleus, protons and neutrons fill the bound levels of the nucleus in accordance with the Pauli exclusion principle, which states that two protons or two neutrons in the same nucleus can not have the same set of quantum numbers. The lower energy levels are filled first. The excited states of the nucleus can be formed by the outermost nucleon moving up to a higher energy level. Deexcitation of a bound level can only occur by gamma emission or by the competing process of internal conversion. The excitation energy is not high enough in these bound states to allow for particle emission.

In the lower-lying levels, the energy levels are spaced far enough apart to be considered discrete levels, and their width is small enough not to overlap one another. However, in the high energy levels, above the 2 MeV range, the single particle shell model is insufficient in detailing the energy levels and widths. At these energies, the levels become very close together, and the widths become relatively large. The density of energy levels increases as the excitation energy is increased. Also, at these higher energy levels, there are more competing modes of decay. The model used to describe the behavior of the nucleus at these higher energies is based on statistical mechanics and thermodynamics. [21]

Table 2.1 displays some discrete energy levels and the spin-parity assignments of the excited ^{239}U nucleus, as shown in Booth et al. [7] and the Nuclear Data Sheets.

Table 2.1: Discrete energy levels in ^{239}U up to 0.950 MeV

Level	Booth et al.	Nuclear Data Sheets
1	0.0 (2.5-)	0.0 (2.5-)
2	.043 (3.5+)	.1338 (.5,1.5-)
3	.097 (4.5+)	.1456 (.5,1.5-)
4	.1331 (.5+)	.1839 (2.5-)
5	.1428 (1.5-)	.6877 (.5,1.5-)
6	.173 (3.5+)	.7157 (.5,1.5-)
7	.1915 (2.5+)	.7500 (.5,1.5-)
8	.220 (3.5+)	.7347 —
9	.2391 (4.5+)	.7392 (.5,1.5-)
10	.3072 (5.5+)	.7459 (.5,1.5-)
11	.685 (.5-)	.7567 (2.5-)
12	.713 (1.5+)	~.800 —
13	.7423 (2.5+)	.8150 (.5,1.5-)
14	.7428 (1.5-)	.8236 (.5,1.5-)
15	.750 (.5-)	.8530 (.5,1.5-)
16	.7986 (3.5-)	.8882 (2.5-)
17	.811 (.5-)	.8933 (2.5-)
18	.8191 (.5-)	.9325 (.5,1.5-)
19	.823 (1.5-)	—
20	.860 (2.5-)	—
21	.943 (4.5-)	—

The usual convention employed in dealing with level densities is to discuss the density of levels instead of the density of states. The level density is the number of levels per MeV of energy. In the lower lying energy region, the level density is relatively small, and in the higher energy region, the level density is relatively large. The energy level densities up to a few MeV can be obtained experimentally from the determination of the population of levels in nuclear reactions or radioactive decay. Slow-neutron resonances can reveal information concerning the level densities in the 6-8 MeV range. Higher levels require the use of statistical mechanics to determine the level densities.

There is a degeneracy of $2J + 1$ states in a level with spin J . The physical observable is the energy level spacing (D), which is the reciprocal of the energy level density (ρ). The evaporation theory of nuclear decay predicts that the level density as a function of energy behaves as:

$$\rho(E) = \frac{1}{D} = \rho_o * \exp [aE^{\frac{1}{2}}], \quad (2.1)$$

where:

- $\rho(E)$ = level density at energy E
- D = spacing between levels (MeV)
- $\rho_o = 1$ to 0.01 (MeV)^{-1} for $A = 20$ to 200
- $a = 1$ to $7 \text{ (MeV)}^{-\frac{1}{2}}$ for $A = 20$ to 200

The constant (a) is called the level density parameter and is proportional to the atomic weight. The value of ρ_o is determined by the level density at a low (about 1 Mev) energy level and the above expression is adjusted for the higher energy levels by the level density parameter. The nucleus can also be characterized [22] by its nuclear temperature (t), which is related to the excitation energy of the nucleus by

the relation:

$$E = at^2 \quad (2.2)$$

2.2 Bethe's Free Gas Model

In the Bethe free gas model [23], the nucleus is considered to be a Fermi gas of free neutrons and protons. These particles are confined to the volume of the nucleus. In this model, the level spacing (inverse of the level density) is found to depend on the mass number (A) and the excitation energy (E).

The spacing between two levels of a given spin I, in the Bethe free gas model, is given by the relationship:

$$D = \frac{432}{2^{\frac{1}{4}}\pi^4} \left(\frac{\log 2}{5} \right)^{\frac{3}{2}} \frac{\zeta}{2I-1} x^4 e^{-x}, \quad (2.3)$$

where:

- $\zeta = \zeta_0(1 - (\pi^2/12)(\beta\zeta_0)^{-2} + \dots)$.
- $\zeta_0 = (N/C)^{\frac{2}{3}}$.
- β^{-1} = average excitation energy of the individual particles.
- N is the total number of particles.
- $C = (\frac{2^{\frac{7}{2}}}{9\pi})(\frac{MR^2}{\hbar^2})^{\frac{3}{2}}$.
- $x = (AE/2.20)^{\frac{1}{2}}$ for excitation energy E in MeV.
- M = particle mass.
- R = nuclear radius.

Since the level density is the reciprocal of the level spacing we can state that the level density in the Bethe formulation is simply:

$$\rho(E, I) = \frac{1}{D} = \frac{2^{\frac{1}{4}}\pi^4}{432} \left(\frac{5}{\log 2} \right)^{\frac{3}{2}} (2I-1)\zeta^{-1} x^{-4} e^x. \quad (2.4)$$

Table 2.2: Spacing of nuclear energy levels of zero angular momentum in eV

$E \cdot A$ (MeV)	spacing (MeV)
100	1×10^7
200	2.4×10^6
400	1.9×10^5
600	2.1×10^4
800	2800
1000	450
1200	85
1500	8.5
1800	1.0

The spacing D_0 is the spacing between levels of zero angular momentum and is simply the value of equation 2.3 times $(2I-1)$. Table 2.2 displays some representative values of the level spacing for given values of the product of the excitation energy (E) and the mass number (A). As seen in the table, the level spacing between successive levels decreases rapidly with excitation energy for a given mass number. If one compares different mass number elements, then for a given excitation energy, the level spacing decreases rapidly with increasing mass number.

For many years experimental observations of nuclear level densities have been interpreted in the framework of the Fermi gas model, and most statistical model calculations have employed level density formulas of the type introduced by Bethe, where the level density exponentially increases with both the excitation energy and the mass number. This simple model does not take into account the odd-even and shell effects so modifications to the original level density formula have been proposed. More modern level density formulations are now discussed and their details examined in the context of the present gamma cascade model.

2.3 Gilbert and Cameron Formulation

In 1965, Gilbert and Cameron [24] developed a composite nuclear-level density formula which contained shell corrections. In this formulation, a constant nuclear temperature model is used for the lower lying nuclear level densities. The regular Fermi gas formula is used at the higher excitation energies. The two methods are joined by fitting the curves tangentially.

The level-density relation adopted for the higher energy levels is essentially similar to Bethe's in that there exists an $e^{\sqrt{\text{Energy}}}$ dependence on the level density. This level density formula is given by the relationship:

$$\rho(U, J) = \frac{\sqrt{\pi} \exp(2\sqrt{aU})}{12 a^{\frac{1}{4}} U^{\frac{5}{4}}} \frac{(2J+1) \exp(-(J+\frac{1}{2})^2/2\sigma^2)}{2\sqrt{2\pi}\sigma^3} (\text{MeV}^{-1}), \quad (2.5)$$

where:

- $\rho(U, J)$ = level density (in MeV^{-1}).
- J = angular momentum.
- U = energy above fully degenerate state (which is at excitation energy U_0).
- σ = spin-dependence parameter.

Note that this representation accounts for the spin J . The observable level density is:

$$\rho(U) = \sum_J \rho(U, J) \simeq \frac{\sqrt{\pi} \exp(2\sqrt{aU})}{12 a^{\frac{1}{4}} U^{\frac{5}{4}}} \frac{1}{\sqrt{2\pi}\sigma} (\text{MeV}^{-1}). \quad (2.6)$$

This observable level density is not the same as the total level density which also includes those levels degenerate in the magnetic quantum number, so the total level density $W(U)$ is a factor of $(2J+1)$ times larger than the observable level density $\rho(U)$. This total level density is given by:

$$W(U) = \sum_J (2J+1) \rho(U, J) = \frac{\sqrt{\pi} \exp(2\sqrt{aU})}{12 a^{\frac{1}{4}} U^{\frac{5}{4}}} (\text{MeV}^{-1}). \quad (2.7)$$

In order to use this expression, one must know the pairing corrected energy (U), the spin dependence parameter (σ), and the level density parameter (a). Note that in the Gilbert and Cameron formulation, the energy U is defined by the total excitation energy E , corrected for pairing effects by subtracting $P(N)$ and $P(Z)$, which are the pairing energies for neutrons and protons respectively.

$$U = E - P(N) - P(Z). \quad (2.8)$$

The spin dependence parameter is given by the relation:

$$\sigma^2 = 0.0888 \cdot a \cdot t \cdot A^{\frac{2}{3}}, \quad (2.9)$$

where $t = \sqrt{U/a}$ and is the thermodynamic temperature of the nucleus. Therefore, σ varies as $U^{\frac{1}{4}}$, which is a slow change with an increase of excitation energy.

The only free parameter left in the formula is the level density parameter. The value used for the parameter for undeformed nuclei is given by:

$$\frac{a}{A} = 0.00917 \cdot S + 0.142, \quad (2.10)$$

and for deformed nuclei by:

$$\frac{a}{A} = 0.00917 \cdot S - 0.120, \quad (2.11)$$

where $S = S(N) - S(Z)$, the total shell correction (in MeV), where $S(N)$ represents the shell correction for neutrons and $S(Z)$ represents the shell corrections for protons. As can be seen by the given relationship, the ratio of the level density parameter to the atomic weight (a/A) is not a constant as in the earlier models such as the Bethe model, which did not account for the shell effects.

The lower levels of the nuclei are generally known. In Gilbert and Cameron's work, they fitted the lower lying levels to:

$$N(E) = \exp[(E - E_0)/T], \quad (2.12)$$

where E_0 and T are parameters determined by the fitting of the upper and lower level density formulas at the point of tangency.

The density of the lower levels may be represented by:

$$\rho_{lower} = \frac{N(E)}{T} \quad (2.13)$$

and the density of the higher levels is given by Equation 2.6. The two curves must be fitted tangentially. The conditions at the point at which the two densities meet are

- $\rho_{lower} = \rho_{upper}$.
- $T = \text{nuclear temperature}$.

This two level formulation is termed a composite level density formula. There are some problems with it, however. Some nuclei will not have a good fit between the upper and lower densities. This may be a result of the absence of information about the low-lying level structure. The nuclei with $A < 40$ and the nuclei with N or Z within 2 units of a magic number tend to give this composite formula problems. Nuclei near the magic numbers have a much smaller number of lower levels up to a given energy than do those nuclei far away from the magic numbers. Therefore fitting the upper and lower level densities at the tangency point for the magic nuclei is not as simple as for the others. Gilbert and Cameron leave the reader with the warning that the error in using this composite level formula is much greater near the magic number nuclei. [24]

2.4 The Back-Shifted Fermi-Gas Model of Dilg et al.

Dilg et al. [25] proposed a parameterization of the back-shifted Fermi gas model proposed by Vonach and Graves [26] in the whole mass range. In this approach, the Fermi gas model is adopted with adjustable parameters representing

the fictive ground state position (Δ) and the level density parameter (a). These parameters are adjusted by the fitting of low energy and resonance data. This parameterization provides a reasonable description of level densities up to 10-20 MeV.

In the Dilg approach the following forms of the spin-dependent and total level densities are adopted from Lang and Le Couteur. [27]

$$\rho(U, J) = \frac{1}{24\sqrt{2}} \frac{(2J+1) \exp[2(a(U-\Delta))^{\frac{1}{2}} - J(J+1)/2\sigma^2]}{\sigma^3 a^{\frac{1}{4}} (U-\Delta-t)^{\frac{5}{4}}}, \quad (2.14)$$

and

$$\rho(U) = \frac{1}{12\sqrt{2}} \frac{1}{\sigma a^{\frac{1}{4}}} \frac{\exp[2(a(U-\Delta))^{\frac{1}{2}}]}{(U-\Delta-t)^{\frac{5}{4}}}, \quad (2.15)$$

where the thermodynamic temperature is defined by:

$$U - \Delta = at^2 - t,$$

where t is the nuclear temperature and a and Δ are the fitted parameters. The fictive ground state position is shifted by the amount Δ because two-body interactions between the nucleons have been ignored.

These level density expressions are derived from the total density of states assuming random coupling of angular momenta. In this treatment, an additional parameter σ^2 is introduced. This spin cut-off parameter is used to describe the spin distribution. At high excitation, the value of the spin cut-off parameter is expected to approach:

$$\sigma_{rigid}^2 \approx 0.0150 A^{\frac{2}{3}} t. \quad (2.16)$$

The back-shifted Fermi expression, Equation 2.14 can be represented by a simpler expression for ^{239}U . [28]

$$\rho(U, J) = G(2J+1) \frac{\exp(-J(J+1)/2\sigma_c^2) \exp(2a^{\frac{1}{2}}(U-\Delta)^{\frac{1}{2}})}{(U-\Delta)^{1.860}}. \quad (2.17)$$

where the value of $G = 0.00010091$, $a = 9.20212$, $\Delta = -0.58$ and $\sigma = 3.7283$.

2.5 Comparison of the Level Density Models

The Bethe formulation has an exponential increase in the level density with both the excitation energy and the mass number. This, however, does not represent the low energy levels well. The constant temperature model predicts the low energy levels well, but does not represent the high energy levels well. The Dilg back-shifted model takes into account the odd-even and shell effects, resulting in a more realistic prediction of the level densities in the low and high energy regions. The model used in this work is a modification of the Dilg back -shifted model, and agrees well with the other models.

Figure 2.1 through Figure 2.3 display level density versus energy for the present work, the Dilg back-shifted model, and the Fermi gas model. The level density is shown in energy levels per MeV. Figure 2.1 displays the level density for $J=1/2$. Figure 2.2 displays the level density for $J=3/2$. Figure 2.3 displays the level density for $J=5/2$. Note that the level density scale is logarithmic.

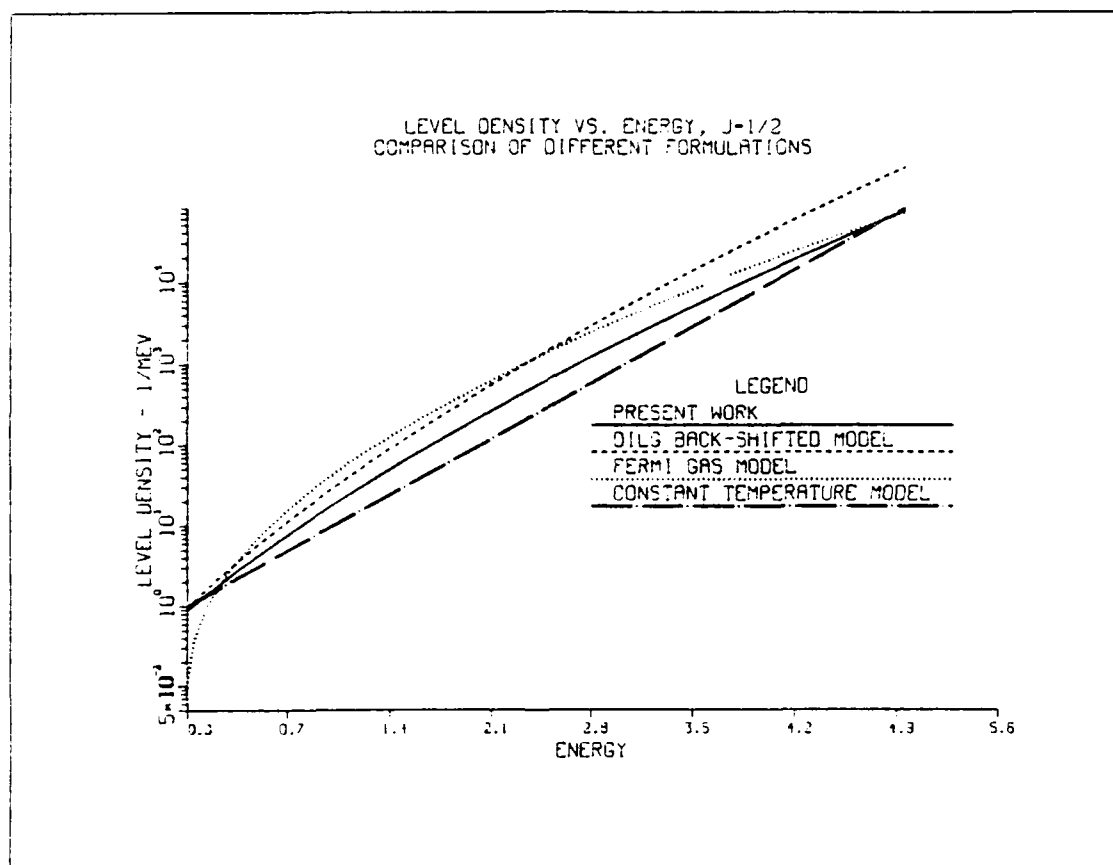


Figure 2.1: Level density versus energy for $J=1/2$

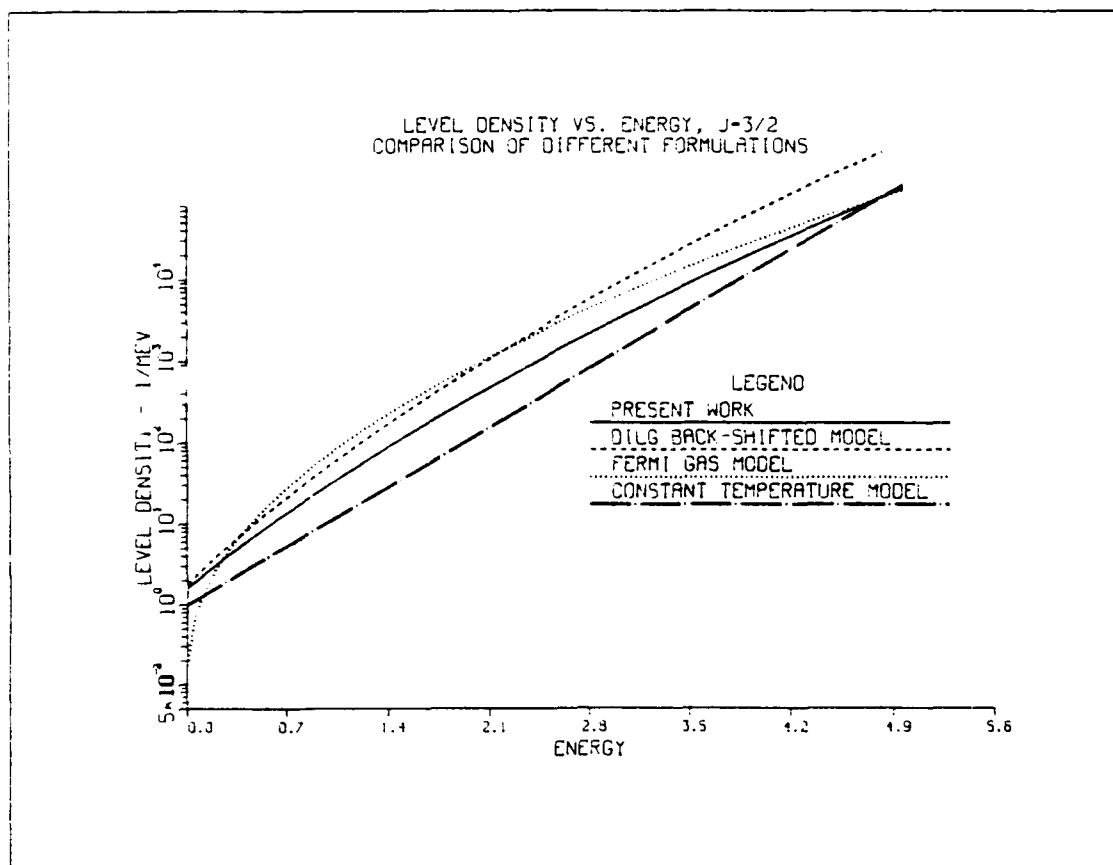


Figure 2.2: Level density versus energy for $J=3/2$

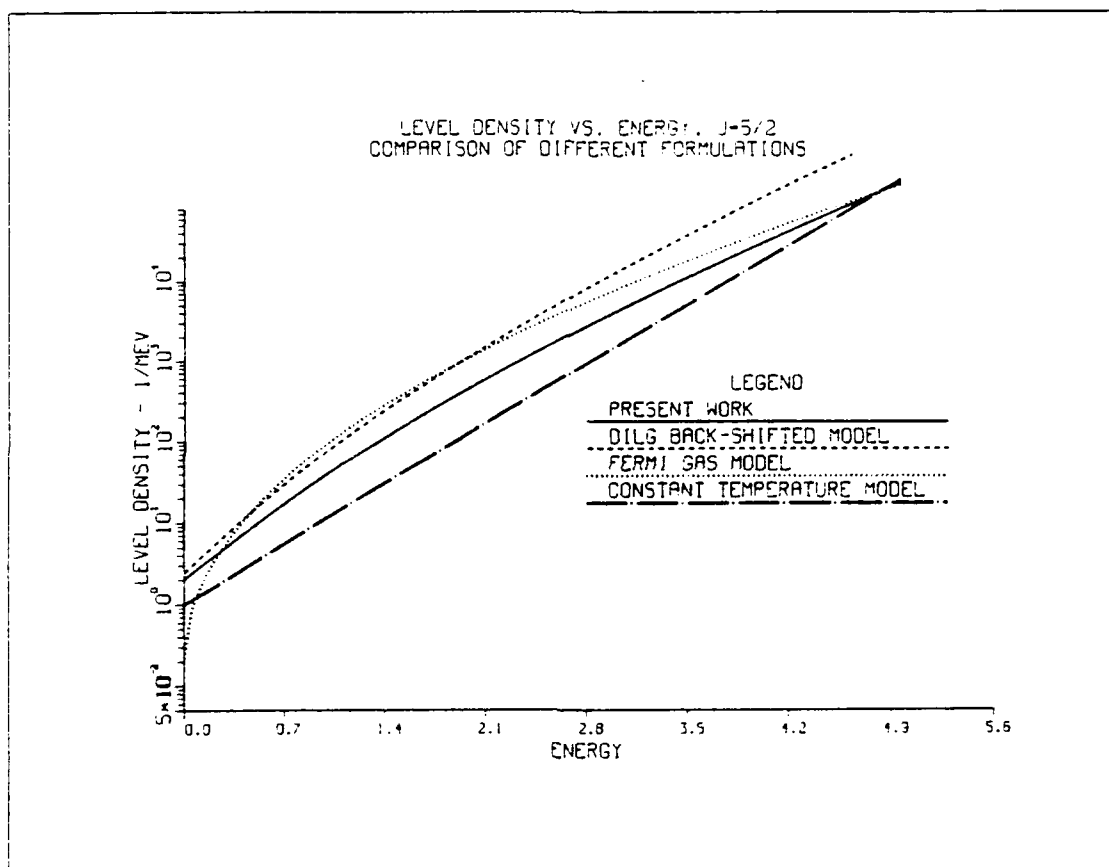
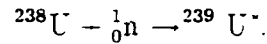


Figure 2.3: Level density versus energy for $J=5/2$

CHAPTER 3

GAMMA TRANSITIONS

A nucleus can be excited in the neutron capture reaction. For example, in the $^{238}\text{U}(n, \gamma)^{239}\text{U}$ reaction, ^{238}U and a neutron will form an excited $^{239}\text{U}^*$ nucleus.



This excited nucleus can then deexcite through gamma decay, or by the competing process of internal conversion. Gamma decay is the process by which a nucleus gives up its excess energy by the release of electromagnetic radiation. The internal conversion process is the result of the interaction of the nucleus and orbital electrons, leading to the emission of an electron with kinetic energy equal to the excitation energy of the nucleus minus the binding energy of the electron in the atom.

$$E_{e^-} = E_{ex} - E_{bind}, \quad (3.1)$$

where E_{e^-} is the electron's kinetic energy upon emission from the atom, E_{ex} is the excitation energy of the nucleus, and E_{bind} is the binding energy of the emitted electron in the atom.

3.1 Energetics Of Gamma Decay

By using conservation of momentum and conservation of energy, one may compare the relative amounts of energy shared among the products of a decaying nucleus. First, assume that the rest mass of the excited nucleus is m_o^* and the rest mass of the final state is m_o . Then by conservation of energy:

$$m_o^*c^2 = m_o c^2 - E_\gamma + T_f, \quad (3.2)$$

and by conservation of momentum:

$$\mathbf{p}_\gamma - \mathbf{p}_f = 0. \quad (3.3)$$

where:

- E_γ = Gamma-ray energy.
- T_f = Energy of the recoil nucleus.
- p_γ = Momentum of the gamma ray.
- p_f = Momentum of the recoil nucleus.

$$T_f = \frac{1}{2} m_o v_f^2 = \frac{p_f^2}{2m_o}, \quad (3.4)$$

and since

$$p_f = p_\gamma, \quad (3.5)$$

the final energy of the recoil nucleus may be expressed in terms of the gamma-ray momentum,

$$T_f = \frac{p_\gamma^2}{2m_o}. \quad (3.6)$$

Here, the relationship between momentum and energy may be used to put this relationship in terms of the gamma-ray energy.

$$T_f = \frac{E_\gamma^2}{2m_o c^2}. \quad (3.7)$$

Using realistic values of gamma-ray energy ($E = 2$ MeV) and the atomic mass number ($A = 239$) for ^{239}U , the calculated value of the nucleus recoil energy is approximately 9.0 eV. This is only 0.0005% of the value of the gamma-ray energy, and may be considered negligible. Therefore, the gamma-ray may be considered to carry off all of the decay energy of the transition. [29]

3.2 Level Width

The level width is related to the mean lifetime of the level. Planck's constant divided by the lifetime of the level is defined as the width of the level.

$$\Gamma = \frac{\hbar}{\tau} \quad (3.8)$$

The uncertainty principle requires the energy level to have some finite width. This is a result of not being able to precisely know the energy and time at the same moment. The level width (Γ) is equal to:

$$\Gamma = \frac{0.66 \times 10^{-15}}{\text{mean lifetime of width}} (\text{eV}). \quad (3.9)$$

In nuclei which have competing modes of decay, the width of the level is simply the sum of the different level widths for each mode of decay.

3.3 Gamma Transitions

When a gamma-ray is emitted from a nucleus, it carries with it some amount of angular momentum. The value of this angular momentum is quantized, and is an integral multiple of Planck's constant ($L\hbar$, where L is an integer greater than or equal to 1). For each value of L , there exists two different characteristic gamma radiations. There is an electric multipole and a magnetic multipole, each with different parities.

When the charge in the nucleus oscillates, a characteristic radiation is emitted. The oscillation of an electric dipole (two charges of equal magnitude separated by a distance) results in the emission of a specific pattern of radiation, given the title of electric dipole radiation. A circulating charge (current loop) will emit another characteristic pattern, given the title of magnetic dipole radiation.

One major difference between the radiation emitted in the classical sense and the radiation emitted in nuclear decay is the parity operation in going from one nuclear level to another. In gamma decay, each multipole moment of order L produces

radiation, taking with it some angular momentum (I). From the law of conservation of angular momentum, it is required that:

$$L = I_i - I_f, \quad (3.10)$$

where the subscripts indicate the initial and final states of the nucleus. The parity change is related to the angular momentum carried off, as shown by the relationships:

- For electric multipole radiation, parity change $\Delta\Pi = (-1)^L$.
- For magnetic multipole radiation, parity change $\Delta\Pi = -(-1)^L$.

The disintegration constant of a transition for a single particle between two states with the same angular momentum is given by the following expressions. For an electric multipole of order L:

$$\lambda_{EL} = 2.4S \left(R_o A^{\frac{1}{3}}\right)^{2L} \left(\frac{E(\text{MeV})}{197}\right)^{2L-1} 10^{21} \text{ sec}^{-1}. \quad (3.11)$$

For a magnetic multipole of order L:

$$\lambda_{ML} = 0.55SA^{-\frac{2}{3}} \left(R_o A^{\frac{1}{3}}\right)^{2L} \left(\frac{E(\text{MeV})}{197}\right)^{2L+1} 10^{21} \text{ sec}^{-1}. \quad (3.12)$$

The value of S is given by:

$$S = \frac{2(L-1)}{L[1 \times 3 \times 5 \times \dots \times (2L+1)]^2} \left(\frac{3}{L-3}\right)^2, \quad (3.13)$$

and is a statistical factor varying with L. R_o is the nuclear radius, and is given by the expression:

$$R_o = 1.2A^{\frac{1}{3}}, \quad (3.14)$$

where A is the atomic mass under consideration.

Using the above relationships for λ_{EL} and λ_{ML} , it is determined that the relative probability of the transition being an electric multipole versus a magnetic multipole is:

$$\lambda_{ML} = \frac{\lambda_{EL}}{4.364 \times A^{\frac{2}{3}}}. \quad (3.15)$$

For the first four electric and magnetic multipoles, the transition probabilities can be shown to be:

$$\begin{aligned}
 \lambda(E1) &= 1.0 \times 10^{14} A^{\frac{2}{3}} E^3 \\
 \lambda(E2) &= 7.3 \times 10^7 A^{\frac{4}{3}} E^5 \\
 \lambda(E3) &= 34 A^2 E^7 \\
 \lambda(E4) &= 1.1 \times 10^{-5} A^{\frac{8}{3}} E^9 \\
 \lambda(M1) &= 5.6 \times 10^{13} E^3 \\
 \lambda(M2) &= 3.5 \times 10^7 A^{\frac{2}{3}} E^5 \\
 \lambda(M3) &= 16 A^{\frac{4}{3}} E^7 \\
 \lambda(M4) &= 4.5 \times 10^{-6} A^2 E^9
 \end{aligned} \tag{3.16}$$

As the multipole order increases, the decay constant (λ) decreases, and this can be interpreted as an increase in the half-life, or a smaller probability of the nuclear transition decaying by that mode. The probability for an electric multipole radiation can be shown to be greater than for a magnetic multipole of the same order by simply dividing the two disintegration constants. A graph for the half-life versus gamma-ray energy is shown for $A = 55$. This graph summarizes the relative likelihood of electromagnetic radiation being emitted in a particular multipole transition. For a given order multipole, it is seen from the graph that the relative probability of having an electric transition is an order of magnitude larger (the magnitude of the half-life is an order of magnitude smaller) than the probability of having a magnetic transition.

Note that this graph is a log-log plot. [29]

3.4 Selection Rules

Classically, the electromagnetic field produced by an oscillating charge (or current) transmits energy and angular momentum. A multipole of order L transfers

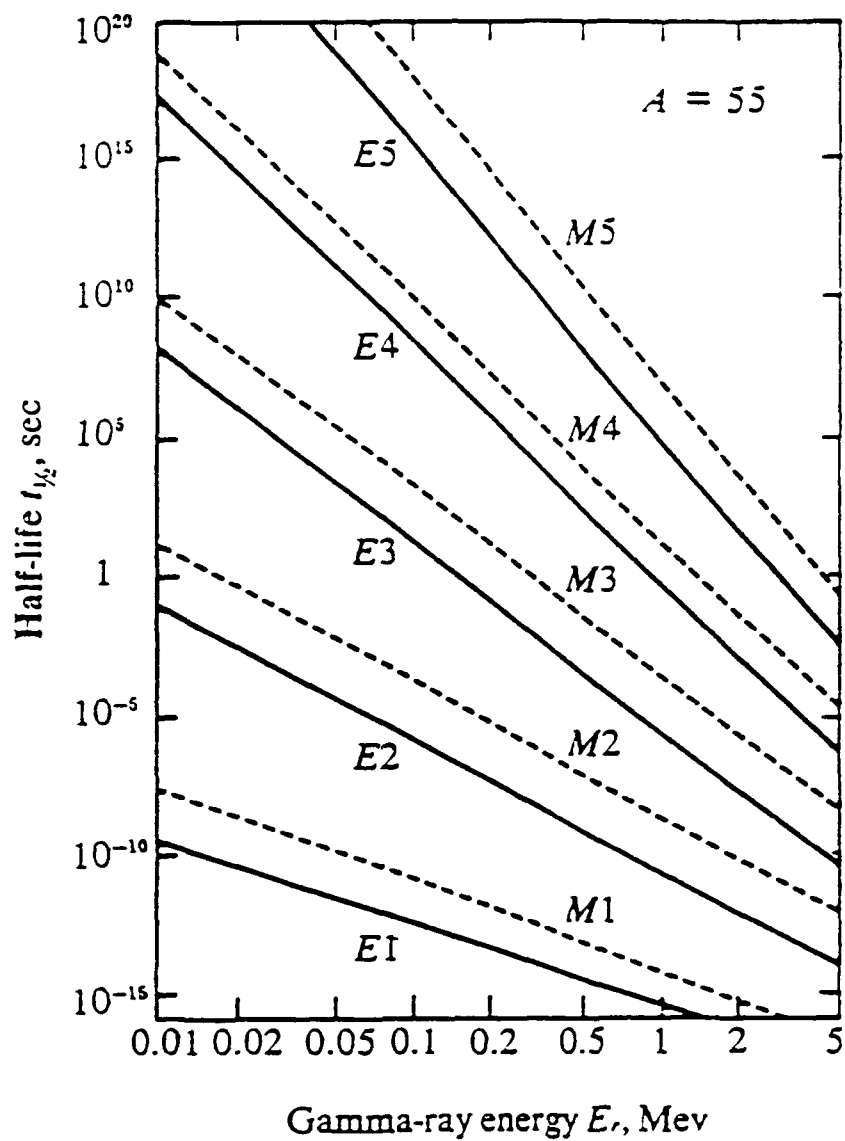


Figure 3.1: Half-life versus gamma-ray energy for different multipoles.

an angular momentum of $L\hbar$ per photon. Consider a nucleus in some initial state (I_i , and π_i) which decays to a final state (I_f , and π_f). Conservation of total angular momentum states that the initial angular momentum of the nucleus must be equal to the final angular momentum of the nucleus plus that angular momentum carried off by the gamma ray.

$$I_i = L + I_f. \quad (3.17)$$

The possible values of L are restricted.

$$|I_i - I_f| \leq L \leq I_i + I_f. \quad (3.18)$$

The dominant transition will have $L = |I_i - I_f|$ because of the strong L dependence of the transition rate.

For example, if $I_i = \frac{3}{2}$ and $I_f = \frac{5}{2}$, then L can be 1, 2, 3, or 4 as determined by:

$$|\frac{3}{2} - \frac{5}{2}| \leq L \leq \frac{3}{2} + \frac{5}{2}. \quad (3.19)$$

The type of dominant radiation emitted (electric or magnetic) depends on the value of L (odd or even) and the relative parity of the initial and final states of the nucleus.

For electric transitions:

$$\Delta\Pi = \text{NO} \Rightarrow \text{radiation will have even } L.$$

$$\Delta\Pi = \text{YES} \Rightarrow \text{radiation will have odd } L.$$

For magnetic transitions:

$$\Delta\Pi = \text{NO} \Rightarrow \text{radiation will have odd } L.$$

$$\Delta\Pi = \text{YES} \Rightarrow \text{radiation will have even } L.$$

That is, if $\pi_i = \pi_f$, ($\Delta\Pi = \text{NO}$) for the example given above ($I_i = \frac{3}{2}$ and $I_f = \frac{5}{2}$), then the radiation will be M1, E2, M3, or E4.

Table 3.1: Classification of gamma rays

Classification	Symbol	L	Parity Change in Nucleus
electric dipole	E1	1	yes
magnetic dipole	M1	1	no
electric quadrapole	E2	2	no
magnetic quadrapole	M2	2	yes
electric octupole	E3	3	yes
magnetic octupole	M3	3	no
electric 2L-pole	EL	L	no for L even, yes for L odd
magnetic 2L-pole	ML	L	yes for L even, no for L odd

In the case $I_i = I_f = 0$, the selection rules predict $L = 0$ which is not permitted in radiative transitions. Internal conversion is allowed, however.

3.5 Classification of Gamma-Rays

Table 3.1 summarizes the classification of gamma transitions [30]. The classification is based on the angular momentum (L) and the type of emission, that is, electric or magnetic.

The symbol E is for the electric transitions and the symbol M is for the magnetic transitions. Note, that for a given transition, the classification of the transition (multipolarity order and type) is dependent on the parity change between the initial and final levels, and the angular momentum difference between the initial and final levels.

3.6 Internal Conversion and Internal Conversion Coefficients

In a nuclear transition, the energy released can be emitted as a photon with energy $E = h\nu$ or it can be transferred to an orbital electron which is ejected with an energy equal to $h\nu - E_{bind(i)}$, where $E_{bind(i)}$ is equal to the binding energy of the electron in the i^{th} shell. This process of ejecting an electron in order to emit the transition energy is called internal conversion. For all electromagnetic transitions.

except for the $L=0$ to $L=0$ transition. gamma emission and internal conversion compete. When considering gamma decay and internal conversion as the only decay processes, the decay constant may be written:

$$\lambda_{total} = \lambda_{\gamma} + \lambda_{e-}, \quad (3.20)$$

where λ_{γ} is the probability for emission of a gamma ray per second, and λ_{e-} is the probability for emission of a conversion electron per second.

The internal conversion coefficient (α) is defined as the ratio of the probability of electron emission to the probability of gamma emission.

$$\alpha = \frac{\lambda_{e-}}{\lambda_{\gamma}}. \quad (3.21)$$

This ratio is a measure of the total number of conversion electrons emitted over a time period divided by the number of gamma rays emitted in the same transition over the same period of time. The internal conversion coefficient is dependent on the shell from which the electron is emitted. The total probability for internal conversion, (λ_{e-}), can be written as the sum of the partial probabilities for ejection in the K, L, M,... shells.

$$\lambda_{e-} = \lambda_{e-K} + \lambda_{e-L} + \lambda_{e-M} + \dots \quad (3.22)$$

The partial coefficients are computed for each shell and are summed to obtain the total conversion coefficient.

$$\alpha = \alpha_K + \alpha_L + \alpha_M + \dots \quad (3.23)$$

Consideration of only the K-shell, L-shell, and M-shell is sufficient, since the partial coefficients decrease rapidly with the increase in the principal quantum number.

In addition to depending on the shell from which the electron is emitted, conversion coefficients depend on the atomic number (Z) of the nucleus and on the transition energy and multipolarity of the radiation which the conversion competes

with The conversion coefficients are presented in tables as functions of atomic number, electron shell, transition energy, and multipolarity. [31]

3.7 Transition Probabilities

The transition probability for a specific type of transition (ϵ) may be determined by dividing the transition rate by the sum of all the transition rates.

$$\text{probability of transition } \epsilon = \lambda_{\epsilon} / \lambda_{\text{total}}. \quad (3.24)$$

This is simply a normalization procedure to result in the fraction of a specific type of transition occurring between two states. The theoretical estimates for the transition rates (disintegration constants) are only approximate. Therefore the transition probabilities are also only approximate.

As previously stated, the probability of a nucleus emitting a gamma-ray decreases with increasing value of L . This means that $2L$ -pole radiation is more probable than $2L+1$ -pole radiation. Also the theory predicts that the intensity of the electric $2L$ -pole radiation is more intense than the magnetic $2L$ -pole radiation. However, this is not necessarily the case in actual decay histories.

3.8 Yrast levels

The lowest energy level for each spin is called an yrast level. The term was suggested by J.R. Grover and is a Swedish word meaning "dizziest" [22]. Most of the energy in such a state is in the form of rotational energy and, therefore, the intrinsic shape of the nucleus may be close to the equilibrium value in the ground state region. Because of this, the various yrast levels of a nucleus share the same intrinsic state and differ only in their rotational motion.

Because of the special position of the yrast levels, it is common for a highly excited nucleus to decay by particle emission down to the yrast level. From the yrast

level, the nucleus will decay to a lower state by gamma emission and then continue the decay process by gamma decay, through lower levels, down to the ground state.

[32]

For an yrast level at excitation energy E_{ex} , the maximum kinetic energy of an emitted particle is

$$E_{part} = E_C - E_{bind} - E_y, \quad (3.25)$$

where

- E_{part} = the maximum kinetic energy of the particle being emitted.
- E_C = the excitation energy of the compound nucleus.
- E_{bind} = the binding energy of the particle being emitted.
- E_y = the energy of the yrast level under consideration.

It is possible for the value of $E_C - E_{bind} - E_y$ to be less than zero while $E_C - E_{bind}$ is greater than zero. In this case, the particle, assuming it is spinless and emitted with zero angular momentum, will not be emitted from the compound nucleus even though the excitation energy of the nucleus is greater than the binding energy of the particle to be emitted. The quantity E_y in effect raises the level at which gamma emission will compete effectively with particle emission. The increase is above the particle emission threshold by several million electron volts. [32]

3.9 Hindrance Factors

The single-particle model assumes that the nucleus consists of an inert core made up of completely filled shells. In this model, the outer shell is not completely filled. The single-particle theory considers the inner shells to move in independent orbits, and that the outer shell determines all of the low energy characteristics of

the nucleus. The interaction between a given nucleon and all others is considered to be a spherically symmetric potential.

The hindrance factor is defined as the ratio of the experimentally determined mean-life (τ_{ex}) for gamma decay to the calculated mean-life (τ_{calc}) for gamma decay using the single-particle model.

$$\text{Hindrance Factor} = \frac{\tau_{ex}}{\tau_{calc}}. \quad (3.26)$$

Since the single-particle model does not take into account all of the collective interactions of the nucleons in the nucleus, the experimentally determined lifetime of the nucleus does not agree with the computed lifetime. This hindrance factor adjusts the computed lifetime to agree with the experimentally determined lifetime. The E1 transition, expected to be the most probable transition, is actually very hindered. Figure 3.2 [33] presents the hindrance factors for the E1 transition in heavy nuclei. In heavy nuclei, the E1 transition is slowed down considerably more than in the light nuclei. In the larger nuclei, states of opposite parity differing by one unit of angular momentum are more likely to be very different in structure. The shell model does not provide the opportunity for the occurrence of such states differing in the level of only one particle.

In light nuclei, the M1 transition rate agrees quite well with the calculated single particle model expectations. In the heavy nuclei, the M1 transition is fairly consistent with the single particle model calculated values, however in the distorted nuclei, the M1 transition is slightly hindered. In contrast with other multipoles, the E2 transition is usually slightly enhanced over the single particle values in both the light and heavy nuclei. Figure 3.3 [33] presents the hindrance factors for the E2 transition in heavy nuclei. This is a result of the enhancement of the collective quadrupole moments over the single particle quadrupole moments. As a result of the enhancement of the E2 rate, it is expected that the M1 and the E2 transition will favorably compete with the E1 transition, determined by the single particle model

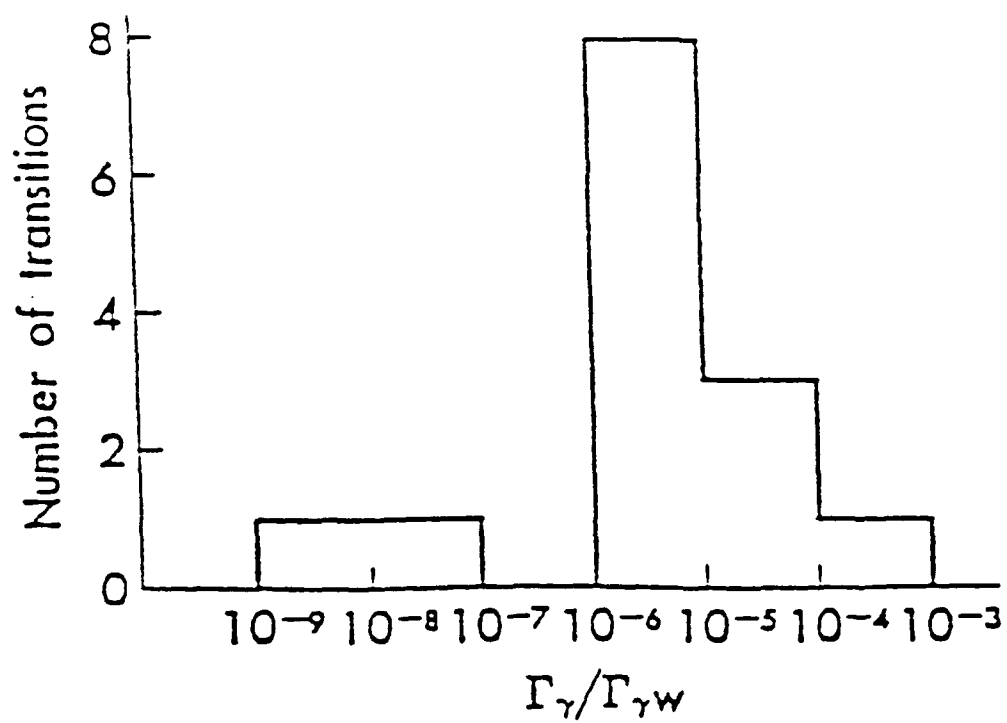


Figure 3.2: Histogram of the values of the hindrance factors for the E1 transitions in heavy nuclei.

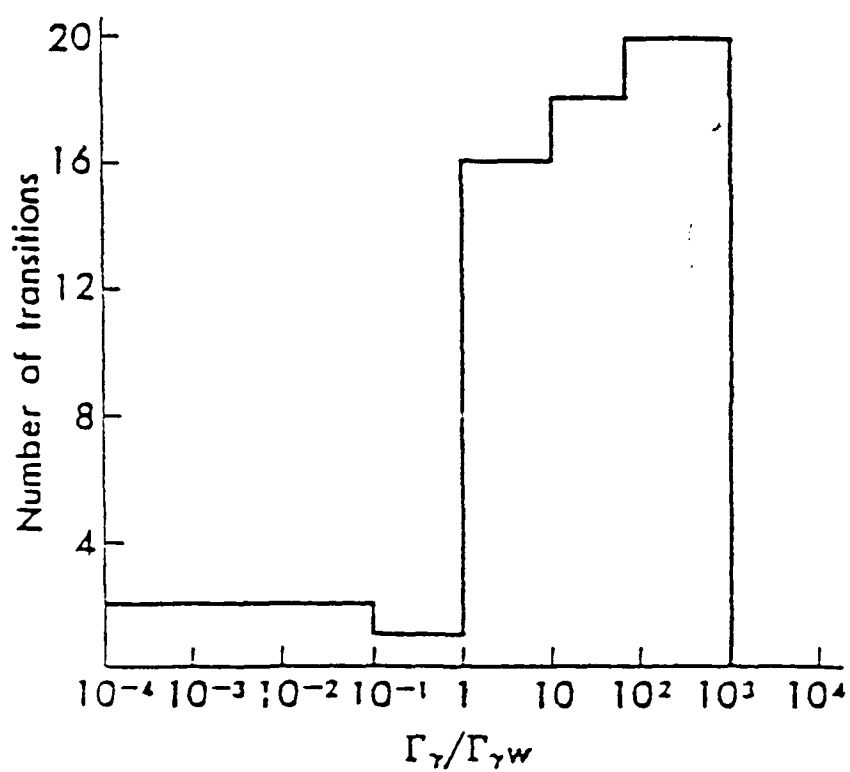


Figure 3.3: Histogram of the values of the hindrance factors for the E2 transitions in heavy nuclei.

to be dominant. [34]

3.10 Angular Distribution of Gamma Rays

In a gamma cascade, there exists a correlation between the direction of the first gamma emitted and the direction of the second gamma emitted. The angular distribution for the second emitted gamma relative to the first emitted gamma is the same for electric and magnetic radiation of the same multipole order (l) and same quantum number (m), which is associated with the z -component of the angular momentum. Therefore, the multipole order, but not the parity of the radiation, may be determined.

The angular-correlation function describes the distribution of angles between successive gammas emitted in a two step cascade. The angular-correlation function $W(\theta)$ for the angle θ between two consecutive gamma rays in the cascade

$$J_1 \rightarrow J \rightarrow J_2,$$

can be shown to be:

$$W(\theta)d\Omega = \sum_{i=0}^{i=L} A_{2i} P_{2i}(\cos\theta) d\Omega, \quad (3.27)$$

where A_{2i} are coefficients which depend on the multipole orders of the two gamma rays and is given by:

$$A_{2i} = F_{2i}(\lambda_1, \lambda_1, J_1, J) F_{2i}(\lambda_2, \lambda_2, J_2, J), \quad (3.28)$$

where F_{2i} are certain combinations of Clebsch-Gordon coefficients and Racah coefficients, and $P_{2i}(\cos\theta)$ are the even Legendre polynomials.

One may analyze the angular distribution of the second gamma ray in a two step cascade by determining the distribution of the energy flow from a radiating system. The Poynting vector S , which is defined by the relationship:

$$S \equiv \frac{c}{4\pi} E \times H. \quad (3.29)$$

describes the energy flow in an electromagnetic wave. If a large sphere is drawn around the radiating system, then at any point on the sphere S is the energy escaping per square centimeter per second.

$$S \cong \frac{c}{4\pi} E^2 \cong \frac{c}{4\pi} H^2. \quad (3.30)$$

The energy emitted into the solid angle $d\Omega$ around the direction (θ, ϕ) is the product of S and the area $R^2 d\Omega$ subtended by the solid angle at the sphere surface.

The electric multipole field of order l, m at point $r = (r, \theta, \phi)$ is given by:

$$E_E = \frac{i}{\kappa} \text{curl} \left[\frac{u_l^-(r)}{\kappa r} X_{l,m}(\theta, \phi) \right], \quad (3.31)$$

and

$$H_E = \frac{u_l^-(r)}{\kappa r} X_{l,m}(\theta, \phi), \quad (3.32)$$

where the outgoing wave is designated by u^- . The magnetic multipole field of order l, m is given by:

$$E_M = \frac{u_l^-(r)}{\kappa r} X_{l,m}(\theta, \phi) \quad (3.33)$$

$$H_M = -\frac{i}{\kappa} \text{curl} \left[\frac{u_l^-(r)}{\kappa r} X_{l,m}(\theta, \phi) \right] \quad (3.34)$$

where $X_{l,m}(\theta, \phi)$ are the vector spherical harmonics defined by:

$$X_{l,m}(\theta, \phi) = \frac{-i r \times \nabla Y_{l,m}(\theta, \phi)}{\sqrt{l(l+1)}}, \quad (3.35)$$

and $Y_{l,m}$ are the scalar spherical harmonics. The angular distribution function $Z_{l,m}(\theta, \phi)$ is defined by:

$$Z_{l,m}(\theta, \phi) \equiv X_{l,m}(\theta, \phi) * X_{l,m}(\theta, \phi), \quad (3.36)$$

or

$$Z_{l,m}(\theta, \phi) = \frac{1}{2} \left[1 - \frac{m(m+1)}{l(l+1)} \right] Y_{l,m+1}^2 + \frac{1}{2} \left[1 - \frac{m(m-1)}{l(l+1)} \right] Y_{l,m-1}^2 - \frac{m^2}{l(l+1)} Y_{l,m}^2. \quad (3.37)$$

The angular distribution of emitted energy is the same for electric and magnetic multipole radiation of the same l and m [17].

For $m=0$ and $l= 1, 2$, and 3 , plots of the angular distribution function (Z) are shown in Figure 3.4, Figure 3.5, Figure 3.6, respectively.

The angular distribution of the second gamma in a two step cascade in which the first gamma ray is emitted isotropically is plotted in Figure 3.7. For this plot, 10,000 isotropic gammas were emitted, followed by a second gamma, distributed by the angular distribution function (Z). The multipole (l) was randomly selected. The angle of the second gamma was added to the angle of the first gamma, in order to orient the second gamma with respect to the 0.00° axis. The gammas were grouped into 18 angle bins.

The results of this analysis show that the gammas emitted in a sample in which a large number of nuclei are undergoing gamma-ray transitions, the gammas will be emitted isotropically in the laboratory coordinate system. This is a result of the random orientation of the nuclei in the sample. The correlation is only between the two gammas emitted relative to each other, and therefore for the randomly oriented nuclei, the first gamma is not initially oriented. [34]

3.11 Expectations of the Single-Particle Model

Based on the single-particle model, a few expectations of some consequence arise. Briefly, they are:

1. The lowest permitted multipole will dominate the gamma-ray transitions.
2. A comparison of an electric multipole emission of order L to a magnetic multipole emission of order L shows that the electric multipole emission is more probable by a factor of approximately 10^2 .
3. Emission of order $L+1$ radiation is less probable than emission of order L radiation by a factor of approximately 10^5 .

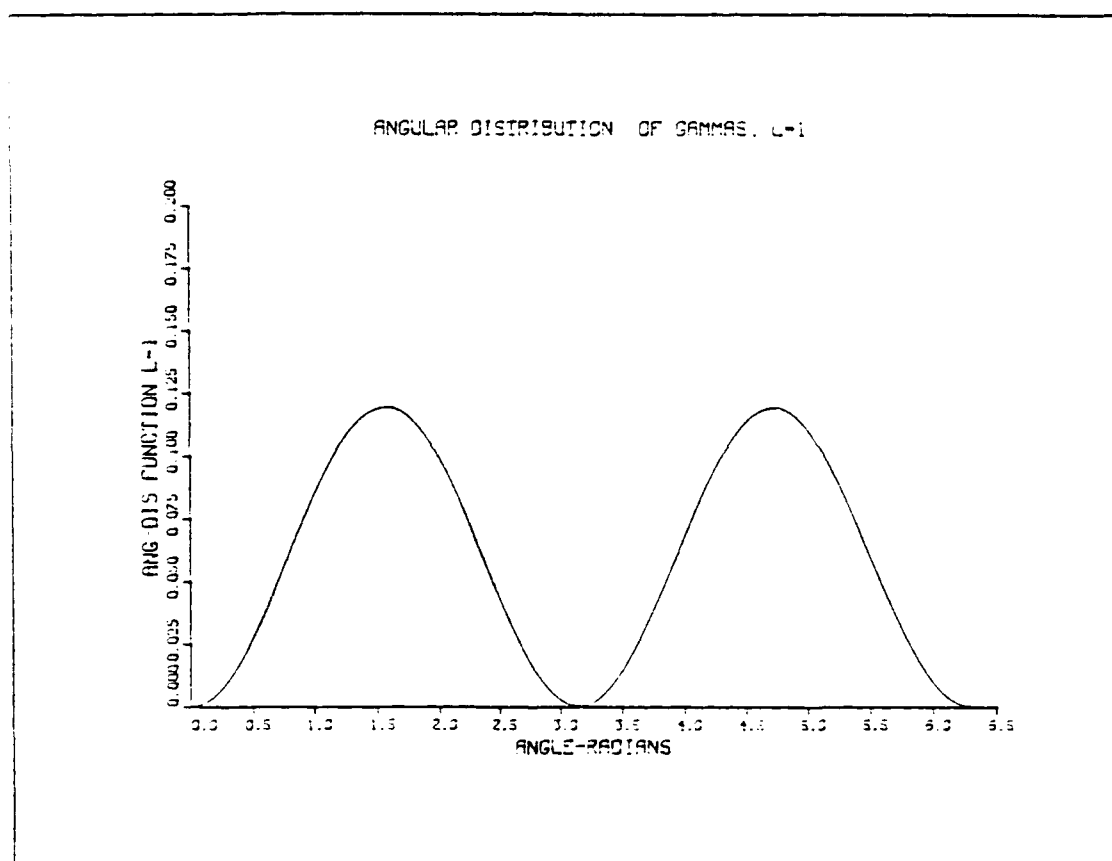


Figure 3.4: Angular distribution of second gammas relative to the first gamma ($l=1$).

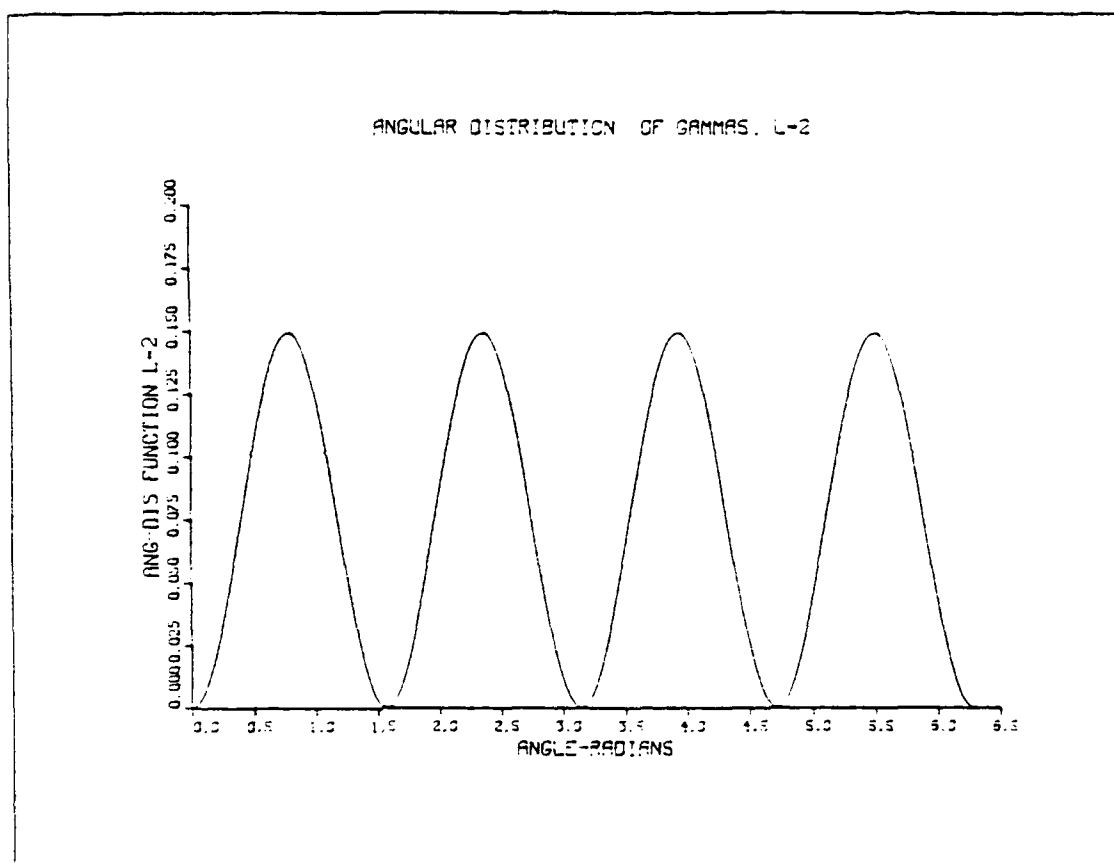


Figure 3.5: Angular distribution of second gammas relative to the first gamma ($l=2$).

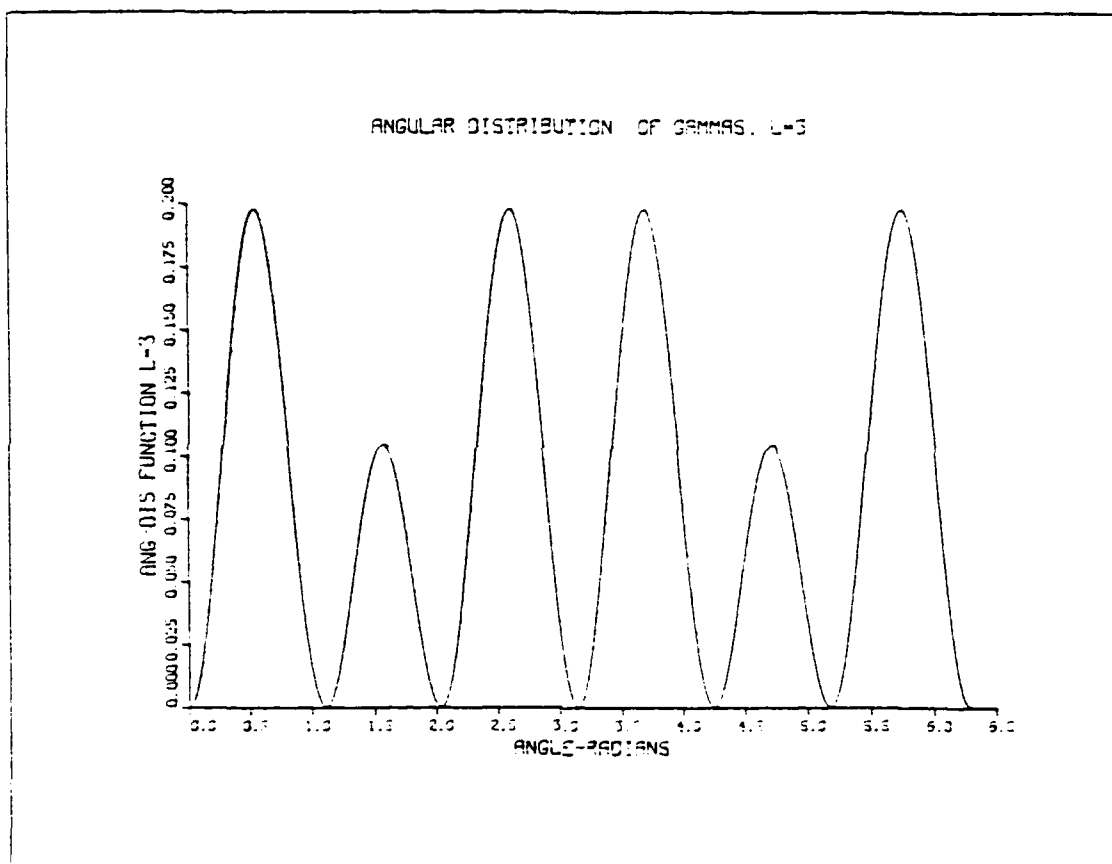


Figure 3.6: Angular distribution of second gammas relative to the first gamma ($l=3$).

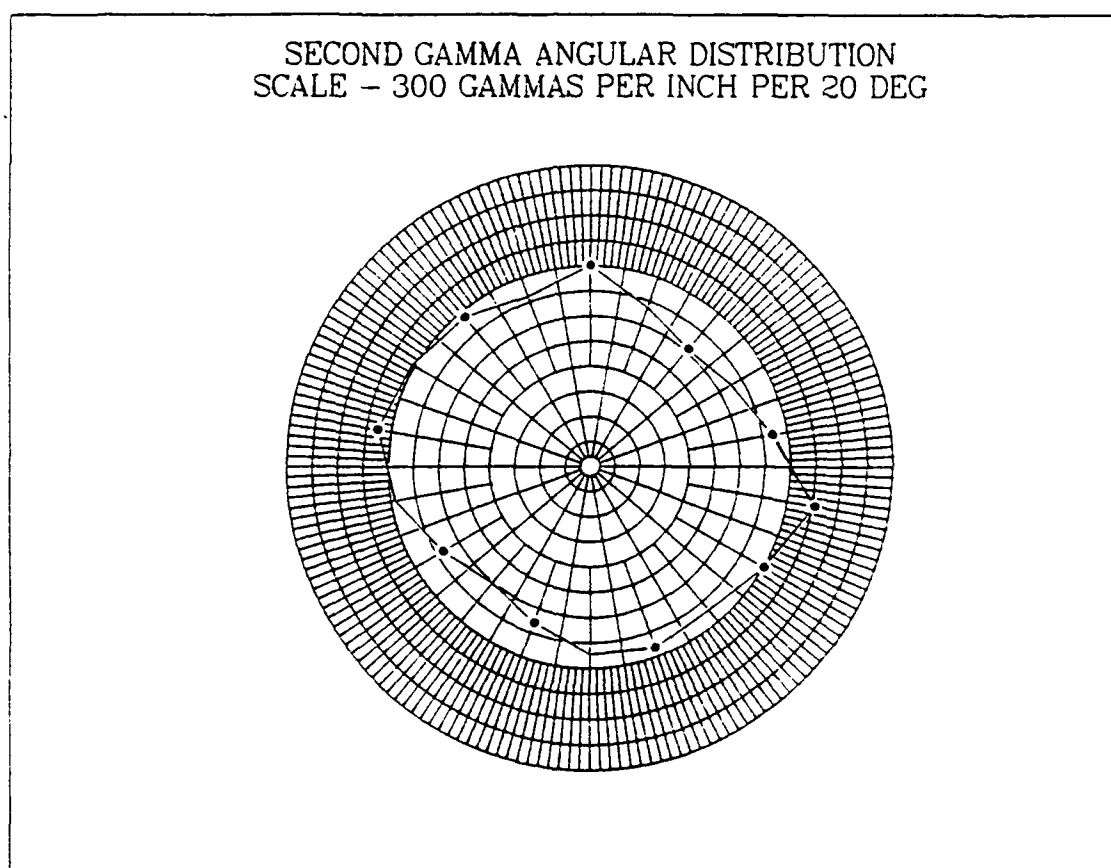


Figure 3.7: Angular distribution of second gammas relative to the first gamma, with the multipole (l) randomly selected for 10,000 isotropic gammas.

These expectations are based on the very general approximations of the single particle model, which do not always hold true. For example, it is sometimes seen that an E2 transition will occur more frequently than an M1 transition. This does not follow the expectations stated above. [34]

CHAPTER 4

THE GAMINT CODE

4.1 Introduction to the GAMINT Code

A gamma cascade code (GAMINT Code) was developed to examine the effect cascades of different makeup have on the response of a capture tank. The GAMINT Code generates a gamma-ray energy spectrum for the neutron capture reaction $^{238}\text{U}(n,\gamma)^{239}\text{U}$. The code also determines the cascade gamma-ray yields, energies, order of emission, and multiplicities by Monte Carlo techniques. Included in this code is the competing process of internal conversion. This code, for the first time, considers the internal conversion process in the gamma cascades produced in the decay of ^{239}U .

Electromagnetic transitions in the continuum energy levels, transitions from the continuum energy levels to the discrete energy levels, and transitions in the discrete levels are considered. In the code, electric and magnetic multipole transitions of type E1 through E4 and M1 through M4 are taken into account.

Figure 4.1 through Figure 4.7 are flow charts of the GAMINT code. These charts summarize the main steps involved in the computer code and are prepared to aid the reader in understanding the general strategy of the code.

4.2 Input to the GAMINT Code

The input to the GAMINT Code is performed in two different ways. There is an external input file and an internal Block Data Subroutine. The external file contains those variables which may require changes. The Block Data subroutine contains those variables which remain fixed. This is done in order to facilitate the mechanics of changing the input to the code.

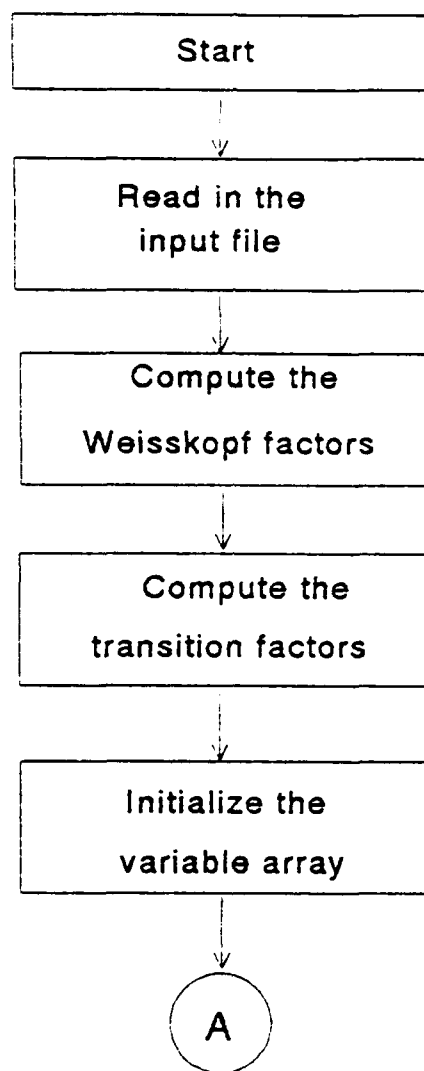


Figure 4.1: Flowchart for the GAMINT code initialization.

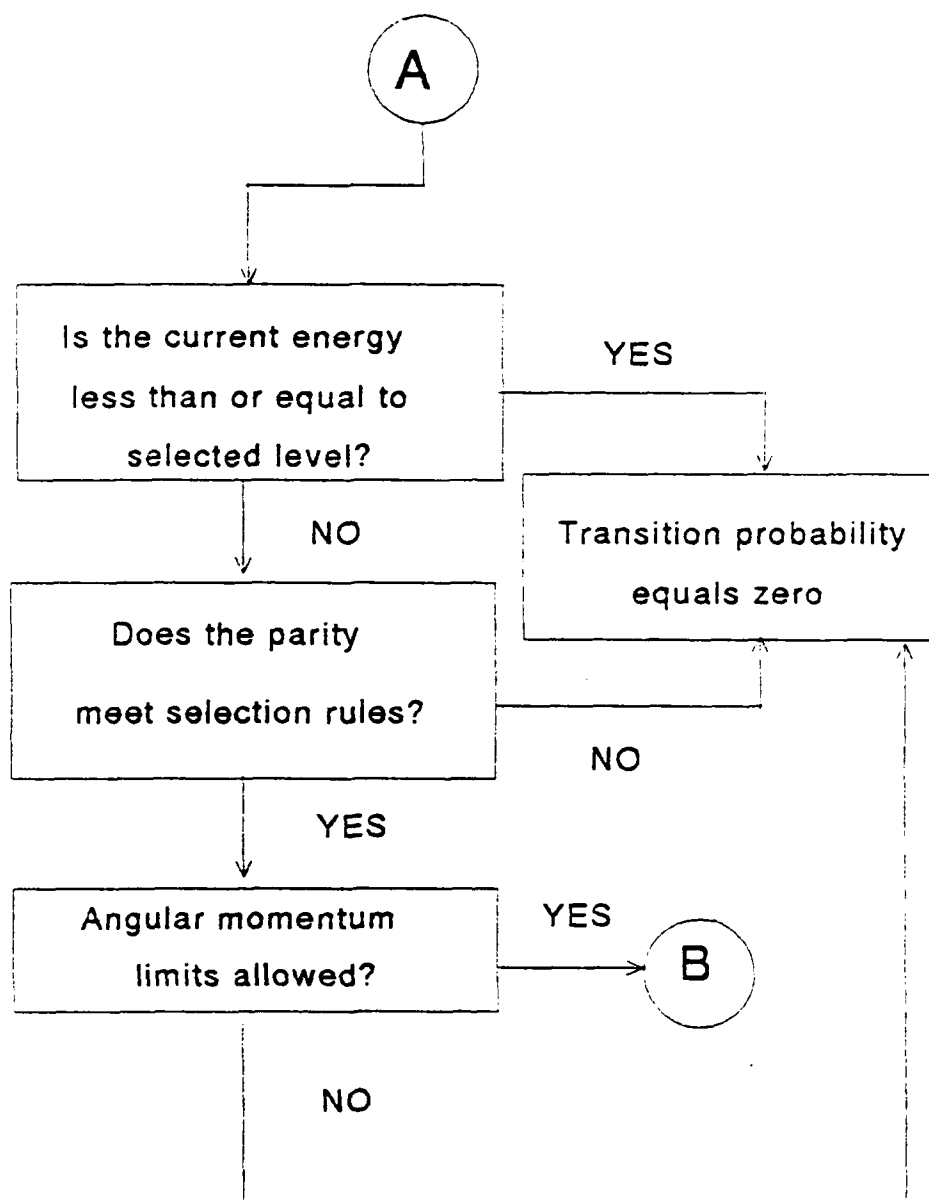


Figure 4.2: Flowchart for the discrete level selection criteria.

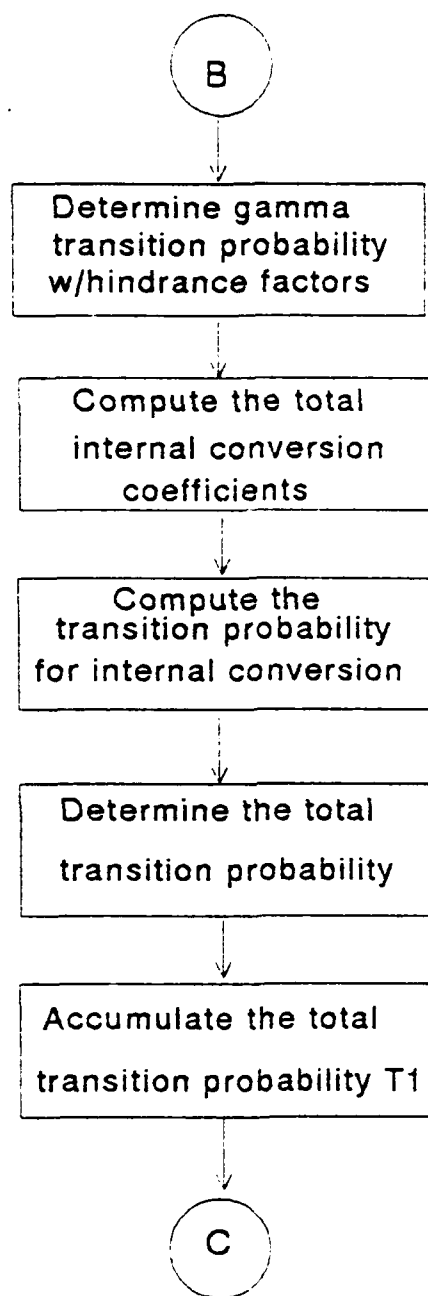


Figure 4.3: Flowchart for the discrete level transition probabilities.

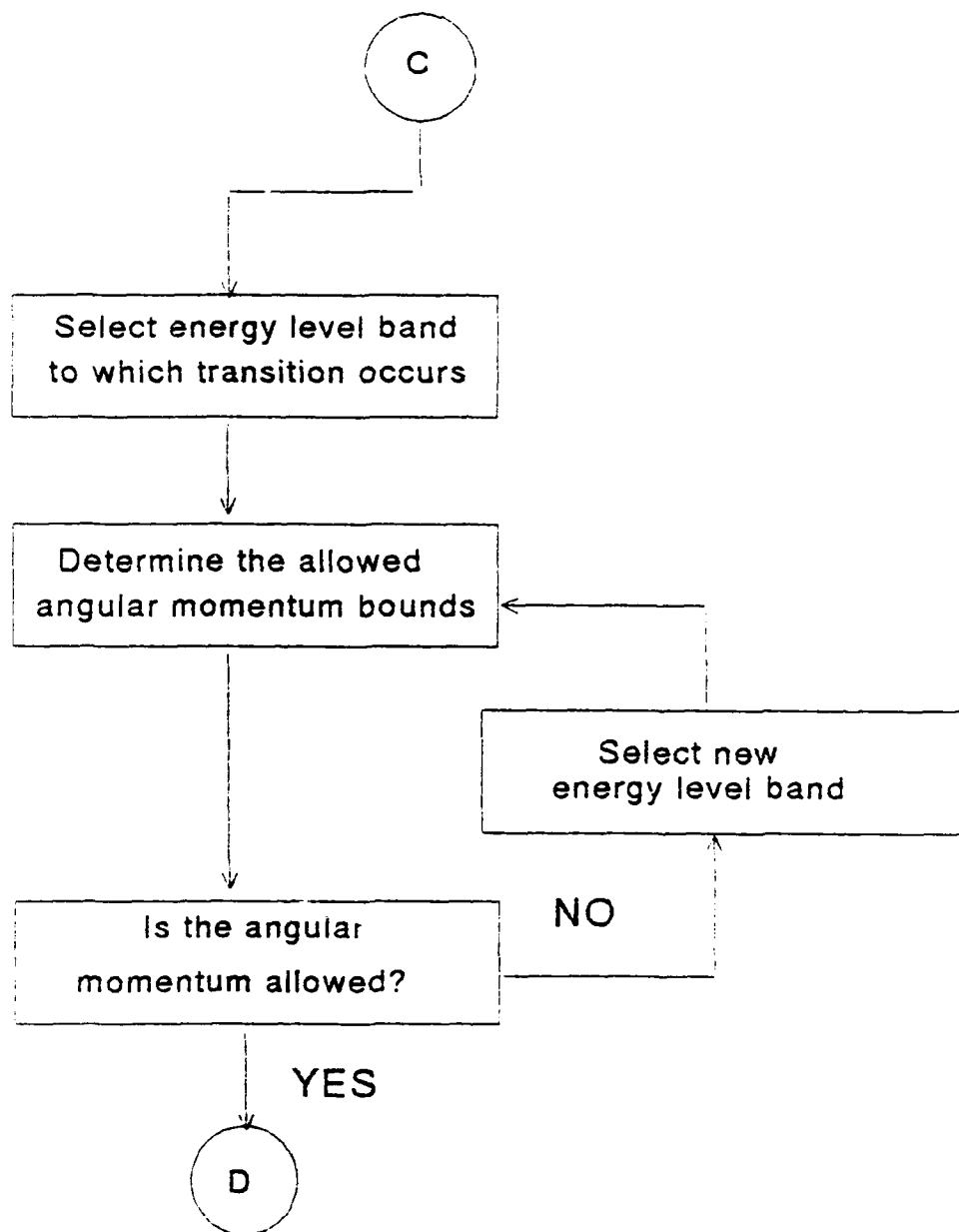


Figure 4.4: Flowchart for the continuum selection criteria.

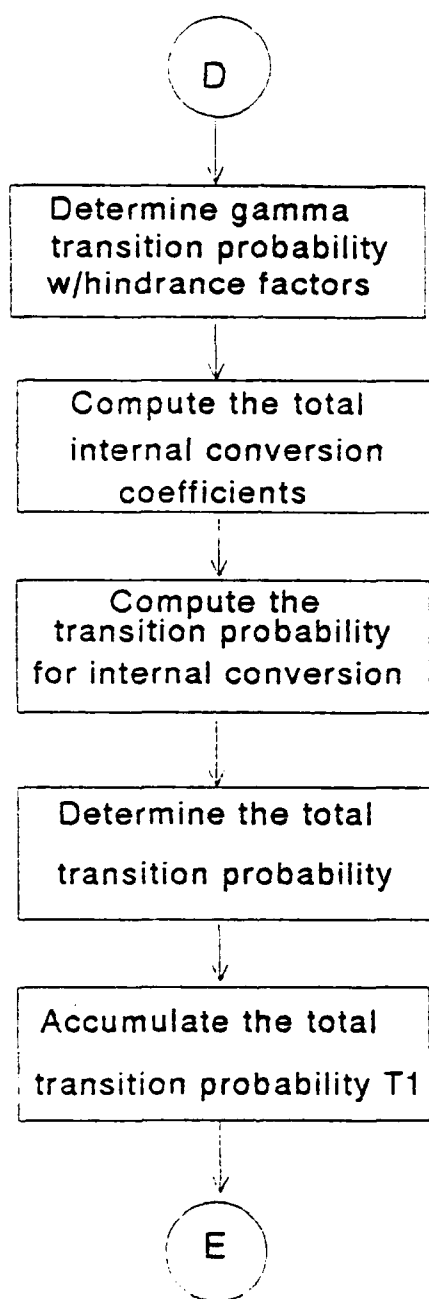


Figure 4.5: Flowchart for the continuum level transitions.

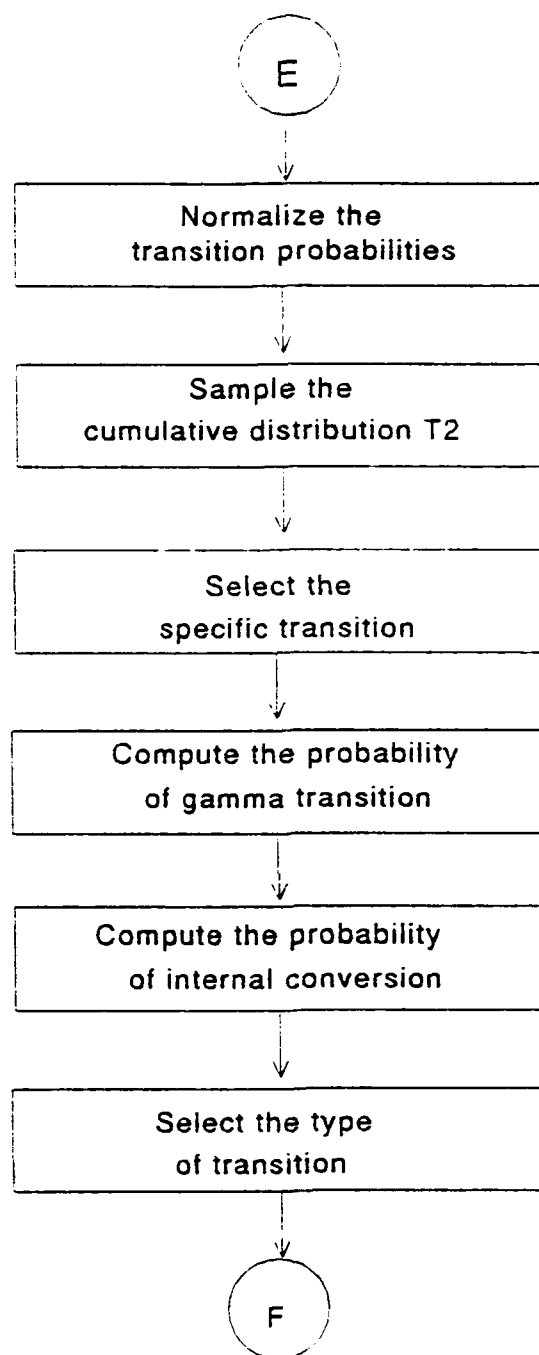


Figure 4.6: Flowchart for the selection of the transition.

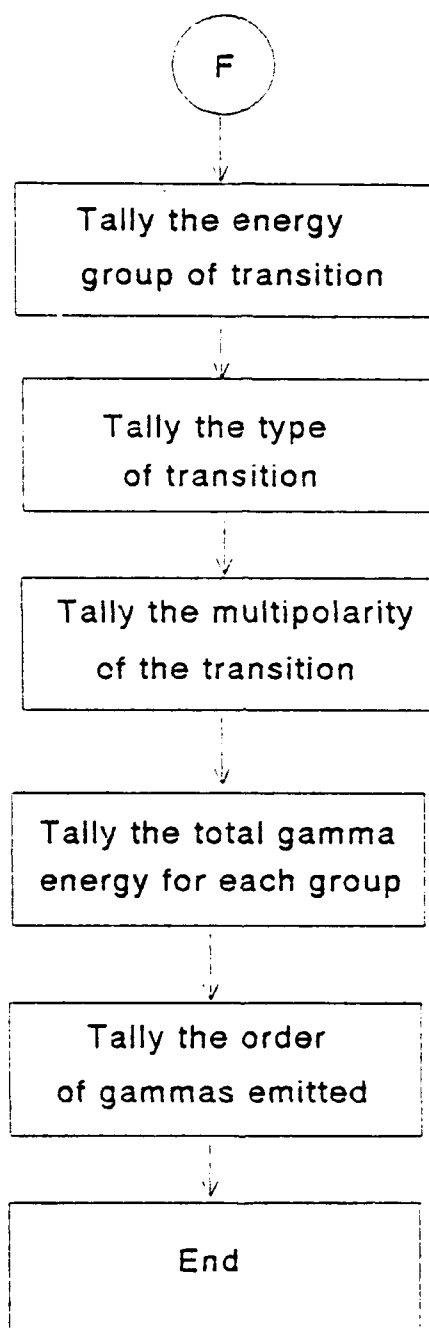


Figure 4.7: Flowchart for the tallies performed in the GAMINT code.

Table 4.1: Input variables to the GAMINT code

Line Number	Input Variable
1	TJ
2	NL,NC,NE,NJ
3	XE,XJ,XP

The initial input into the GAMINT code consists of a three line input file read into the main program from the external file GAMINT5. Line 1 of the input file contains the job title (TJ) which may be conveniently changed to keep track of the current application. Line 2 contains the number of multipoles used in the calculation (NL), the number of cascades to be executed (NC), the number of energy level bands to be used in the energy continuum (NE), and the value of the largest level spin used in the continuum region (NJ). Line 3 contains the initial nucleus energy (XE), the initial nucleus spin (XJ), and the initial nucleus parity (XP). This line is specific to the nucleus under consideration and facilitates the input of nuclei excited above 4.803 MeV neutron separation energy. These inputs may be easily changed in order to perform analysis on the cascade process.

Table 4.1 summarizes the input variables contained in the GAMINT5 input file.

Internal to the GAMINT Code is a Block Data subroutine which is used to initialize the values of the variables labeled in the common statements in the code. This subroutine contains the following input.

- Atomic weight of the compound nucleus: (AW)
- Level density parameter: (AE)
- Level density parameter for spin: (SJ)
- Number of gamma energy groups: (NG)

- Number of discrete levels: (NVD)
- Number of values for internal conversion coefficient in table for a given shell: (NV)
- Cutoff energy between the discrete levels and the continuum: (CD)
- Upper energy of the IG-th group: EG(IG)
- Hindrance factors for a particular multipole transition of moment IL, for electric transitions (IP = 1) or magnetic transitions (IP = 2): HF(IL,IP)
- Statistical factor for the particular transition of moment IL: SL(IL)
- Spin of the discrete level-IV: VJ(IV)
- Parity of the discrete level-IV: VP(IV)
- Energy of the discrete level-IV: VE(IV)
- Maximum transition energy in given shell-NS for internal conversion coefficient table: ETM(NS)
- Internal conversion coefficient for shell-NS, multipole type-IP, moment-IL, and I-th energy in table: AL(NS,IP,IL,I)

4.3 Details of the GAMINT Code

As shown in the flowchart shown in Figure 4.1, the program begins by reading in the input file (GAMINT5). This information is printed out in the output file in order to allow the user to check the accuracy of the code input.

The code then calculates the Weisskopf factors for the electric and magnetic dipoles. These values are stored in arrays RP(1) and RP(2), respectively. If RP(1)

Table 4.2: Discrete energy levels in ^{239}U

Level	Energy (MeV)	spin-parity
1	0.0	2.5-
2	.043	3.5+
3	.097	4.5-
4	.133	.5+
5	.144	1.5-
6	.165	5.5-
7	.173	3.5-
8	.191	2.5+
9	.220	3.5-
10	.229	4.5+
11	.300	5.5+
12	.307	4.5+
13	.373	6.5+
14	.696	.5-
15	.715	1.5+
16	.735	1.5+
17	.742	1.5-
18	.754	.5-
19	.799	3.5-
20	.812	.5-
21	.821	1.5-
22	.854	2.5-
23	.894	5.5-
24	.930	2.5-
25	.943	4.5-

is set equal to 1.0, then $RP(2)$ is simply::

$$RP(2) = \frac{RP(1)}{4.364 * AW * 0.66667}, \quad (4.1)$$

as shown in Equation 3.15 in Section 3.3. The factor ($RP(IP)$) is the relative probability of being an electric multipole ($IP=1$) versus a magnetic multipole ($IP=2$) transition. The magnetic multipole transition is less probable than the electric multipole of the same order since the above ratio is less than 1.000.

The code then initializes the common variables through the use of the Block Data subroutine. In the Block Data sub-routine, the known discrete levels of ^{239}U are read into the program. Table 4.2 [16] displays the energy levels and the spin-parity assignments of the excited ^{239}U nucleus used in this program. There are 25 well known levels up to the 0.95 MeV cutoff energy (CD).

The transition rates for gamma-ray transitions, based on the Weisskopf model, are then determined from all of the continuum bands and discrete levels down to all lower levels. To calculate these rates, the transition factors ($RL(IL)$) must be calculated for the all multipole moments (IL). The transition factor consists of those terms of the transition rate which the electric and magnetic multipole rates have in common.

$$RL(IL) = SL(IL) * (AW * 0.66667 * IL) * \frac{(1.82307E21)}{164.443 * (2 * IL + 1)}. \quad (4.2)$$

The transition rate for a transition between two discrete levels is then the product of the Weisskopf factor $RP(IP)$, the transition factor $RL(IL)$, the hindrance factor $HF(IL,IP)$, and the transition energy (ET) raised to the $2*IL-1$ power.

$$PV(IL,IP,IV) = RP(IP) * RL(IL) * HF(IL,IP) * (ET * (2 * IL - 1)). \quad (4.3)$$

In this calculation, the E1 transition rate is hindered by multiplying the calculated transition rate by a hindrance factor of 1.0×10^{-6} [34]. The E2 transition is enhanced by multiplying the calculated transition rate by a hindrance factor of 10.0 [35]. All

Table 4.3: Transition probabilities (per second) for discrete level transitions

Transition Energy	E1	M1	E2	M2
.1	3.85×10^6	5.60×10^{10}	1.08×10^7	1.35×10^4
.2	3.08×10^7	4.48×10^{11}	3.48×10^8	4.32×10^5
.3	1.04×10^8	1.51×10^{12}	2.63×10^9	3.28×10^6
.4	2.47×10^8	3.58×10^{12}	1.11×10^{10}	1.38×10^7
.5	4.82×10^8	7.00×10^{12}	3.39×10^{10}	4.21×10^7
.6	8.32×10^8	1.21×10^{13}	8.43×10^{10}	1.05×10^8
.7	1.32×10^9	1.93×10^{13}	1.82×10^{11}	2.27×10^8
.8	1.97×10^9	2.87×10^{13}	3.55×10^{11}	4.42×10^8
.9	2.81×10^9	4.08×10^{13}	6.40×10^{11}	7.96×10^8
1.0	3.85×10^9	5.60×10^{13}	1.08×10^{12}	1.35×10^9

other transitions have a hindrance factor set equal to 1.0. There exists no evidence for hindrance factors of other multipolarities. However, these other multipolarities contribute very little to the process. Table 4.3 shows the discrete transition probabilities (sec^{-1}) for the E1, M1, E2, and M2 transitions for selected gamma transition energies.

The transition rate between a continuum level band and a lower lying level includes a spin term. Using the back-shifted fermi gas model in Equation 2.17, Section 2.4 with the level density parameter (a) set equal to 9.20212, the fictive ground state position (Δ) set equal to -0.58, and the spin parameter set equal to 3.7283, the transition rate for the continuum levels down to lower lying states becomes:

$$\begin{aligned}
 PT(IL,IP,IJ,IE) = & RP(IP) * RL(IL) * ET * (2. * IL - 1) * DE * (2. * RJ - 1.) \\
 & * HF(IL,IP) * EXP(-RJ * (RJ - 1)/SJ) \\
 & * .00010091 * EXP(9.7494 * SQRT(EE - .58))/(EE - .58) * 1.86000.
 \end{aligned}
 \tag{4.4}$$

4.4 Treatment of Internal Conversion

The internal conversion rate for each of the possible transitions is also determined. Since internal conversion is considered an additional decay process, it increases the total decay rate. The total transition rate λ is the sum of the transition rate due to a gamma transition λ_γ and the transition rate due to an internal conversion transition λ_e .

$$\lambda = \lambda_\gamma + \lambda_e. \quad (4.5)$$

Once the transition rates $PV(IL,IP,IV)$ for transitions from discrete levels and the transition rates $PT(IL,IP,IJ,IE)$ for transitions from the continuum bands are known, the internal conversion coefficients (ALT) are determined. The coefficients are returned from the FIT subroutine, and by using the definition of the internal conversion coefficient (Equation 3.21, Section 3.6), together with the known gamma transition rate, the internal conversion rate is computed.

In the discrete transitions:

$$PE(IL,IP,IV) = PV(IL,IP,IV) * ALT. \quad (4.6)$$

In the continuum bands to lower level transitions:

$$PC(IL,IP,IJ,IE) = PT(IL,IP,IJ,IE) * ALT. \quad (4.7)$$

The internal conversion coefficients are determined by a procedure published by Hager and Seltzer [31]. The conversion coefficients can be determined for the four lowest electric and magnetic multipole moments ($E1, \dots, E4, M1, \dots, M4$), for electrons in the K-, L-, or M-shells. The table values for internal conversion coefficients are shown in Figure 4.8 through Figure 4.10. These values are entered into the code through the Block Data subroutine. In order to determine the internal conversion coefficient for transition energies between any two given values, a cubic spline interpolation subroutine (SPLINE) provides a piece-wise polynomial fit to the data. This insures that the accuracy of the table is preserved.

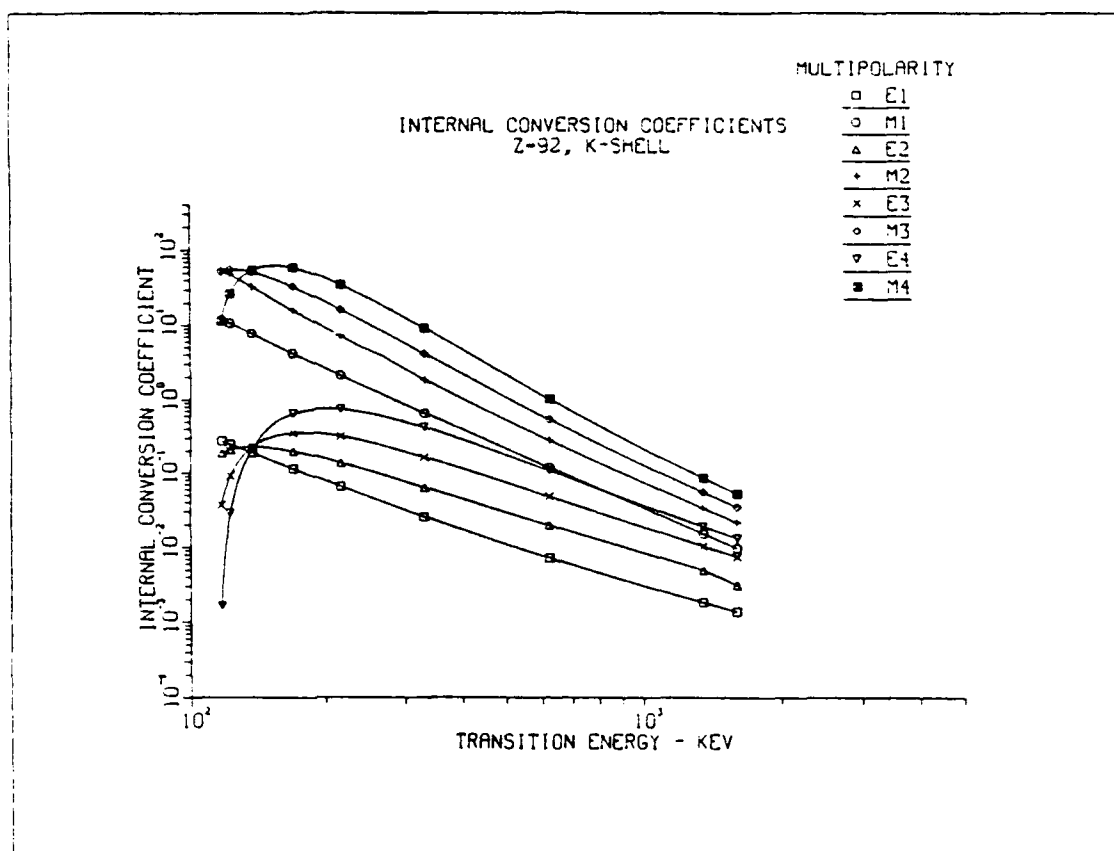


Figure 4.8: Internal conversion coefficients for K-shell conversion used in the GAMINT Code

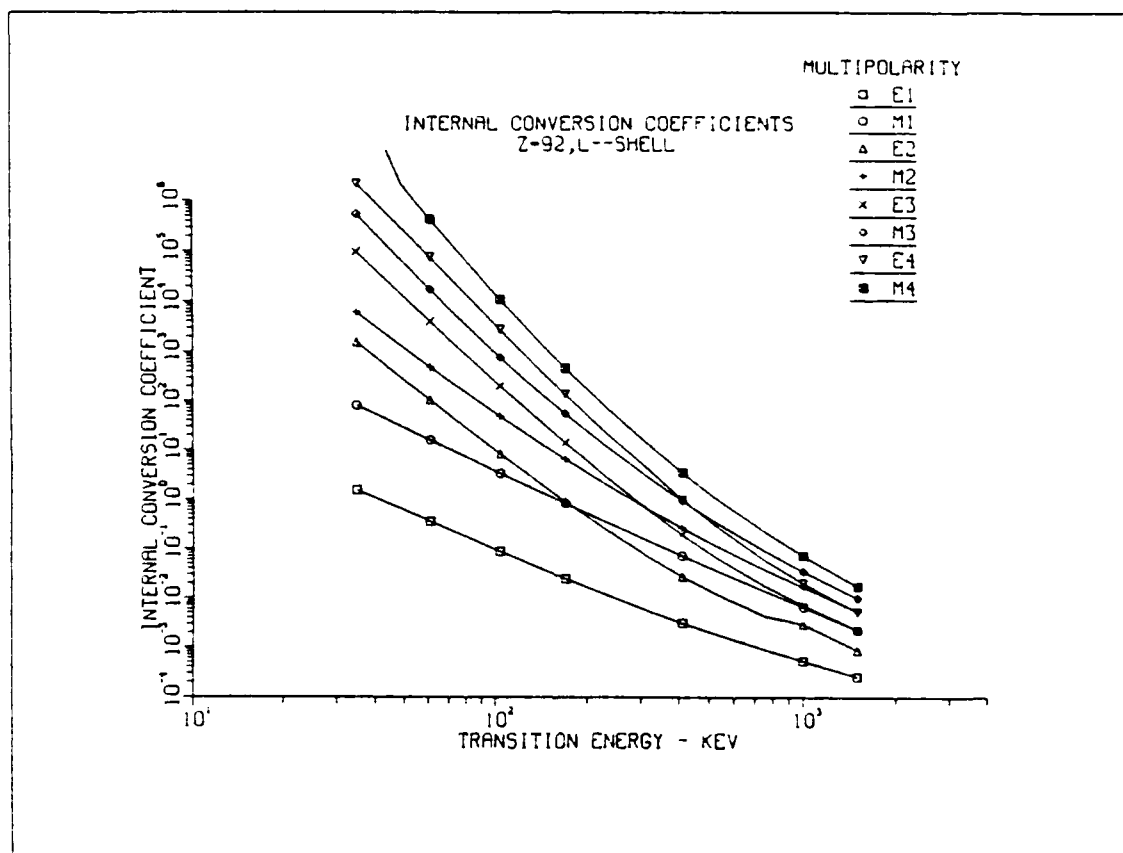


Figure 4.9: Internal conversion coefficients for L-shell conversion used in the GAMINT Code

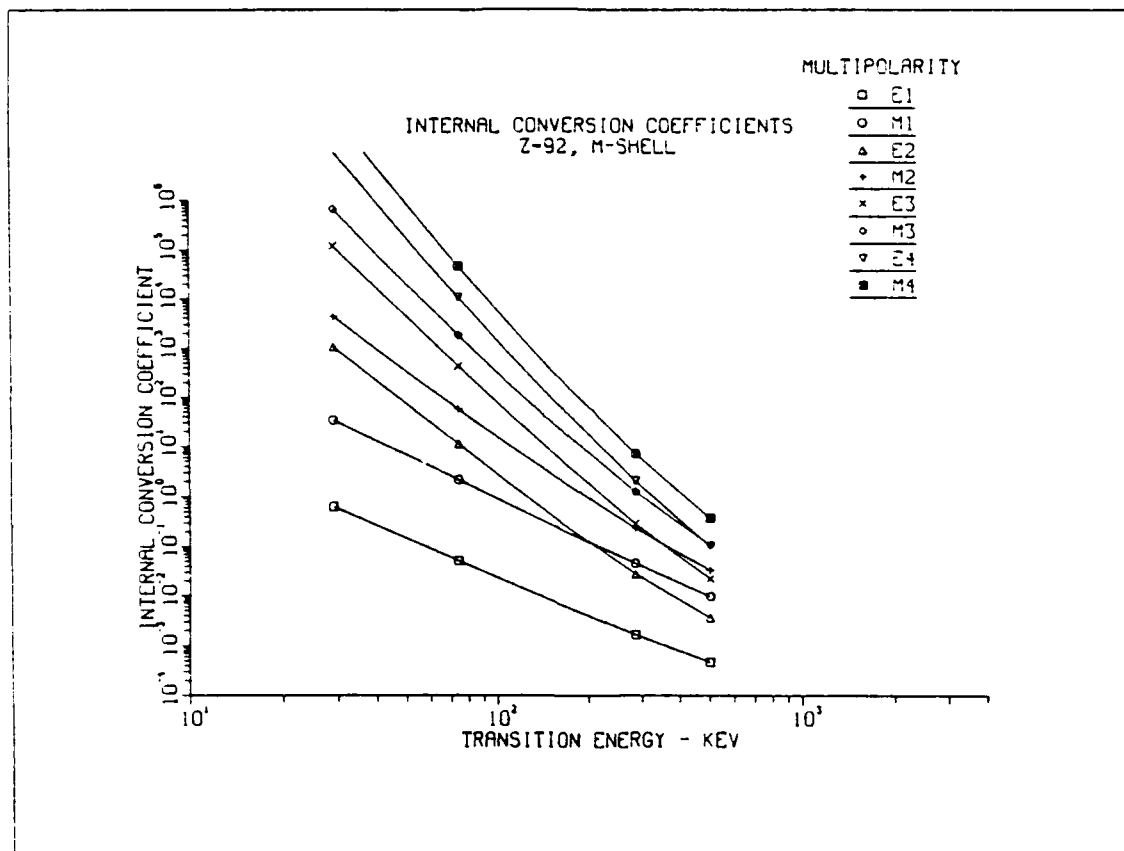


Figure 4.10: Internal conversion coefficients for M-shell conversion used in the GAMINT Code

The subroutine FIT serves as an input-output controlling routine and this subroutine calls the subroutine SPLINE in which the actual curve interpolation is performed. In the main program it is necessary to determine the internal conversion coefficient for each gamma-ray transition. A call is made to Subroutine FIT in a loop over the three electron shells. Since the table values are in KeV, the transition energy (in MeV) is multiplied by a factor of 1000.0 and this value is used as the energy interpolation value. Each of the three shells have a different number of known values in the table. Each shell has associated with it a number NV(NS) to indicate the number of table values. When the call to FIT is made, the important parameters passed into the subroutine include the electron shell (NS), the number of values in table NV(NS) for shell NS, and the transition energy (ETT). The important parameter passed back to the main program through the common statement is the internal conversion coefficient for the given electron shell ALV(NS). A value is obtained for the conversion coefficient for each of the three shells (K,L, and M) by calling the FIT subroutine three times, once for each shell. These three values are summed to give the total internal conversion coefficient α (ALT).

$$ALT = ALV(1) + ALV(2) + ALV(3), \quad (4.8)$$

where ALV(NS), (NS=1,2,3) represents the partial internal conversion coefficients. The three values for the electron shell conversion coefficient are summed in the main program.

4.5 Transition Selection

The total transition rates for all transitions are determined by summing the transition rate for gamma decay and the transition rate for internal conversion. For a discrete to discrete level transition, the total transition rate is:

$$TT(IL,IP,IV) = PV(IL,IP,IV) + PE(IL,IP,IV). \quad (4.9)$$

and for a continuum band to lower level transition, the total transition rate is:

$$TU(IL,IP,IJ,IE) = PT(IL,IP,IJ,IE) + PT(IL,IP,IJ,IE). \quad (4.10)$$

The total transition rates are summed in a temporary variable (T1) and each individual rate is divided by T1 in order to normalize the total transition rate for a particular transition.

$$TT(IL,IP,IV) = TT(IL,IP,IV)/T1. \quad (4.11)$$

and

$$TU(IL,IP,IJ,IE) = TU(IL,IP,IJ,IE)/T1. \quad (4.12)$$

A cumulative probability distribution (T2) is created by summing the normalized rates and sampled with a random number to select a transition.

$$T2 = \sum_{IL,IP,IV} TT(IL,IP,IV), \quad (4.13)$$

and

$$T2 = \sum_{IL,IP,IJ,IE} TU(IL,IP,IJ,IE). \quad (4.14)$$

A simple rejection technique is used to select the transition. The random number is generated in the GGUBS subroutine in the IMSLDPLIB routine library on MTS. This random number is then compared to the cumulative probability, as the normalized cumulative distribution is built, to select the transition (if the random number is less than the cumulative probability) or reject the transition (if the random number is greater than the cumulative probability). When rejected, the transition selection process is performed again.

Once the transition is selected, another random number selection determines if the transition occurs by gamma decay or by internal conversion. In this selection process, the gamma transition probability is divided by the sum of the gamma and

internal conversion probabilities. For the discrete transitions, the gamma transition probability is:

$$PG = PV(IL,IP,IV)/(PV(IL,IP,IV) + PE(IL,IP,IV)). \quad (4.15)$$

This number represents the gamma transition probability for a particular transition energy, given that transition is selected. The probability for internal conversion, given a particular transition occurs, is simply:

$$PI = PE(IL,IP,IV)/(PV(IL,IP,IV) + PE(IL,IP,IV)). \quad (4.16)$$

The sum of the gamma transition probability and the internal conversion probability is unity. The above procedure is also performed for the continuous level transitions. The gamma transition probability, given a transition occurs, is:

$$PH = PT(IL,IP,IJ,IE)/(PT(IL,IP,IJ,IE) + PC(IL,IP,IJ,IE)), \quad (4.17)$$

and the internal conversion transition probability, given a particular transition occurs, is:

$$PJ = PC(IL,IP,IJ,IE)/(PT(IL,IP,IJ,IE) + PC(IL,IP,IJ,IE)). \quad (4.18)$$

The new random number is generated in the GGUBS subroutine and compared to the gamma transition probability. If the random number is less than the gamma transition probability, the transition proceeds by gamma emission. If not, internal conversion occurs. This procedure is continued until the ground state is reached.

4.6 Tallies Performed by the GAMINT Code

The GAMINT code performs as many iterations as programmed into the input file. During each of the iterations, information is tallied for analysis. The specific items of interest which the code can keep track of are

- The energy group of the transition.
- The type of the transition (gamma ray or internal conversion).
- The multipolarity of the transition.
- The total gamma-ray energy for each group.
- The order of the gamma-ray emitted in the cascade.

This information serves as the basis for the analysis of the gamma cascades in the decay of the excited ^{239}U nucleus.

CHAPTER 5

RESULTS

5.1 Results of the GAMINT Code

The GAMINT Code was implemented with the following input data in the input file GAMINT5.

- Job title (TJ): GAMMA SPEC CALCULATION W/I.C.
- Number of multipoles used in calculation (NL): 3
- Number of cascades executed (NC): 1000
- Number of energy level bands to be used in the energy continuum (NE): 100
- Largest level spin used in the continuum region (NJ): 10
- Initial nucleus energy (XE): $4.8030 < XE < 7.3000$
- Initial nucleus spin (XJ): 0.50000
- Initial nucleus parity (XP): 1.0000

The number of cascades (NC) in the input file determines how many decays to ground state (program loops) will be considered. The initial excitation energy (XE) may be changed to allow for the generation of a spectrum based on a different initial excitation energy. The number of level bands considered in the continuum may be varied, however, 100 proved to be a sufficient number of bands to use.

The GAMINT Code determines the energy, multiplicity, and order of each gamma ray in the gamma cascades emitted in the decay of the excited ^{239}U nucleus. The code output also contains useful information such as the number of conversion electrons per cascade for each of the selected energy groups. The same input file

was run through the FGAMA Code which produces a spectrum without any consideration for internal conversion process. The spectra from the two codes were drawn on the same graph using the DISSPLA Graphics Package on the MTS computer system at Rensselaer. This plot is shown in Figure 5.1.

A comparison shows that in the low energy region, the number of gamma rays emitted is greatly suppressed when internal conversion is considered. This is because the low energy transitions in a high-Z nucleus are more likely to occur through the internal conversion process than the gamma-ray emission process. This is expected because the internal conversion coefficient decreases rapidly with energy. In the higher energy region, internal conversion has little effect on the number of gamma-rays produced. It is seen however that the spectrum with internal conversion is slightly higher than the spectrum without internal conversion.

A gamma-ray emission ratio was determined by dividing the gamma-ray multiplicity by the sum of the gamma-ray multiplicity and the internal conversion multiplicity. A value of unity for this ratio indicates that the internal conversion process has no impact on the number of gamma rays emitted in a particular energy group. A value for the ratio of less than unity indicates that the internal conversion process decreases the number of gamma rays emitted in a particular energy group. The plot, shown in Figure 5.2, reveals that the lower energy gamma-rays are suppressed as a result of the favorable competition of the internal conversion process.

Figure 5.3 displays the fraction of total gamma ray energy released per energy group. For this plot, the gamma ray energies were summed into their respective energy bins and the result was divided by the total gamma ray energy released. This results in a normalized spectrum.

Figure 5.4 displays the multipolarity of the gamma rays emitted in the decay of ^{239}U . The M1 transition is enhanced by a factor of 10 in this decay. The E1 transition is hindered by a factor of a million. This leads to the majority of the

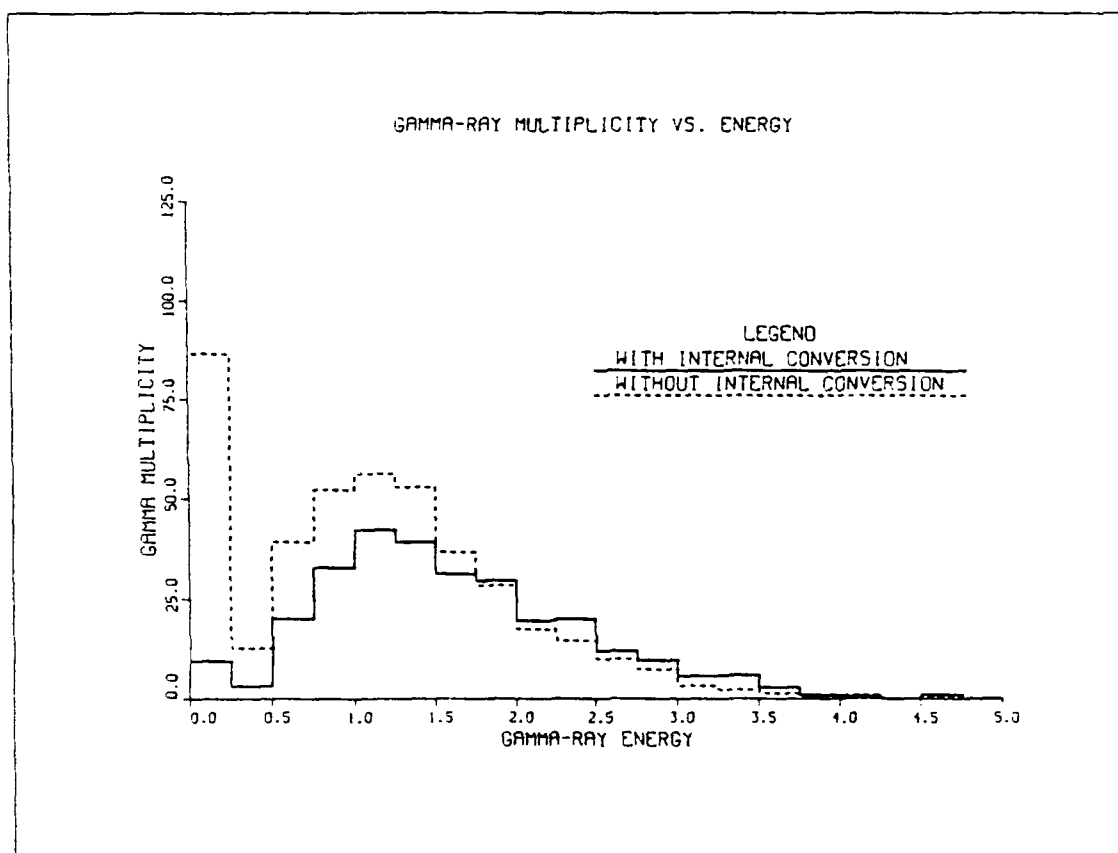


Figure 5.1: Gamma-ray multiplicity versus transition energy.

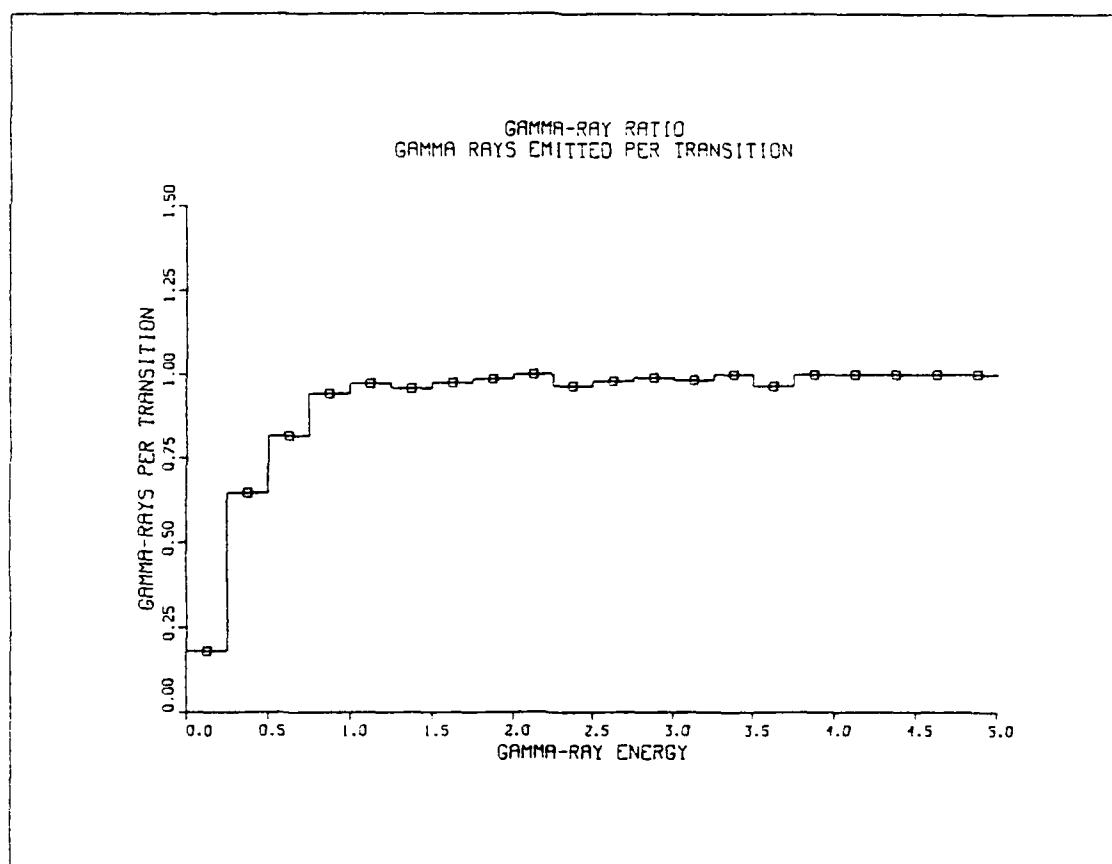


Figure 5.2: Gamma-ray emission ratio

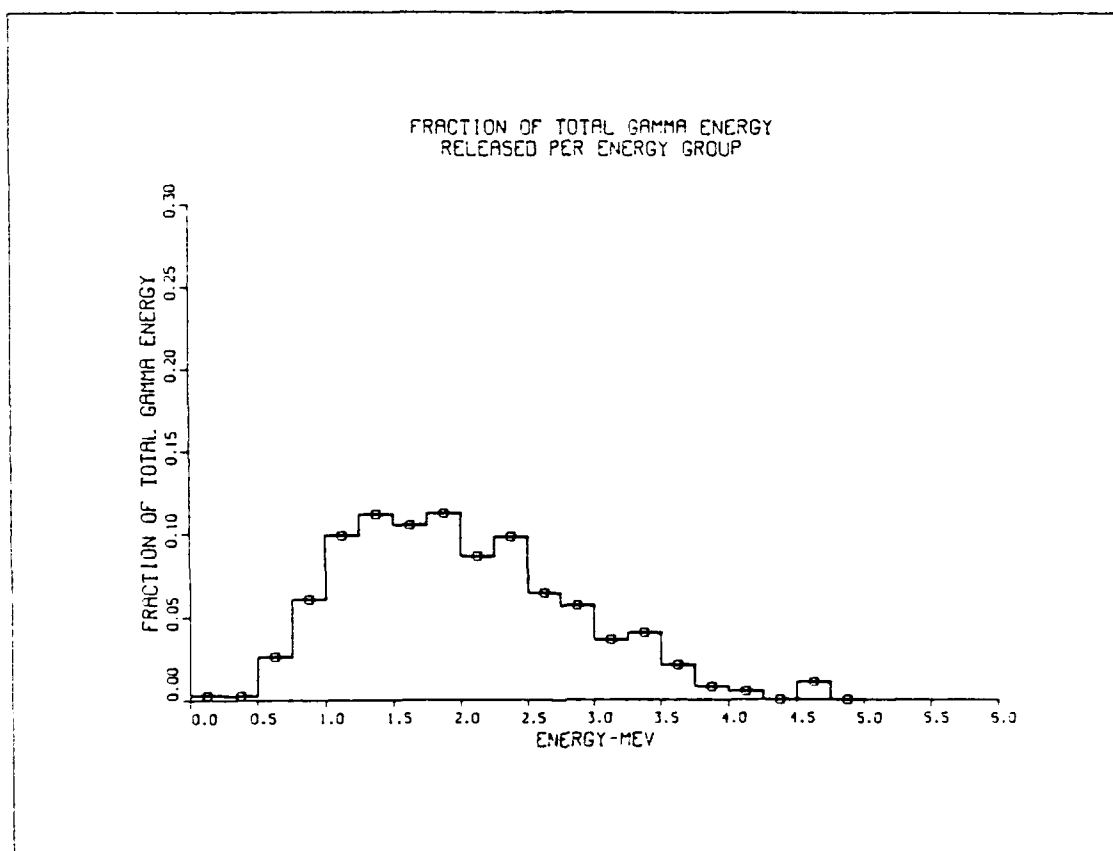


Figure 5.3: Fraction of total gamma-ray energy released per energy group.

transitions being magnetic dipole (M1).

The GAMINT code allows one to determine the order in which the gamma rays are emitted from the compound ^{239}U nucleus. The plot shown in Figure 5.5 was constructed showing the frequency with which the n -th gamma ray (where $n = 1, 2, \dots, 7$) is emitted in the cascade for a given energy. The frequency is shown on a per cascade basis. The first gamma ray emitted in a cascade is larger on the average than the other gamma rays, with a peak around 1.9 MeV. The second gamma ray is smaller on the average than the first gamma ray, with a peak around 1.3 MeV. The third gamma ray has a peak around 1.2 MeV. The fourth gamma ray has a peak around 0.8 MeV. For the few cascades with more than four gamma rays in the cascade, the energy of these gamma rays is in the 0.0 to 0.5 MeV region.

Figure 5.6 through Figure 5.9 are scatter plots of the first gamma ray emitted in a cascade versus the n^{th} gamma (for $n=2, 3, 4, 5$). As the value of n gets larger, there are fewer cascades with that number of gamma rays in it. Therefore, as n increases, more cascades have values of zero for the n -th gamma ray and there are more points lying on the first gamma ray axis, indicating a value of zero for the n -th gamma ray. These plots contain information on 1000 cascades.

Figure 5.10 is a scatter plot of the first gamma emitted in the cascade versus the last gamma emitted in the same cascade. The lone point in the upper right hand corner of the plot is the superposition of the cascades with only one gamma ray from the 4.803 MeV level down to ground state. Therefore the first gamma ray is the last gamma ray for these cascades.

A 3-dimensional plot was constructed to show the gamma-ray spectrum for different excitation energies. In Figure 5.11, the gamma ray spectrum is displayed for initial excitation energy from 4.803 MeV, up to 7.3000 MeV. The cutoff level of 7.3000 MeV was selected because of consideration for the yrast level in the excited ^{239}U nucleus. For excitation energies above 7.3000 MeV, particle emission will occur.

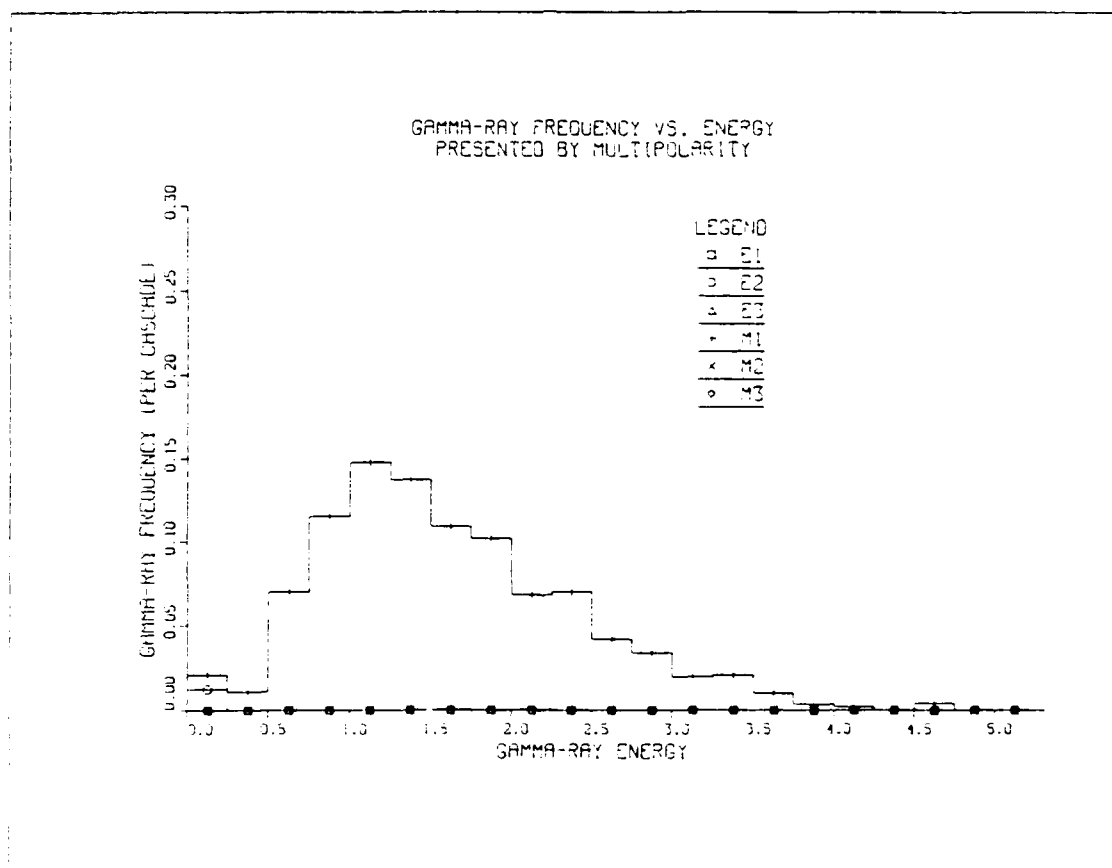


Figure 5.4: Gamma-ray frequency versus energy presented by multipolarity

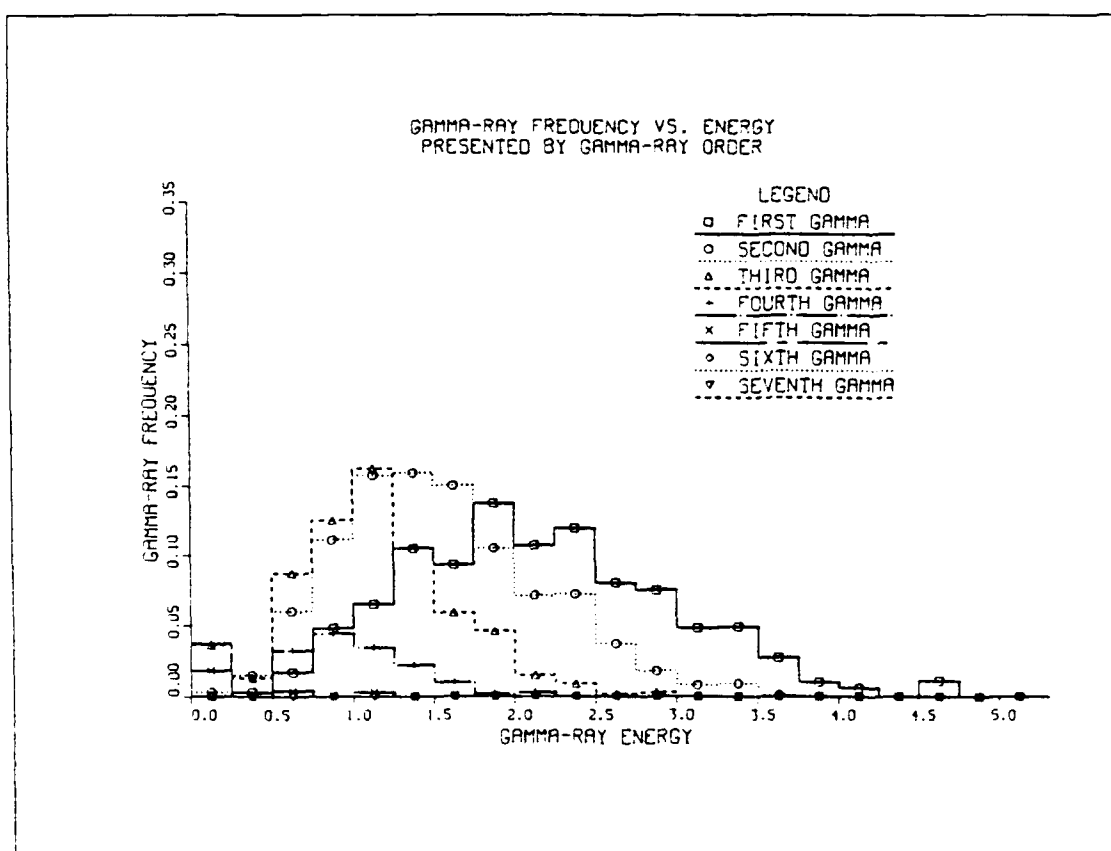


Figure 5.5: Gamma-ray frequency versus energy presented by gamma-ray order.

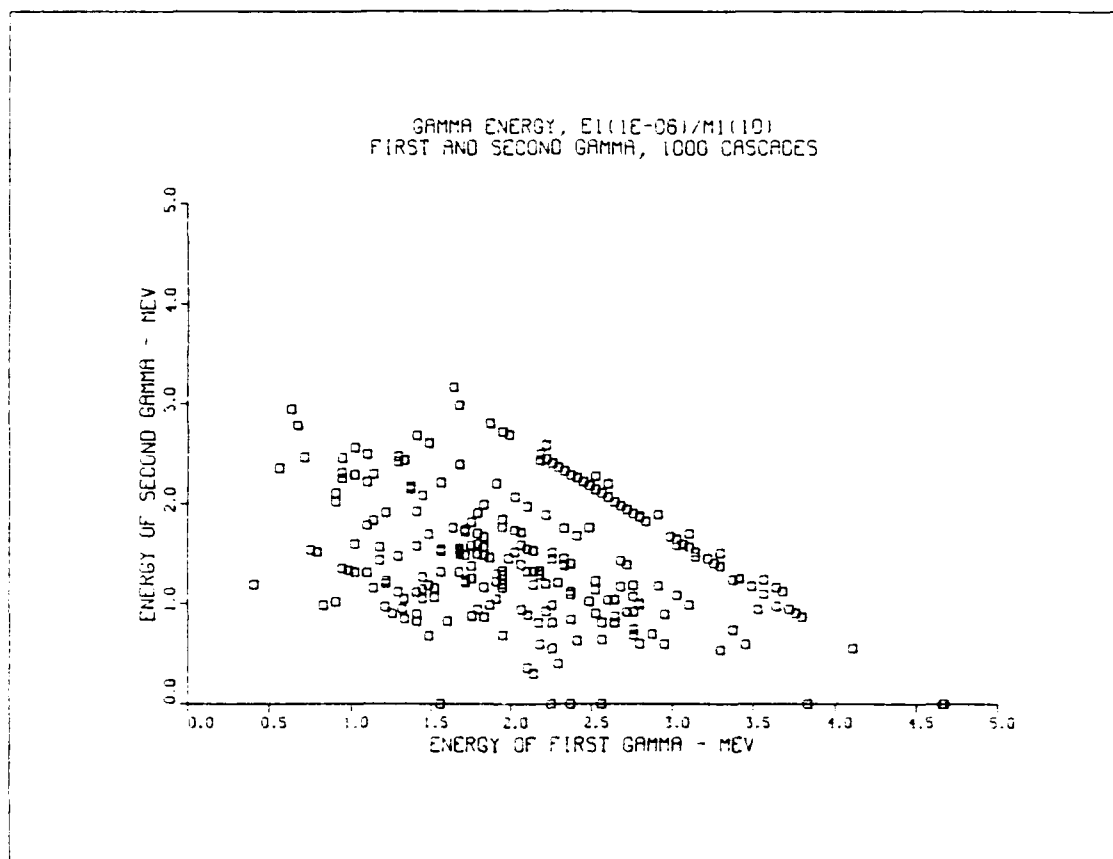


Figure 5.6: Gamma Ray Energy for the First and Second Gamma Rays

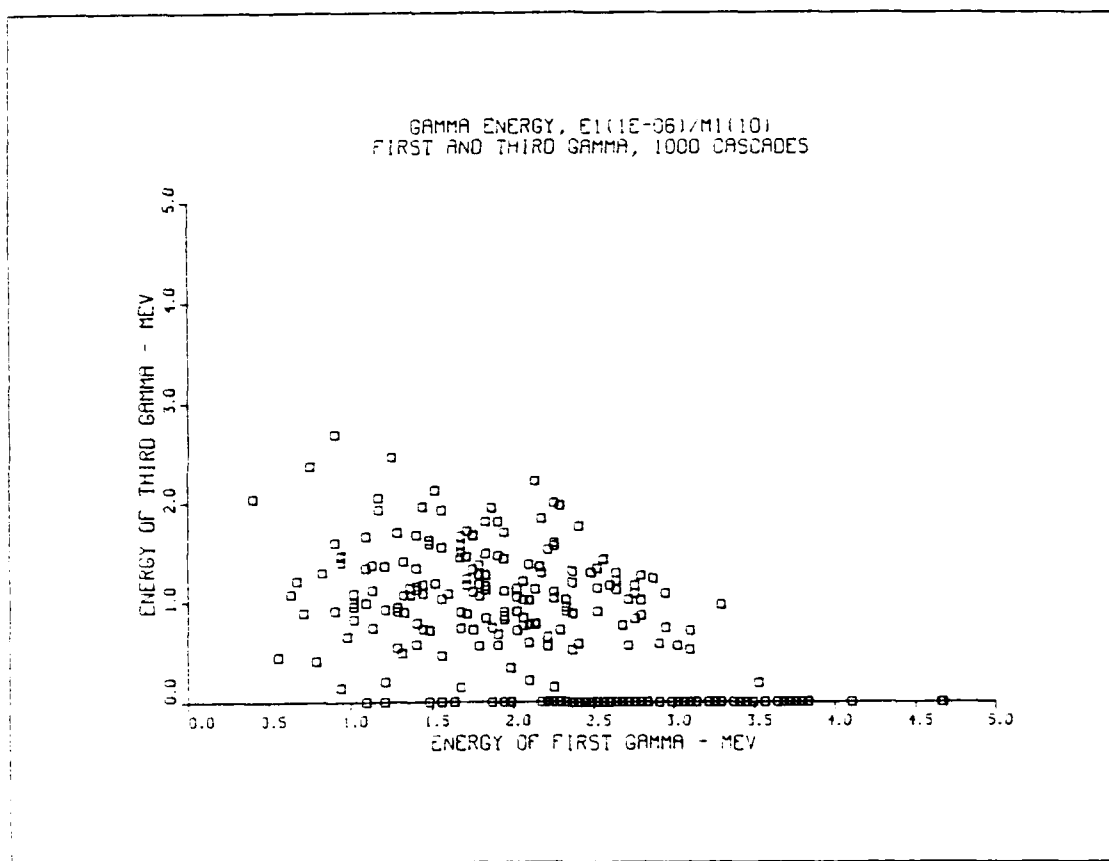


Figure 5.7: Gamma Ray Energy for the First and Third Gamma Rays

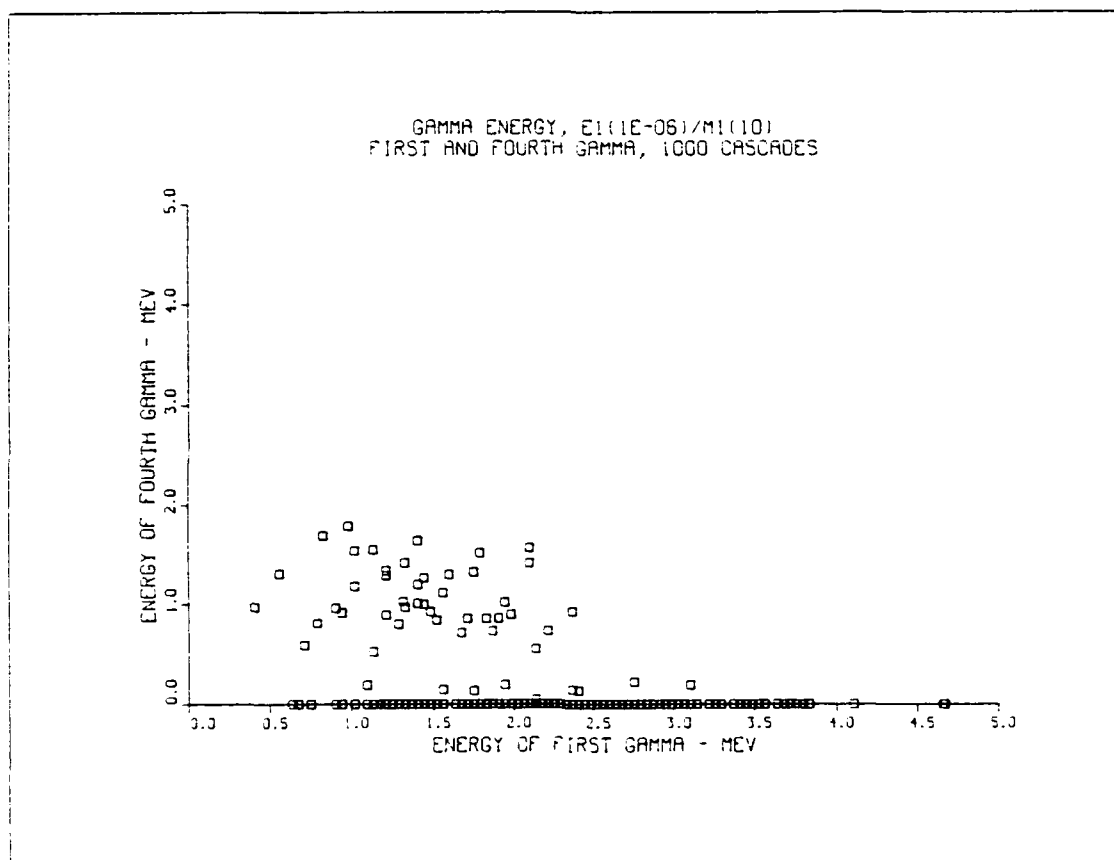


Figure 5.8: Gamma Ray Energy for the First and Fourth Gamma Rays

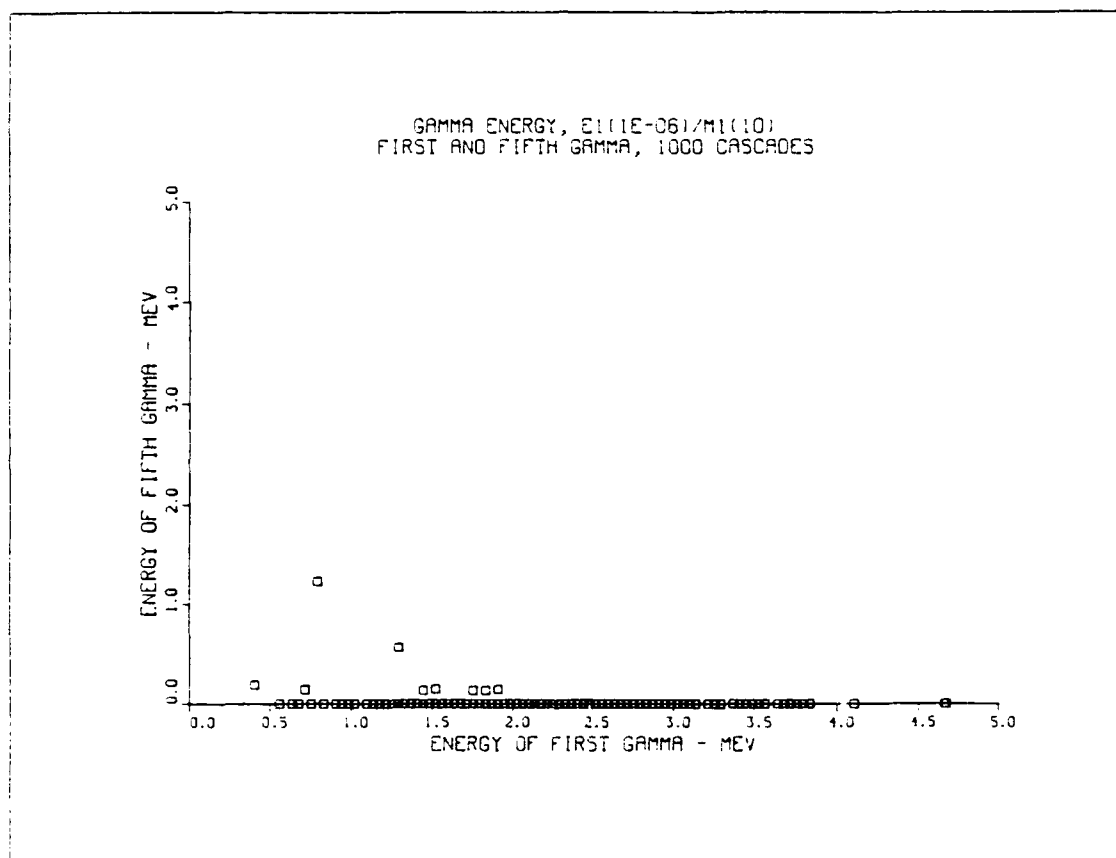


Figure 5.9: Gamma Ray Energy for the First and Fifth Gamma Rays

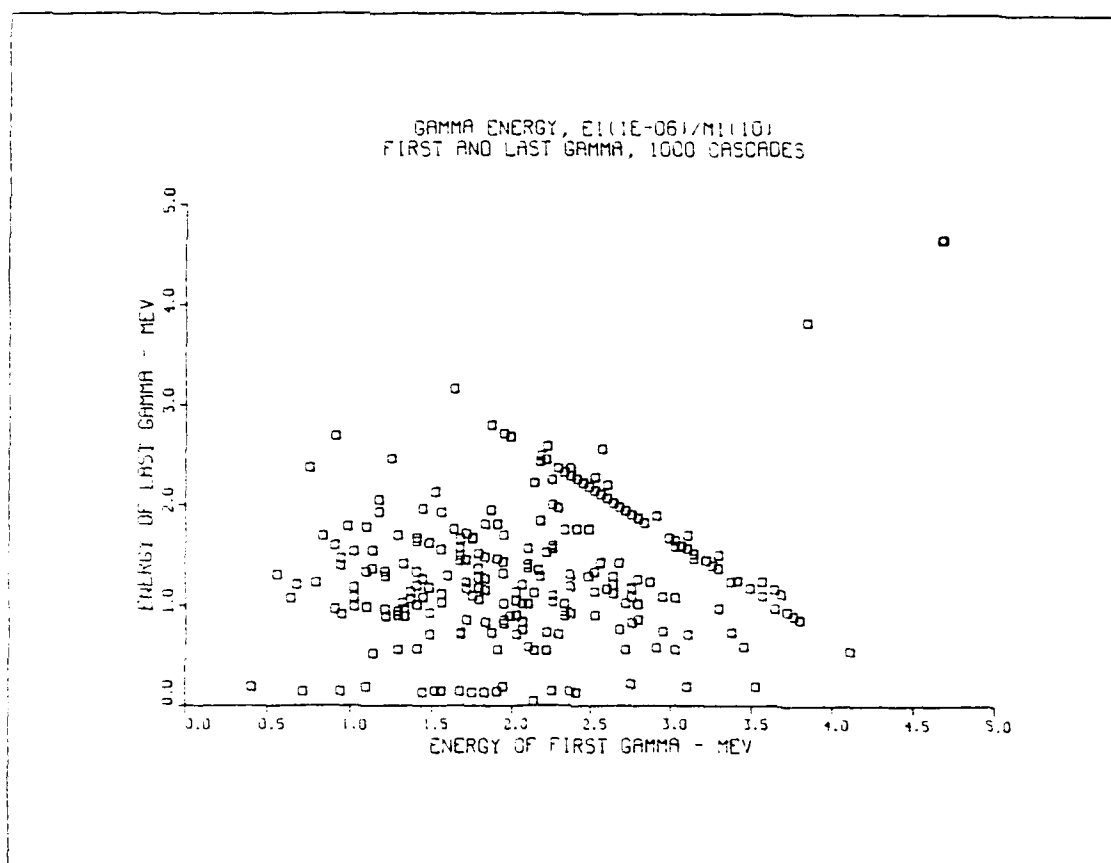


Figure 5.10: Gamma Ray Energy for the First and Last Gamma Rays

This regime is not considered in this work. The higher excitation energy nuclei exhibit spectrum shapes similar to the lower energy spectrum, however there is a slight shift to the higher energy gamma rays. This is to be expected as a result of the increased initial excitation energy.

Figure 5.12 through Figure 5.15 show the angular distribution of the n^{th} gamma ray emitted in the decay of ^{239}U formed in the thermal neutron capture reaction $^{238}\text{U}(n,\gamma)^{239}\text{U}$. In this analysis, 1000 cascades were considered. The angular distribution probabilities of the second gamma ray relative to the first gamma ray was computed using a Monte Carlo program based on the angular distribution function shown in Equation 3.37 in Section 3.10.

Each of the plots shown in Figure 5.12 through Figure 5.15, are based on the first gamma ray being emitted at a preferred direction of 0.00° . Figure 5.12 shows the direction of the second gamma ray with respect to the first gamma ray. Note, since the M1 transition is enhanced in the decay of ^{239}U , the angular distribution of the second gamma ray, relative to the first gamma ray emitted in a preferred direction, is a dipole. We see, however, that some of the gamma rays fall outside of the dipole distribution. This is a result of other than dipole transitions occurring in the 1000 cascades examined.

Figure 5.13 shows the third gamma ray angular distribution, relative to the first gamma ray emitted along the preferred 0.00° axis. The probability in this case is determined by multiplying the probability of the second gamma in the cascade by the probability of the third gamma in the cascade. This is because the third gamma ray direction and probability is dependent on the direction of the second gamma ray in the cascade, which in turn is dependent on the first gamma-ray direction. The first gamma ray is assumed to be emitted in the preferred direction with a probability of unity. Again, due to other than M1 transitions, there are some gamma rays falling outside of a dipole emission signature.

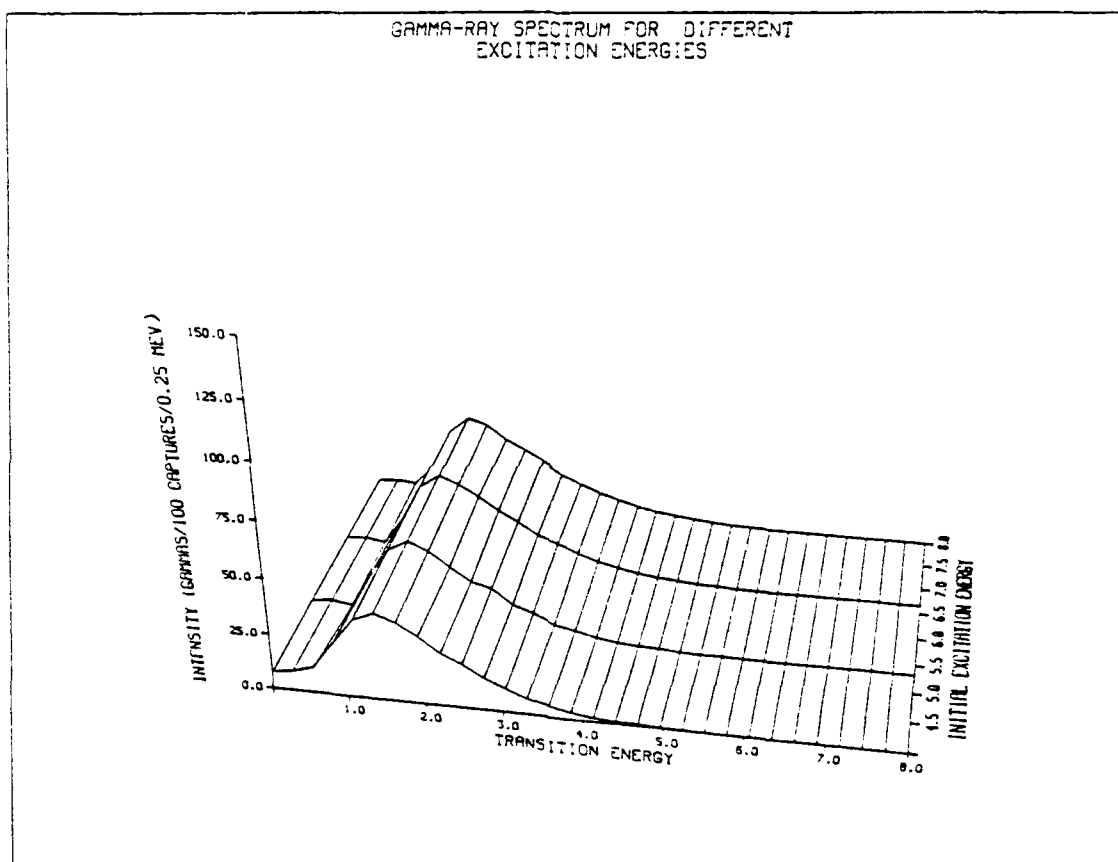


Figure 5.11: Gamma-ray spectrum for different excitation energies.

As the number n ($n=2,3,4,5$) of the gamma ray in the cascade increases, the physical number of points plotted in the distribution decreases. This occurs because the number of gamma rays in the cascades varies.

5.2 Comparison to Published Results

The spectrum generated by the GAMINT code is compared to the calculated spectrum of Takahashi, to the experimental spectrum of John et al., and to the experimental data of Campion, in Figure 5.16. The spectrum determined by John et al. is only reported for energies above 1.00 MeV. The results of the GAMINT code are presented in terms of gamma-ray intensity in photons per 100 capture events per 0.25 MeV bin. The Takahashi spectrum is reported in 0.25 MeV bins. The data of Campion is plotted for several energies in the 0.5 MeV to 0.6 MeV region. Campion's data is also given for 3.58 MeV, 3.66 MeV, and 4.06 MeV.

The similarities in the spectra occur in the gross structure. In Takahashi's spectrum, there is a spike below 0.2 MeV. In the GAMINT code spectrum this spike is absent, a direct result of internal conversion competition. Around 0.3 MeV the spectrum drops very abruptly. This absence of gamma rays in the 0.3 MeV region is due to the lack of transitions that allow for the selection rule criteria for energy transition of 0.2 to 0.3 MeV. The preponderance of the low energy gamma rays emitted from the excited ^{239}U nucleus are emitted in the lower lying discrete level transitions.

The GAMINT code predicts a much lower gamma ray intensity in the 0 to 1.0 MeV region and a higher gamma ray intensity in the 1.0 to 1.5 MeV region than does Takahashi. The spectrum predicted by the GAMINT code is depressed at lower energies, as expected, because of the strong competition from internal conversion. Internal conversion was not considered in the Takahashi calculation.

The transitions in the continuum region contribute to a large peak in the 1.2

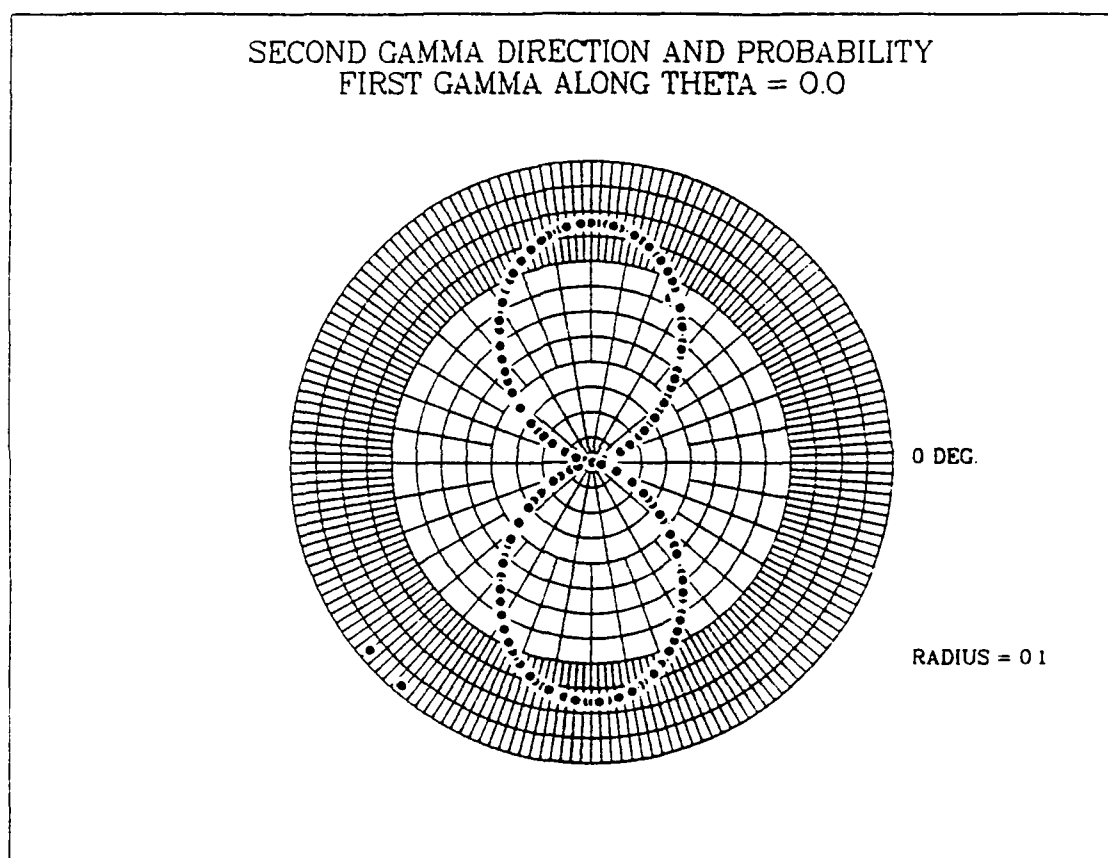


Figure 5.12: Angular distribution of second gamma relative to first gamma.

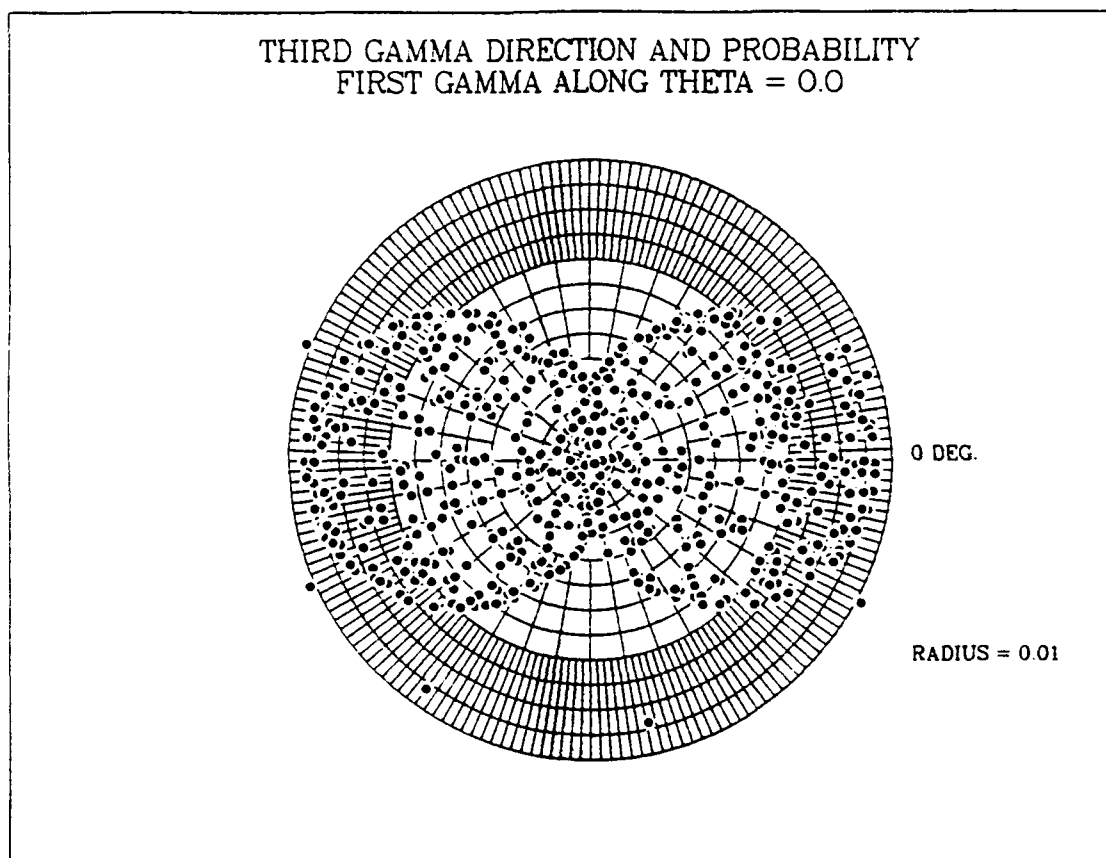


Figure 5.13: Angular distribution of third gamma relative to first gamma.

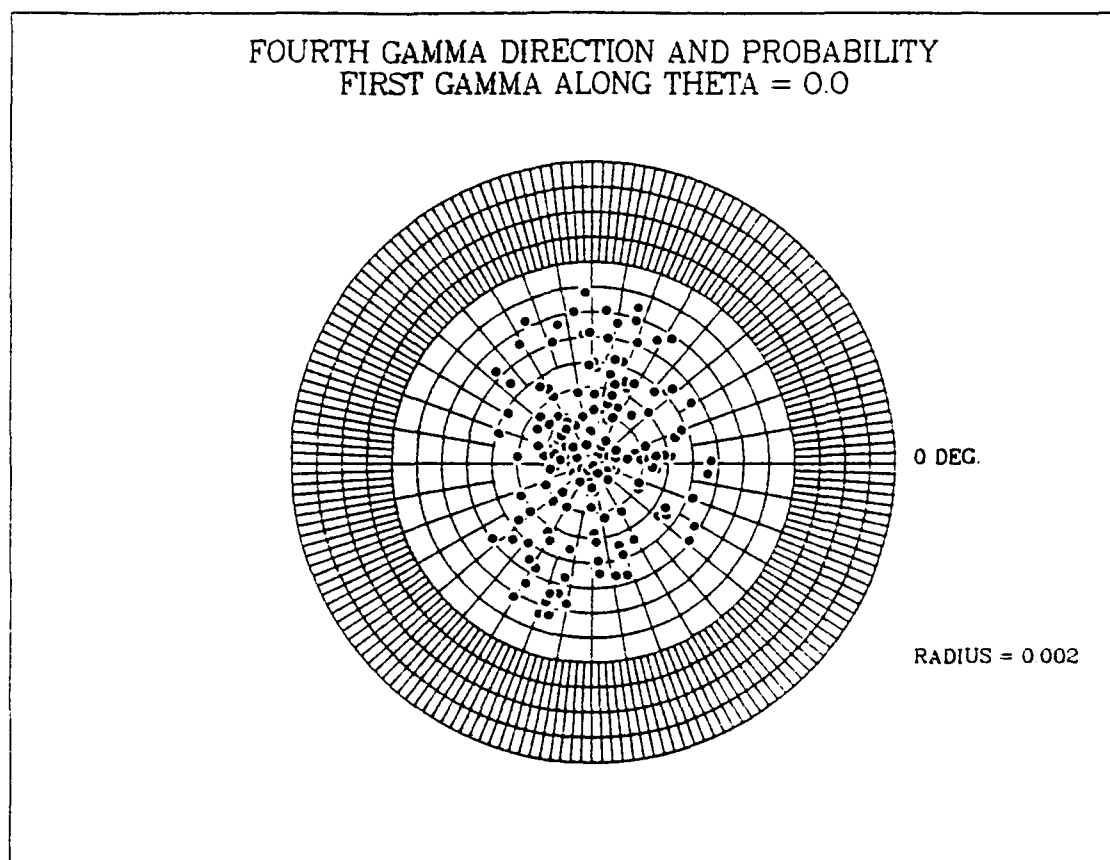


Figure 5.14: Angular distribution of fourth gamma relative to first gamma.

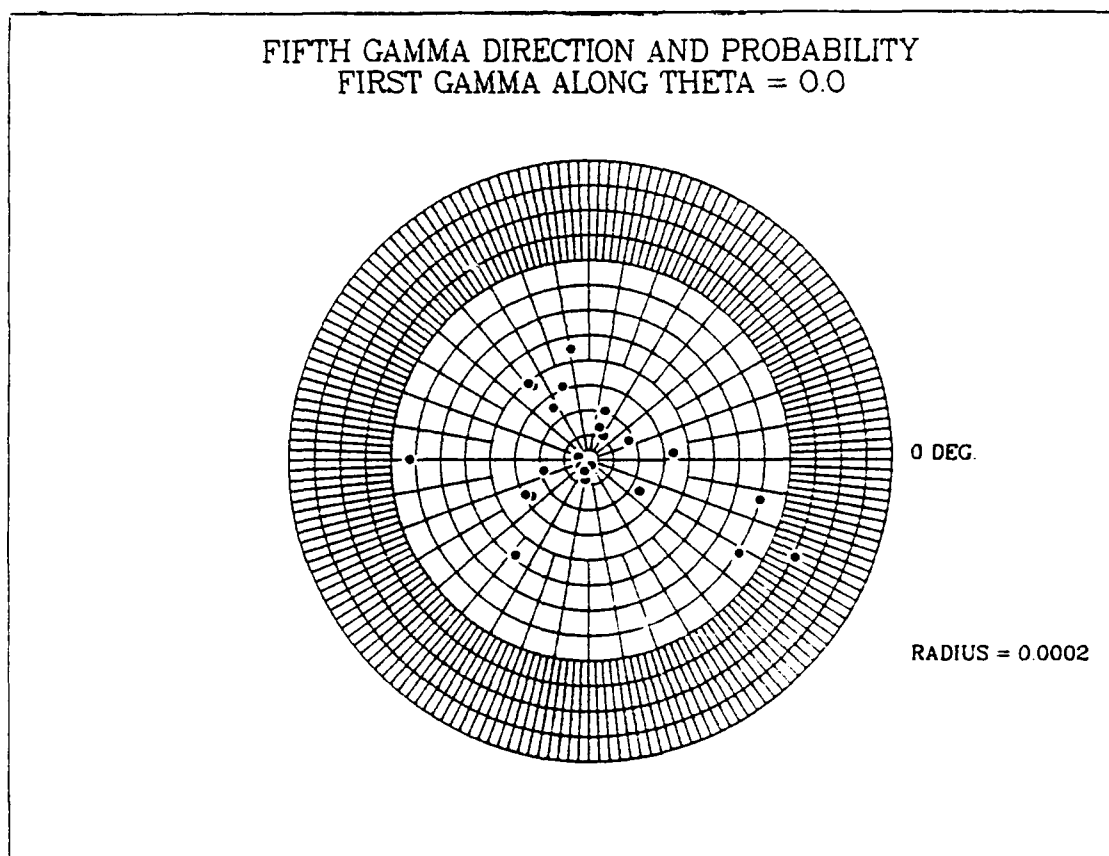


Figure 5.15: Angular distribution of fifth gamma relative to first gamma.

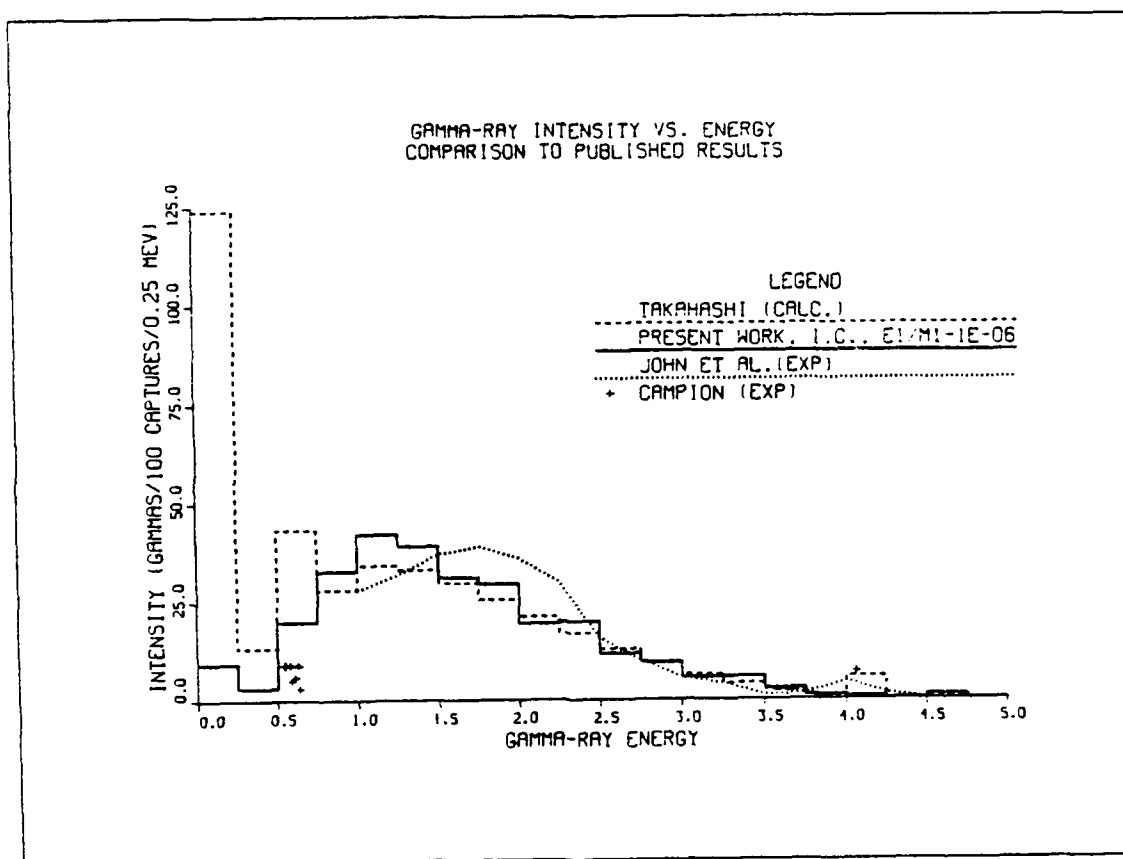


Figure 5.16: Comparison to published results.

MeV region. In both calculated spectra, the peak of the gamma ray spectrum is shifted to lower energies than the experimentally determined spectrum of John et al. The effect of the single particle model on the average energy of the spectrum is to shift it to lower energy, since the model only considers vibrational spectra and neglects the rotational spectra found in the actual nucleus. The collective motion, in the form of vibration and rotation, in a large nuclei such as ^{239}U will lead to a gamma rays of higher average energy, due to the larger transitions in the rotational bands. [36]

CHAPTER 6

SIMULATION OF CAPTURE TANK RESPONSE USING MICROSHIELD

Neutron transmission and self-indication ratio measurements have been performed [2] for $^{238}\text{U}(n, \gamma)$ at the Rensselaer Polytechnic Institute Linear Accelerator and recently elsewhere [3] [4] in order to determine resonance self-shielding. A preliminary analysis of the data of Byoun et al. [5] by Harris et al. [6] examined the capture tank efficiencies for average s-wave and p-wave neutron capture. The self-indication ratio depends on the gamma cascade multiplicities, as well as average spectra, however. Because the capture tank responds to the combined effect of the gamma rays of various energies from a cascade, as transported through intervening material, the cascade structure has a profound effect on the response. This work for the first time analyzes the multiple gammas in the individual cascades, the transport, and the resulting energy deposition in the capture tank. The GAMINT Code (gamma cascade model) was developed to simulate the deexcitation of the excited ^{239}U nucleus provides the gamma source for this transport model. The GAMINT Code predicts the energy and order of emission of each gamma in a cascade. This is important in the study of the energy deposition for the individual cascades, since the percentage of gamma-ray energy reaching the capture tank is highly dependent on the energy of the individual gamma rays in the cascade. Therefore the cascade makeup will have a profound effect on the energy deposited by the individual cascades.

6.1 Introduction to the Microshield Program

The Microshield Program [37] was used to perform gamma transport calculations between the capture sample and the capture tank. This program was selected because of its incorporation of buildup factors, its capability to include user defined

materials, and its capability to define energy groups for the gamma-ray source spectrum. This particular version of Microshield operates on an IBM personal computer.

Shield materials determine the radiation attenuation and buildup characteristics for the Microshield calculation of the dose rate at a chosen point. Materials are specified for each of the shield regions for the particular geometry selected. The Microshield program provides a listing of built-in materials, or the user may create a custom material for each of the shield regions. The custom materials may be entered by selecting one of the built in materials and entering a default density, or by entering a default name, default density, and the number of atoms of each element in the material.

The buildup factors which may be selected are Taylor formulation, geometric progression, Berger formulation, or no buildup. The buildup factor corrects for the contribution of photon scattering at the dose point. In the Microshield program, the buildup factor for each differential source volume is calculated during the kernel integration. Values of the line-of-sight distance between the source kernel and the dose point, are calculated for each new source point. The attenuation mean free paths are determined and used for the build up factor calculation. This shielding mean free path is used for all of the materials between the source and the dose point. Interpolation for energy is done for the buildup formula calculations. A linear interpolation scheme is used for the Taylor and Berger correlations, and a logarithmic interpolation is used for the geometric progression method.

For mixed materials and several shields, the combined attenuation exponent is determined by the relationship:

$$\mu r = \sum_{k=1}^{shields} t_k \times \sum_{i=1}^{materials} [(\mu/\rho)_i * \rho_i], \quad (6.1)$$

where:

- μr = number of shielding mean free paths.

- $(\mu/\rho)_i$ = energy dependent mass attenuation coefficient of material i in shield k .
- ρ_i = density of material i in shield k .
- t_k = thickness of shield k between source and dose point.

Microshield looks up values for mass attenuation coefficients by material type, interpolates for energy, multiplies by the individual material density, and sums to obtain the linear attenuation coefficient for each of the shield regions. The linear attenuation coefficients are then multiplied by the path length through each shield and summed over all shields.

The custom material densities are determined by an atomic weight ratio for the atoms of a particular species within the custom material.

$$\rho_i = \rho_{bulk} * \frac{N_i * A_i}{\sum_i N_i * A_i}, \quad (6.2)$$

where the bulk density is the density for the overall custom material, N_i is the number density of the i^{th} species, and A_i is the atomic weight of the i^{th} species.

The effective atomic weights (EAW_i) of the custom materials is the total molecular weight divided by the number of atoms.

$$EAW_i = \frac{\sum_i N_i * A_i}{\sum_i N_i}. \quad (6.3)$$

The mass attenuation coefficient for the custom material is the sum of the density-weighted individual species.

$$\mu/\rho = \sum_i [(\mu/\rho)_i * (\rho_i/\rho_{bulk})]. \quad (6.4)$$

The effective atomic number is used for the interpolation of buildup factors. Microshield uses an effective atomic number for the custom materials.

$$EAN_{custom} = \frac{\sum_i \frac{\rho_i * Z_i}{A_i}}{\sum_i \frac{\rho_i}{A_i}}, \quad (6.5)$$

where Z_i is the atomic number of the atoms of species i . For mixed materials, the effective atomic number is determined by:

$$EAN_{mixed} = \frac{\sum_i \frac{d_i \cdot EAN_i}{EAW_i}}{\sum_i \frac{d_i}{EAW_i}}, \quad (6.6)$$

where d_i is the density of material in shield i , and the subscript i refers to the mixed materials. [37]

6.2 Description of the Physical System

The physical system modelled in this analysis consists of a 1.25 m. diameter capture tank filled with a xylene based scintillator. A neutron-beam tube in the tank contains the capture sample which is a 0.0792 cm. thick, 7.8 cm. diameter disk of ^{238}U . Surrounding the capture sample is a 4.95 cm. thick annulus of ^6LiH and the beam tube wall.

6.3 Microshield Model

In order to simplify the geometry for the physical set up described above, the cylindrical geometry has been converted to a spherical geometry by equating the chord length of the cylinder (\bar{c}_{cyl}) to that of the sphere (\bar{c}_{sphere}). This will give equivalent results in the Monte Carlo transport through the two geometries. [38]

$$\bar{c}_{cyl} = \bar{c}_{sphere}. \quad (6.7)$$

For a cylinder of diameter d and thickness t , the mean chord length may be written as:

$$\bar{c}_{cyl} = \frac{4 * \frac{\pi}{4} * d^2 * t}{2 * \frac{\pi}{4} * d^2}. \quad (6.8)$$

This expression simplifies to

$$\bar{c}_{cyl} = 2 * t. \quad (6.9)$$

For a sphere of diameter d , the mean chord length is the radius. Therefore the equivalent cylinder may be approximated as a sphere with a radius equal to twice the thickness of the cylinder.

For this Microshield work, four cases are analyzed. The cases considered are

- Off-resonant capture without internal conversion
- Resonant capture without internal conversion
- Off-resonant capture with internal conversion
- Resonant capture with internal conversion

Setup 1: In the off-resonant neutron capture case, the captures are uniformly distributed throughout the cylinder. This cylinder has a thickness of 0.0790 cm. Therefore the equivalent sphere has a radius of 0.1584 cm. The gamma rays originate uniformly throughout the sphere.

Setup 2: In the resonant neutron capture case, the captures occur primarily in the front face of the cylinder, since there is a high probability for capture. The equivalent sphere is made to be the same size as in setup 1, however, in order to model this situation on Microshield, the following procedure is performed. First the gammas emitted into the disk from the active region of the face are considered. In this case the active source region is made much smaller and located in the center of the sphere. The surrounding material is also U^{238} and this is equivalent to the inactive region of the cylinder. In addition, the gammas emitted away from the face are modelled by a small sphere. The surrounding material is replaced by a vacuum in order to maintain the model integrity. The two answers are added, resulting in a description of the resonant capture case.

6.4 Results of the Microshield Model

Table 6.1 shows the probabilities of transport of gammas of various energies from capture sample to capture tank for the case of resonant capture. Table 6.2 shows the probabilities of transport of gammas for the case of off-resonant capture. Note that lower energy gamma rays are not likely to reach the capture tank. Internal conversion diminishes the low energy gamma yield and results in a total gamma energy which differs from cascade to cascade.

Figure 6.1 displays a plot for the case of resonant capture without internal conversion for 100 representative cascades. Since no internal conversion is considered in this case, the total available gamma energy for each cascade is 4.803 MeV. The mean gamma energy deposited by a cascade in the capture tank is 3.17 MeV.

Figure 6.2 displays a plot for the case of off-resonant capture without internal conversion. As in the previous case, no internal conversion is considered so the total available gamma energy for each cascade is 4.803 MeV. The mean gamma energy deposited by a cascade in the capture tank is 3.08 MeV.

Figure 6.3 displays a plot for the case of resonant capture with internal conversion. Since internal conversion is considered, the total available gamma energy for each cascade is less than 4.803 MeV. For the 100 representative gamma cascades, the average available energy is 4.56 MeV. The mean gamma energy deposited in the capture tank is 3.15 MeV.

Figure 6.4 displays a plot for the case of off-resonant capture with internal conversion. As in the previous case, the total available gamma energy for each cascade is less than 4.803 MeV. For this case the average available energy per gamma cascade is also 4.56 MeV. The mean gamma energy deposited in the capture tank is 3.07 MeV.

Table 6.3 displays the average energy that reached the tank for a cascade for the cases considered. It is shown in this analysis that for either the resonant or the

Table 6.1: Probability of transport of gammas of various energies from capture sample to capture tank for resonant capture

Group Number	Mean Energy (MeV)	Probability of Gamma Reaching Capture Tank
1	4.875	0.80
2	4.625	0.79
3	4.375	0.79
4	4.125	0.78
5	3.875	0.78
6	3.625	0.77
7	3.375	0.76
8	3.125	0.75
9	2.875	0.74
10	2.625	0.73
11	2.375	0.72
12	2.125	0.72
13	1.875	0.71
14	1.625	0.69
15	1.375	0.67
16	1.125	0.63
17	0.875	0.59
18	0.625	0.51
19	0.375	0.39
20	0.125	0.16

Table 6.2: Probability of transport of gammas of various energies from capture sample to capture tank for off-resonant capture

Group Number	Mean Energy (MeV)	Probability of Gamma Reaching Capture Tank
1	4.875	0.78
2	4.625	0.78
3	4.375	0.77
4	4.125	0.76
5	3.875	0.76
6	3.625	0.75
7	3.375	0.74
8	3.125	0.73
9	2.875	0.73
10	2.625	0.72
11	2.375	0.71
12	2.125	0.70
13	1.875	0.69
14	1.625	0.67
15	1.375	0.65
16	1.125	0.61
17	0.875	0.57
18	0.625	0.49
19	0.375	0.35
20	0.125	0.10

Table 6.3: Energy Deposited in Tank by a Cascade

	Resonant	Off-resonant
No I.C.	3.17	3.08
With I.C.	3.15	3.07

off-resonant case, the average amount of energy reaching the tank is only slightly different between internal conversion and the no internal conversion cascades. There is a larger difference between the resonant and off-resonant cases if one considers either the internal conversion case or the no internal conversion case. The off-resonant case has a greater amount of uranium to transport through, since the capture is uniformly distributed throughout the disk. The result is a slight decrease in the net amount of energy reaching the tank. The cases in which internal conversion is considered have fewer low energy gamma rays to start with than the cases in which no internal conversion is considered. However, this difference has less effect on the energy deposited in the tank than does the position of the capture in the disk.

The spectra of the cascade energy reaching the tank for the cases considered are shown in Figure 6.5 through Figure 6.8.

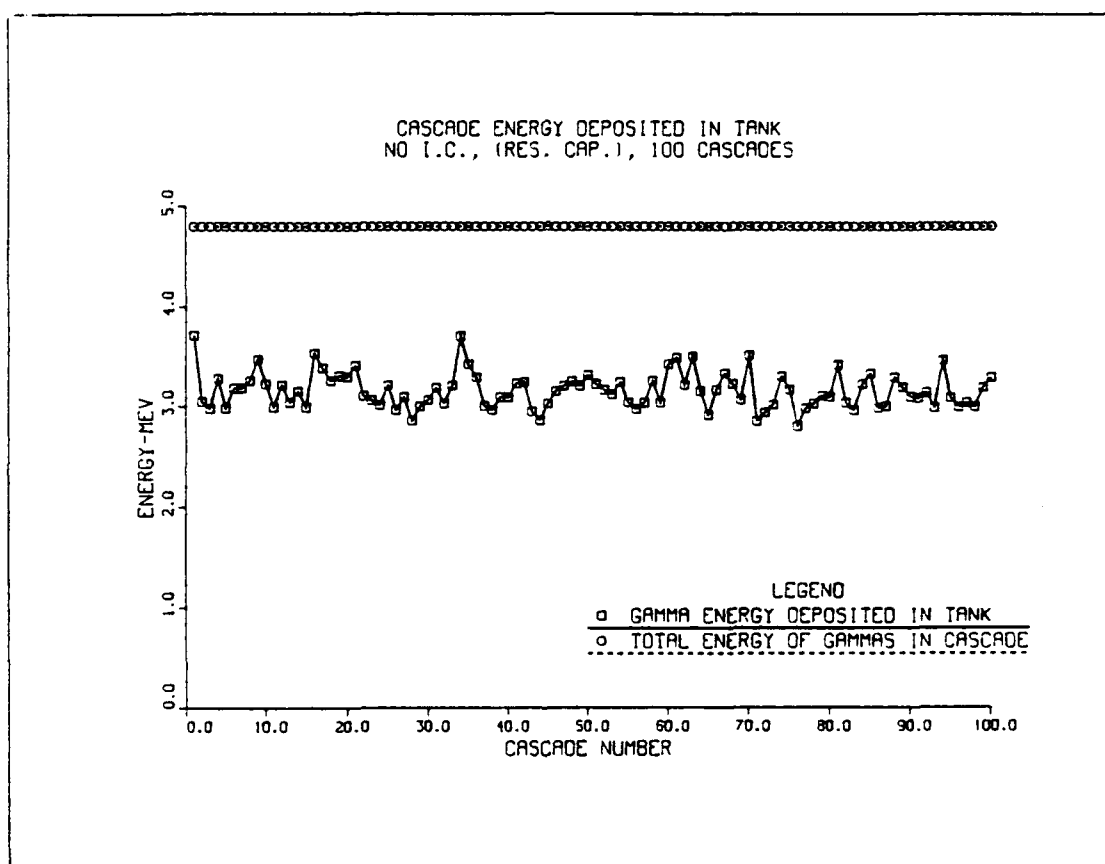


Figure 6.1: Total gamma cascade energy deposited in capture tank for 100 representative cascades (resonant capture, no internal conversion)

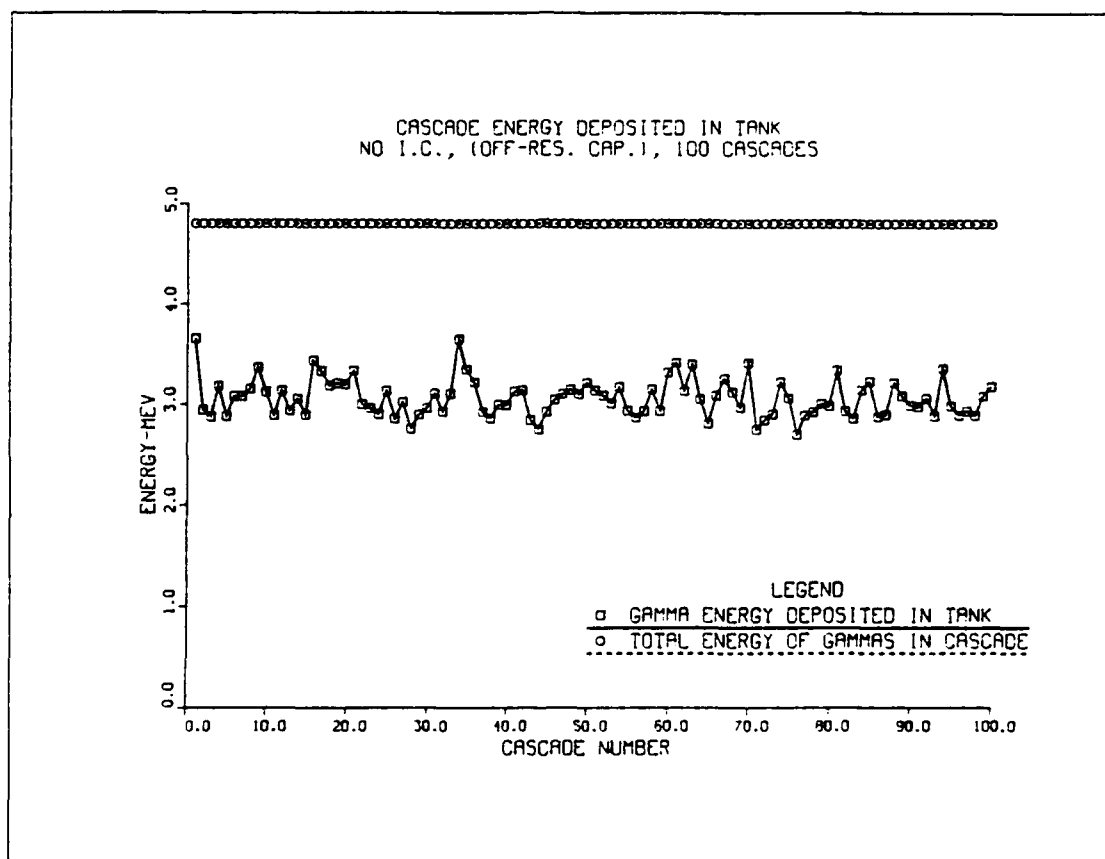


Figure 6.2: Total gamma cascade energy deposited in capture tank for 100 representative cascades (off-resonant capture, no internal conversion)

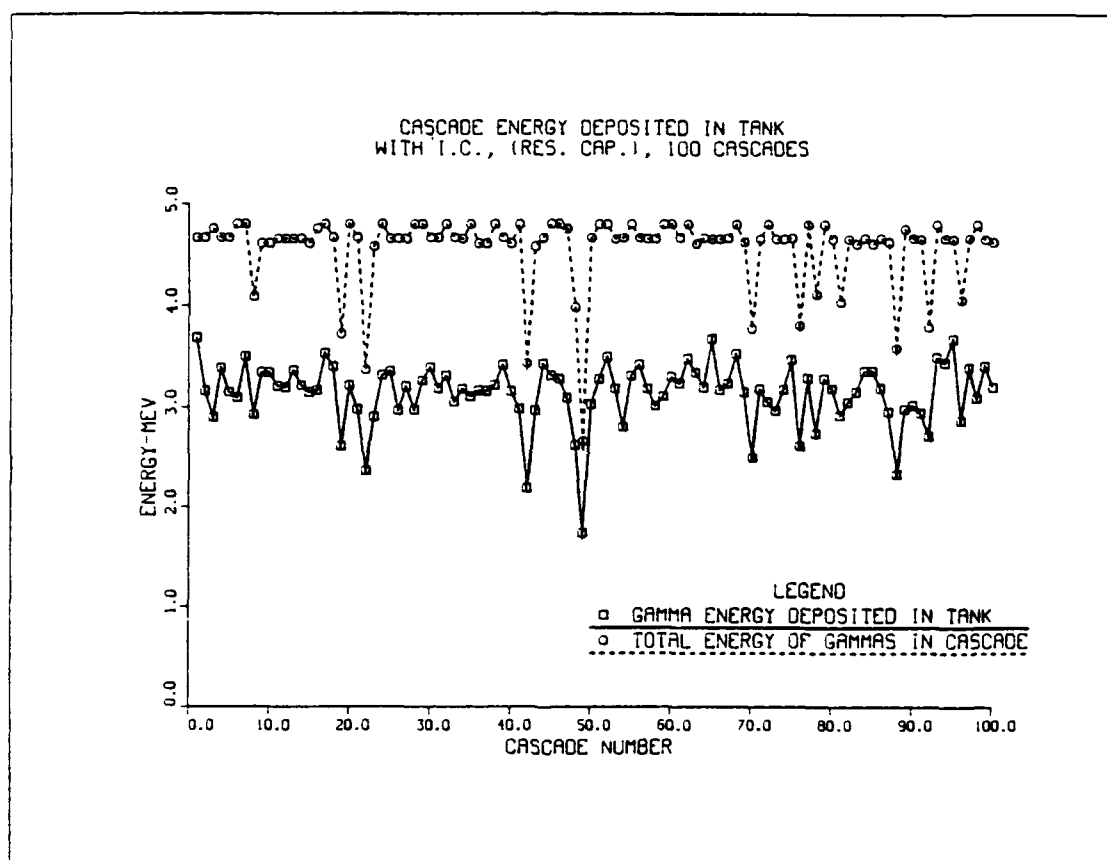


Figure 6.3: Total gamma cascade energy deposited in capture tank for 100 representative cascades (resonant capture, internal conversion)

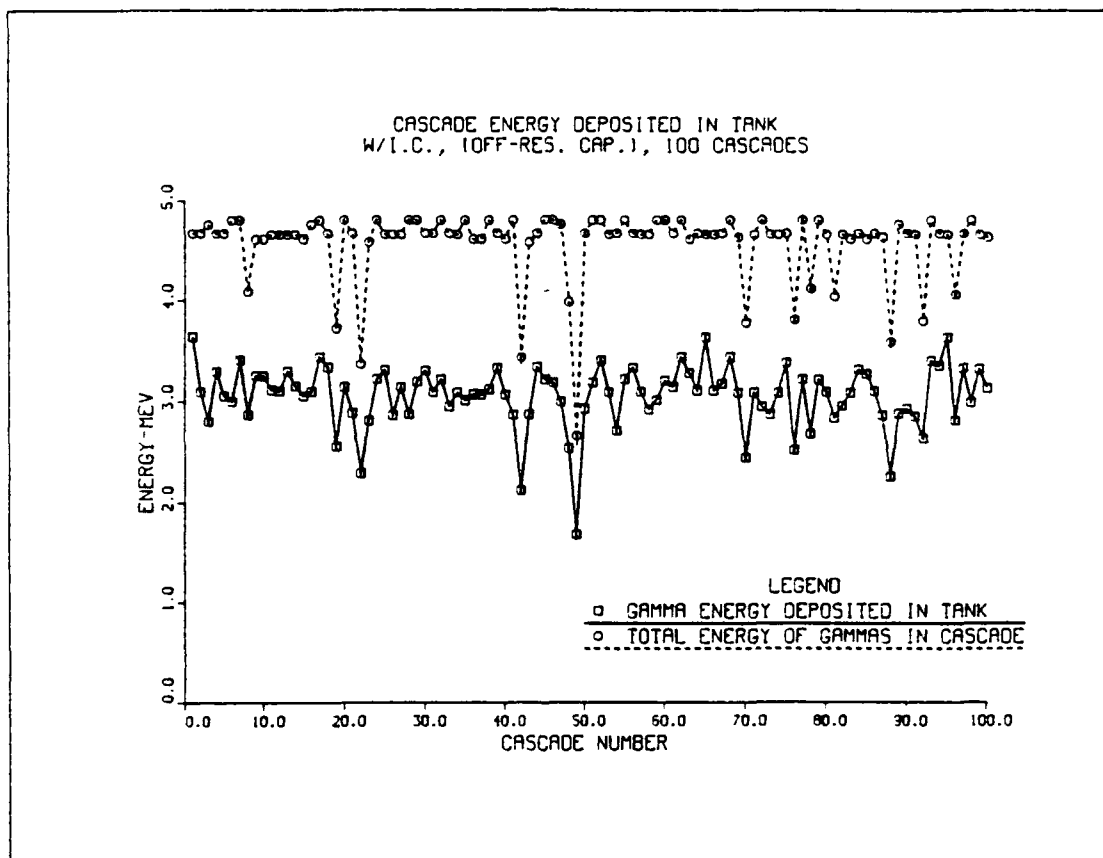


Figure 6.4: Total gamma cascade energy deposited in capture tank for 100 representative cascades (off-resonant capture, internal conversion)

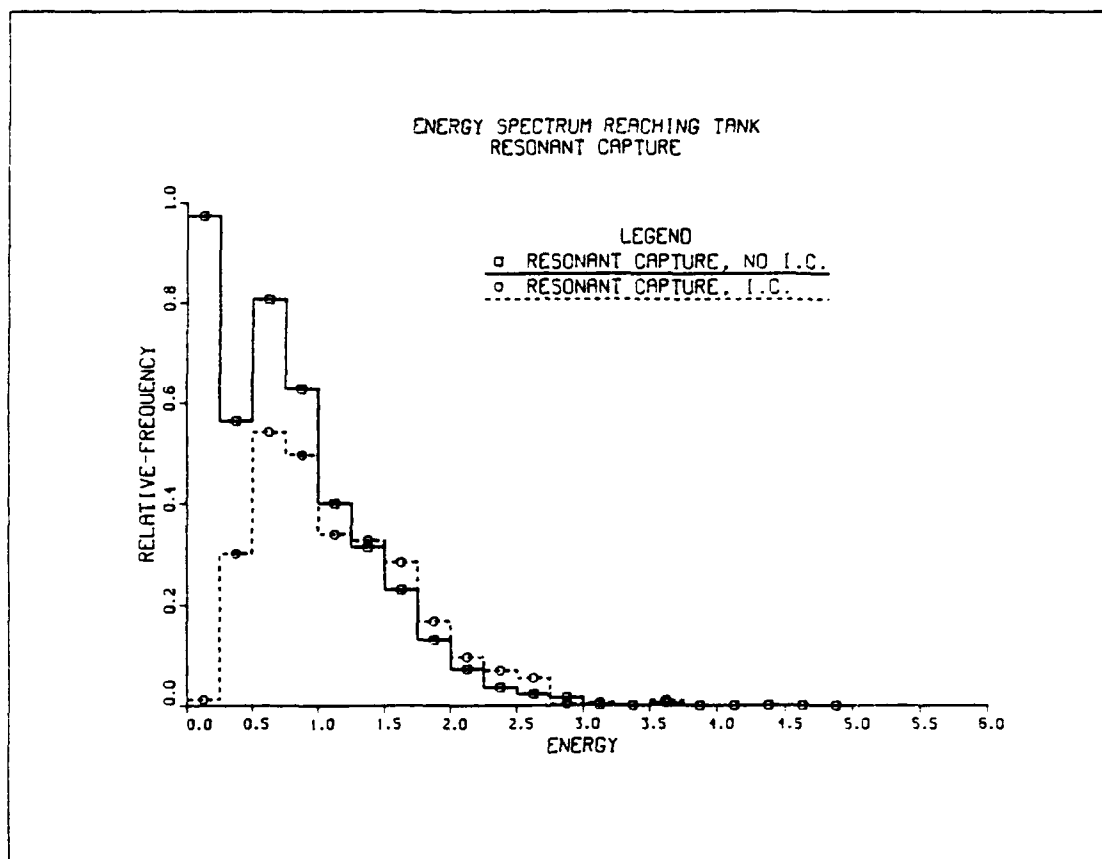


Figure 6.5: Spectrum of cascade gamma energy deposited in capture tank (resonant capture)

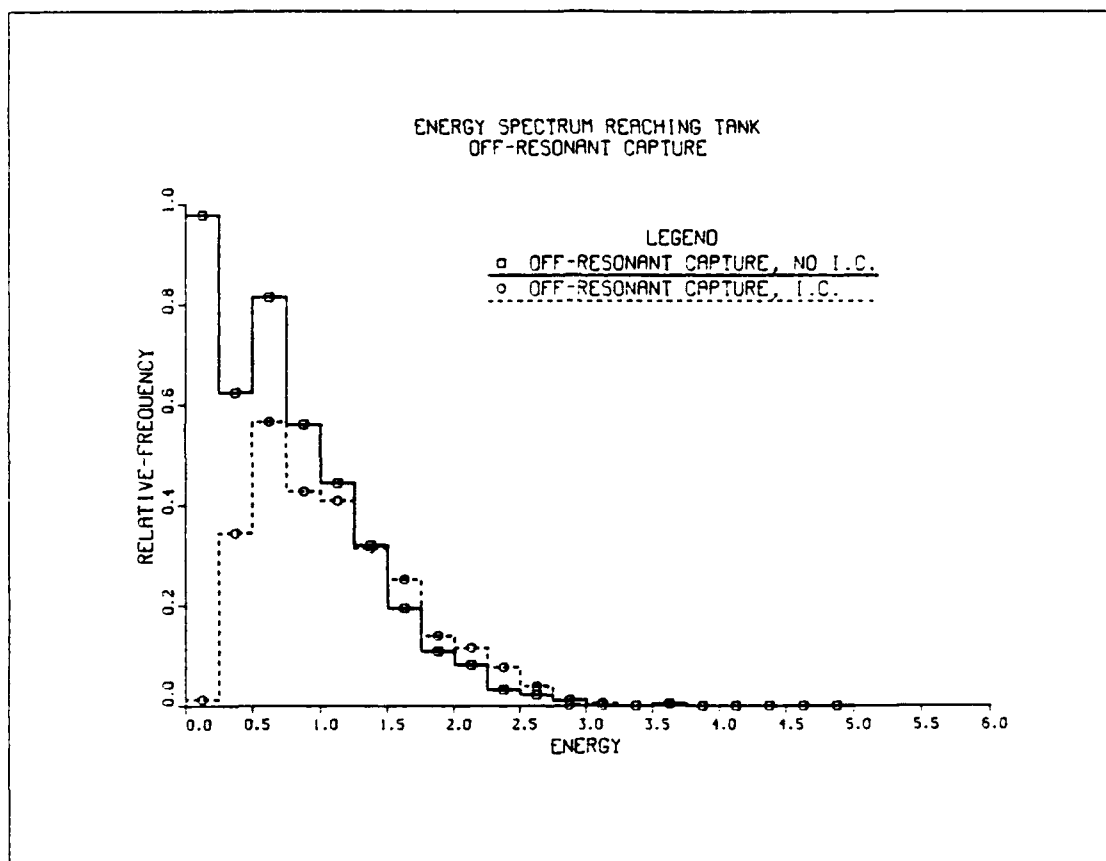


Figure 6.6: Spectrum of cascade gamma energy deposited in capture tank (off-resonant capture)

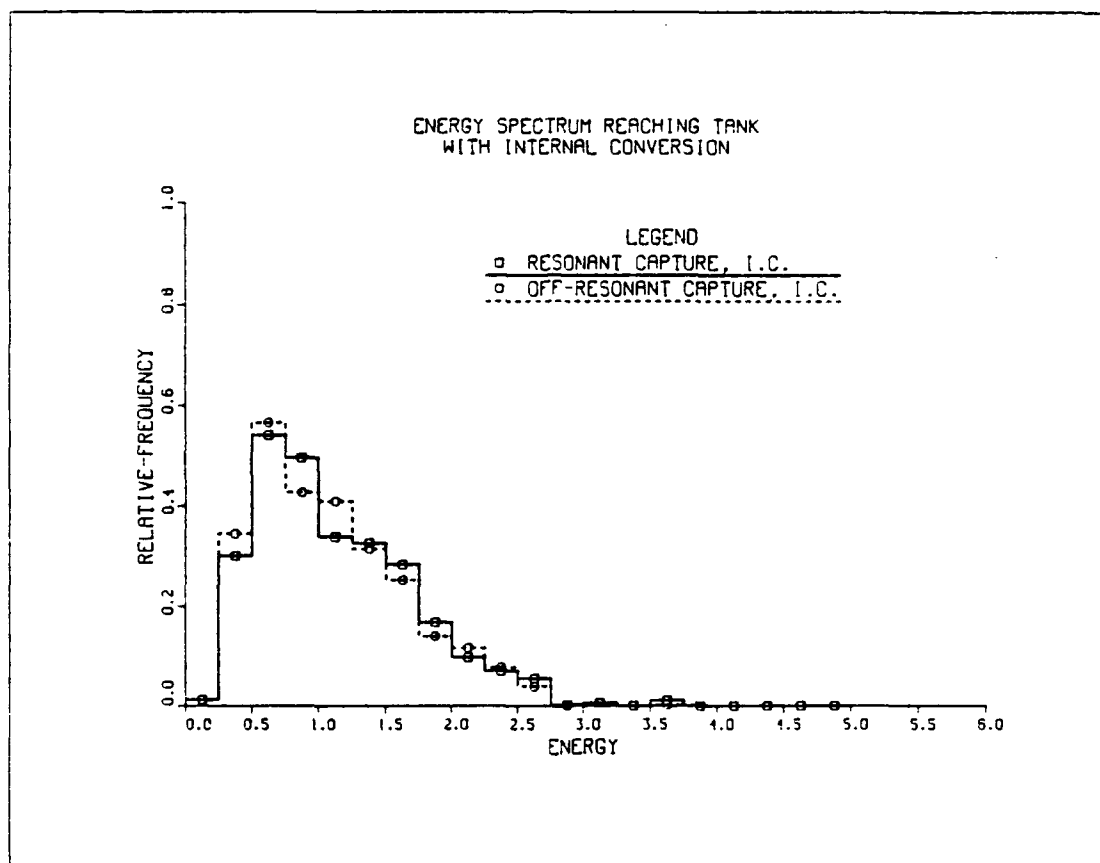


Figure 6.7: Spectrum of cascade gamma energy deposited in capture tank (internal conversion)

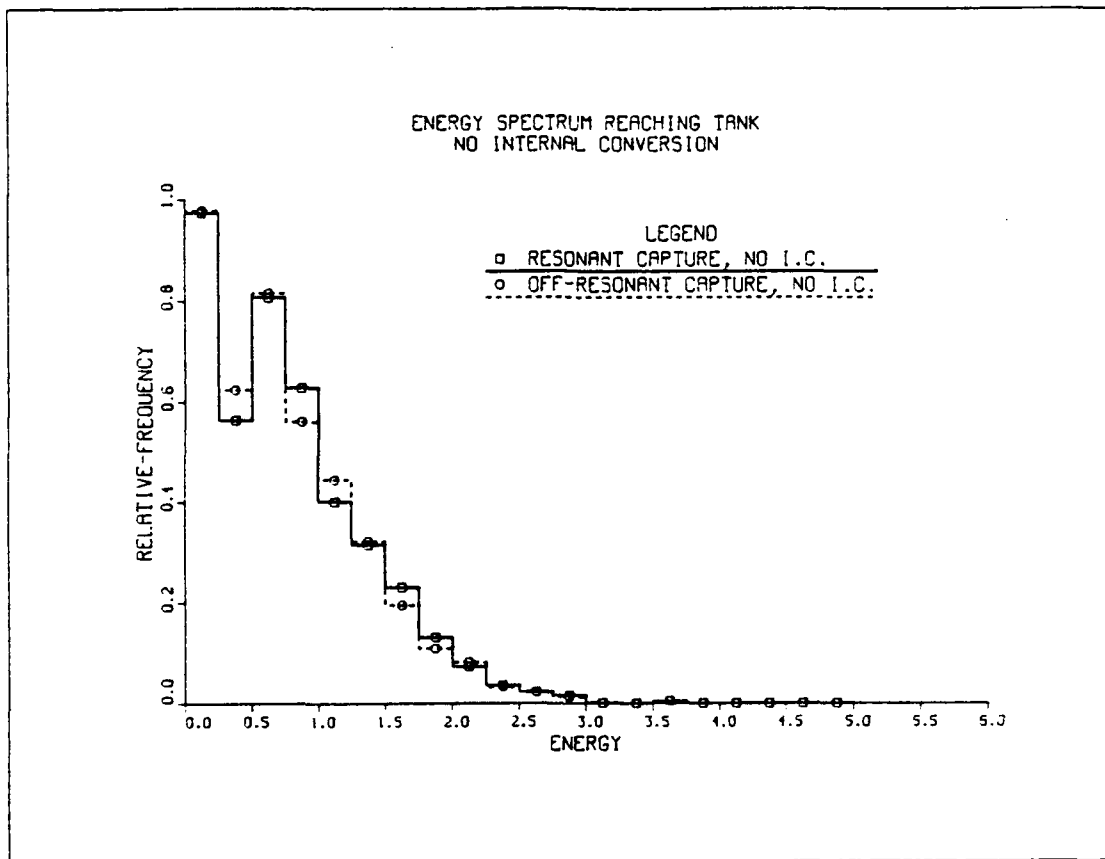


Figure 6.8: Spectrum of cascade gamma energy deposited in capture tank (no internal conversion)

CHAPTER 7

DISCUSSION AND CONCLUSION

The work done in this thesis is the development of a gamma ray cascade code for the $^{238}\text{U}(n,\gamma)^{239}\text{U}$ reaction for the determination of the response of a capture tank to gamma ray cascades. The results of this thesis may be extended to capture tanks other than the one used at Rensselaer Polytechnic Institute, as well as other neutron capture detectors [39]. In this work, the following has been accomplished.

(1) A gamma cascade model has been created which predicts the energy of the gamma rays emitted in a cascade, the order of emission of the gamma rays in a cascade, the multipolarity of the transitions in the decay of the ^{239}U nucleus, the multiplicity of the gamma rays in each cascade, the angular distribution of the gamma rays relative to the first emitted gamma ray, and predicts the spectrum of neutron capture reactions in ^{238}U excited up to the yrast level.

(2) For the first time, the effect of internal conversion on the gamma cascade energy has been analyzed in a cascade simulation and applied to an applications problem. Internal conversion dominates the low energy portion of the spectrum, affecting the number of low energy gamma rays emitted from the source. The gross structure of the spectrum determined in this work agrees well with other calculated and experimental spectra. However, due to the inclusion of internal conversion, the low energy gamma transitions are significantly diminished in the present work. The low energy gamma rays are favorably attenuated in the transport of the source spectrum through the material in a capture tank. It is found that the energy deposition in the tank is not contingent on whether or not internal conversion is considered at the source.

(3) The response of the capture tank used in experiments at Rensselaer has been analyzed. The cases examined are resonant capture with and without internal

conversion, and off-resonant capture with and without internal conversion. As discussed above, the internal conversion had negligible effect on the average cascade energy deposited in the tank. The off-resonant capture occurs randomly in the capture sample, and due to self-shielding, the energy deposition in the tank was slightly lower than for resonant capture. In the resonant capture case, the gamma rays originate near the face of the capture sample, decreasing the amount of self-shielding in the sample. The source spectrum for s-wave and p-wave neutrons was compared and found to be virtually the same. Therefore the position of the capture reaction in the sample has more effect on the energy deposited in the capture tank than the other factors examined.

(4) The methodology and the findings of this work are also relevant to any capture tank or other gamma-ray detectors. By using the results of the gamma-ray cascade transport calculations, one may determine an optimum discriminator level by maximizing the number of cascades which have an energy exceeding the discriminator setting. This will result in more light collection for a given number of captures.

In order to determine if the single particle model is an acceptable model to use in describing the decay of the excited ^{239}U nucleus, one must know how deformed the nucleus is. Examination of the Nilsson diagram for ^{239}U shows that the nucleus is only slightly deformed, and therefore the single particle model gives an acceptable prediction of the gamma decay of this nucleus. However, because rotational bands are actually present, the single particle model will predict an average gamma-ray energy lower than the collective model and this is seen in the shifting of the calculated spectrum to lower energy. A gamma cascade code based on the collective model is only possible if the level spacings, with the rotational bands included, are known. This is not the case, so further experimental and theoretical work in determining the collective model level spacings would allow for a more accurate cascade model.

Future work on this gamma cascade simulation should also incorporate particle emission for those excitation energies above the yrast level. Further improvements may be made by expanding the number of nuclides which may be examined.

LITERATURE CITED

- [1] B. Schwartzschild, "A New Generation of Gamma Detectors for Nuclear Physics", *Physics Today*, p.21, (1991).
- [2] T.Y. Byoun, PhD Thesis, Rensselaer Polytechnic Institute, (1973).
- [3] M.V. Bokovko, V.N. Kononov, G.N. Manturov, E.D. Poletaev, V.V. Sinita, and A.A. Voevodskij, INDC(CCP)-322/L, (1988).
- [4] H.Oigawa, Y. Fujita, K. Kobayashi, S. Yamamoto, and I. Kimura, "Self-Shielding Factors for Neutron Capture Reactions of Uranium-238 and Thorium-232 in Energy Range of 1-35 KeV", *Journal of Nuclear Science and Technology*, 28[10], 8799, (1991).
- [5] T.Y. Byoun, R.C. Block, and T. Semler, "Temperature-Dependent Transmission and Self-Indication Measurements Upon Depleted U in the Unresolved Region", *Kiamesha Lake Conference - 72091*, p.1115, (1973).
- [6] D.R.Harris, R.C.Block, R.N.Hwang, "Analysis of U-238 Self-Indication Experiments", *Nuclear Data for Basic and Applied Science*, Santa Fe, (1985).
- [7] R.S. Booth, J.E. White, S.K. Penny, and K.J. Yost, *Nuclear Science and Engineering*, 47, p.8, (1972).
- [8] H. Takahashi, *Nuclear Science and Engineering*, 51, p.296, (1973).
- [9] N. Yamamuro, K. Udagawa, and T. Natsume, "Calculation of Capture Cross Sections and Gamma-Ray Spectra following the Interaction of Neutrons with Ta-181 and Au-197", Unpublished Paper.
- [10] P.J. Champion, J.W. Knowles, G. Manning, and G.A. Bartholomew, *Canadian Journal of Physics*, 37, p.377, (1959).
- [11] J. John and V.J. Orphan, "Gamma Rays From Resonant Capture of Neutrons in U-238", GA-10186, Gulf General Atomic, (1970).
- [12] K.J. Yost, *Nuclear Science and Engineering*, 32, p.62, (1968).
- [13] K.J. Yost, P.H. Pitkanen, and C.Y. Fu, *Nuclear Science and Engineering*, 39, p.379, (1970).
- [14] J.R.Stehn, M.D. Goldberg, R. Wiener-Chasman, S.F. Mughabghab, B.A. Magurno, and V.M. May, BNL-325, 2nd. ed., Suppl. 2, Brookhaven National Laboratory, (1965).

- [15] L.V. Gorshev and G.A. Bartholomew, Nuclear Data Tables, A5, (1969).
- [16] R.K. Sheline, W.N. Shelton, T. Udagawa, E.T. Journey, and H.T. Motz, Physical Review, 151, p.1011, (1966).
- [17] J. Blatt, and V. Weisskopf, Theoretical Nuclear Physics, Springer-Verlag, New York, (1952).
- [18] K.J. Yost, J.E. White, and C.Y. Fu, Transactions of the American Nuclear Society, 13, p.866, (1970).
- [19] B.B. Kinsey, G.A. Bartholomew, Canadian Journal of Physics, 31, p.537, (1953).
- [20] J. John, V.J. Orphan, C.G. Hoot, Transactions of the American Nuclear Society, 13, p.865, (1970).
- [21] R. Evans, The Atomic Nucleus, Krieger Publishing Company, Malabar, (1955).
- [22] G. Friedlander, J.W. Kennedy, E.S. Macias, and J.M. Miller, Nuclear and Radiochemistry, John Wiley and Sons, New York, (1981).
- [23] H.A. Bethe, "An Attempt to Calculate the Number of Energy Levels of a Heavy Nucleus", Physical Review, 50, p.332, (1936).
- [24] A. Gilbert and A. G. W. Cameron, "A Composite Nuclear Level Density Formula With Shell Corrections", Canadian Journal of Physics, 43, p.1446, (1965).
- [25] W. Dilg, W. Schantl, and H. Vonach, "Level Density Parameters for the Back-Shifted Fermi Gas Model in the Mass Range $40 < A < 250$ ", Nuclear Physics, A217, p.269, (1973).
- [26] H. Vonach, and M. Graves, Nuclear Physics, A127, p.289, (1969).
- [27] J.M.B. Lang, and K.J. Le Couteur, "Statistics of Nuclear Levels", Proceedings of the Physical Society, A67, p.586, (1954).
- [28] D.R. Harris, unpublished work.
- [29] W. Meyerhof, Elements of Nuclear Physics, McGraw-Hill Book Company, New York, (1967).
- [30] D.R. Harris, Lecture Notes, Applied Atomic and Nuclear Physics I, Rensselaer Polytechnic Institute, Troy, New York, (1989).
- [31] R.S. Hager, and E.C. Seltzer, Internal Conversion Coefficients, Academic Press, New York, (1973).

- [32] S. Wong, Introductory Nuclear Physics, Prentice Hall, Englewood Cliffs, (1990).
- [33] D.H. Wilkinson, Nuclear Spectroscopy, ed. F. Ajzenberg-Selove, New York, Academic Press, (1960).
- [34] M. Preston, Physics of the Nucleus, Addison-Wesley Publishing Company, Reading, (1962).
- [35] D.L. Price, R.E. Chrien, O.A. Wasson, M.R. Bhat, M. Beer, M.A. Lone, and R. Graves, Nuclear Physics, A121, p.630, (1968).
- [36] I.L. Preiss, private communication, (Apr. 1992).
- [37] Microshield Version 3, Grove Engineering, Rockville, (1987).
- [38] D.R. Harris, private communication, (Dec. 1991).
- [39] R.C. Block, P.J. Marano, N.J. Drindak, F. Feiner, K.W. Seeman, and R.E. Slovacek, "A Multiplicity Detector for Accurate Low Energy Capture Measurement", Nuclear Data for Science and Technology, MITO, p.383, (1988).
- [40] R.C. Block, D.R. Harris, S.H. Kim, K. Kobayashi, U-238 Resonance Self-Indication Capture Measurements and Analysis, EPRI NP-996, (Feb. 1979).
- [41] E. Fermi, Nuclear Physics, University of Chicago, (1949).
- [42] F.H. Frohner, "Evaluation of the Unresolved Resonance Range of U-238", Nuclear Science and Engineering, 103, p.119, (1989).
- [43] D.R. Harris, R.C. Block, S.H. Kim, K. Kobayashi, "Uranium-238 Resonance Self-Indication Capture Measurements", Nuclear Science and Engineering, 80, p.263, (1982).
- [44] M. Preston, and R. Bhaduri, Structure of the Nucleus, Addison-Wesley Publishing Company, Reading, (1975).
- [45] M.E. Rose, Internal Conversion Coefficients, North Holland Publishing Company, Amsterdam, (1958).
- [46] M.E. Rose, L.C. Biedenharn, and G.B. Arfken, "Internal Conversion Angular Correlations", Physical Review, 85, p.5, (1955).
- [47] M.E. Rose, G.H. Goertzel, and B.I. Spinrad, "The Internal Conversion Coefficients, I: The K-Shell", Physical Review, 83, p. 79, (1951).
- [48] E. Segré, Experimental Nuclear Physics, John Wiley and Sons, Inc., New York, (1964).

APPENDIX A

GAMINT SOURCE CODE

```

C      PROGRAM GAMINT3 (INPUT,OUTPUT)
C *GAMINT COMPUTES GAMMA ENERGY SPECTRUM AND MULTIPLICITY
C FROM NUCLEAR DEEXCITATION WITH INTERNAL CONVERSION
C INCLUDED.
C ALSO COMPUTES PULSE HEIGHT DISTRIBUTION IN A CAPTURE TANK.
C
C
      REAL E1(3),E2(3),AL(3,2,4,23),ALV(3),ALT,CG(40),CI(40)
      1,TJ(20),PV(3,2,25),PT(3,2,40,1000),SG(40),EO(1000,10)
      2,VJ(30),VP(30),VE(30),EG(40),DP(20),SL(3),CD
      3,RP(2),AW,AE,SJ,GE,HF(3,2),RL(3),PS(50),PF(5),SA(40)
      4,PE(3,2,25),TT(3,2,25),PC(3,2,40,1000),GN(10,40)
      5,TU(3,2,40,1000),SE(40),SB(40),ETM(3),TL(1000,10)
      6,TP(1000,10),EINT(40),EINTN(40),ETS(1000),PGE(40)
      7,TH(1000),ETH(1000),TG(1000,40),TI(1000,40),CM(40,2,3)
      INTEGER NS,IP,IC,NA,NP,NV(3),NG,NVD,II
      COMMON/PASS/TJ,PV,PT,SG,EO
      1,E1,E2,NS,IP,IL,IC,NA,AL,NP,ETT,ALV,ALT,CG,CI
      2,VJ,VP,VE,EG,DP,SL,NG,NV,CD,NVD
      3,RP,AW,AE,SJ,GE,HF,RL,PS,PF,SA
      4,PE,TT,PC,GN,II,PGE
      5,TU,SE,SB,ETM,TL,TP
      6,EINT,EINTN,ETS,TH,ETH,TG,TI,CM
      DIMENSION RN(10)
      DOUBLE PRECISION DSEED

```

C DATA

```

      READ (5,10) TJ
      WRITE(6,20) TJ

      READ (5,12) NL,NC,NE,NJ
      WRITE(6,22) NL,NC,NE,NJ

      READ (5,11) XE,XJ,XP

      SEED =7.0

      DSEED=SEED

      WRITE(6,21) XE,XJ,XP,SEED

```

C DETERMINE WEISSKOPF FACTORS FOR ELECTRIC (1) AND MAGNETIC (2)

C DIPOLES

```

      RP(1)=1.

      RP(2)=1./(4.364*AW**(.666667))

```

C DETERMINE TRANSITION FACTORS FOR 2*IL POLE

```

      DO 80 IL=1,NL

      RL(IL)=SL(IL)*(AW**(.666667*IL))*(1.82307E21)/

      1(164.443**(2*IL+1))

      80 CONTINUE

```

C DATA OUTPUT

```

      WRITE(6,21) AW,AE,SJ,GE,CD

      WRITE(6,22) NG,NVD

      WRITE(6,21) (EG(IG),IG=1,NG)

      WRITE(6,21) (DP(IG),IG=1,NG)

      WRITE(6,21) (SL(IL),IL=1,NL)

      WRITE(6,21) (RL(IL),IL=1,NL)

      WRITE(6,21) (RP(IP),IP=1,2)

      DO 82 IP=1,2

      82 WRITE(6,21) (HF(IL,IP),IL=1,NL)

      DO 90 IV=1,NVD

```



```
90 WRITE(6,21) VJ(IV),VP(IV),VE(IV)
```

```
WRITE(6,21) (PF(IU),IU=1,5)
```

```
WRITE(6,26)
```

```
C INITIALIZE
```

```
LA=1111
```

```
LB=2222
```

```
LC=3333
```

```
LD=4444
```

```
LE=5555
```

```
ZA=1.1111111
```

```
ZB=2.2222222
```

```
ZC=3.3333333
```

```
ZD=4.4444444
```

```
ZE=5.5555555
```

```
I1=0
```

```
I2=0
```

```
GNX=0.0
```

```
SJ=SJ*SJ*2.
```

```
PGE(21)=.80
```

```
PGE(22)=.79
```

```
PGE(23)=.79
```

```
PGE(24)=.78
```

```
PGE(25)=.78
```

```
PGE(26)=.77
```

```
PGE(27)=.76
```

```
PGE(28)=.75
```

```
PGE(29)=.74
```

```
PGE(30)=.73
```

```
PGE(31)=.72
```

```
PGE(32)=.72
PGE(33)=.71
PGE(34)=.69
PGE(35)=.67
PGE(36)=.63
PGE(37)=.59
PGE(38)=.51
PGE(39)=.39
PGE(40)=.16
DO 92 I=1,20
92 PGE(I)=0.0
DO 96 INT=1,NG
IGT=NG-INT+1
EINT(IGT)=0.0
EINTN(IGT)=0.0
96 CONTINUE
DO 97 IC=1,NC
ETH(IC)=0.0
TH(IC)=0.0
DO 97 IG=1,NG
97 TG(IC,IG)=0.0
DO 100 IG=1,NG
CG(IG)=0.0
CI(IG)=0.0
SE(IG)=0.0
SG(IG)=0.0
DO 100 II=1,10
100 GN(II,IG)=0.0
DO 101 ID=1,50
```

```
101 PS(ID)=0.
    DO 103 IC=1,NC
    DO 103 II=1,10
    TL(IC,II)=0.0
    TP(IC,II)=0.0
103 EO(IC,II)=0.0
    EF=0.
    DO 98 IPT=1,2
    DO 98 ILT=1,NL
    DO 98 IGT=1,NG
    98 CM(IGT,IPT,ILT)=0.0

C CASCADES
    DO 160 IC=1,NC
    II=1
    CE=XE
    CJ=XJ
    CP=XP
    IT=0
    ED=0.

C COMPUTE RATES. WEISSKOPF RATES WITH HINDRANCE FACTORS HF
112 T1=0.
    DO 140 IL=1,NL
    DO 140 IP=1,2

C TRANSITION RATES TO DISCRETE LEVELS
    DO 110 IV=1,NVD
    PV(IL,IP,IV)=0.
    PE(IL,IP,IV)=0.
    ALT=0.0
    ETT=0.0
```

```

      TT(IL,IP,IV)=0.
      IF(CE.LE.VE(IV)) GO TO 107
      IF(CP*(-1.)*(IP+IL+1).NE.VP(IV)) GO TO 107
      I1=ABS(CJ-VJ(IV))
      I2=CJ+VJ(IV)
102  IF(IL.EQ.I1) GO TO 104
      I1=I1+1
      IF(I1.GT.I2) GO TO 107
      GO TO 102
104  PV(IL,IP,IV)=RP(IP)*RL(IL)*(CE-VE(IV))**(2*IL+1)
      PV(IL,IP,IV)=PV(IL,IP,IV)*HF(IL,IP)
      IF(IL.EQ.1) PV(IL,IP,IV)=PV(IL,IP,IV)*(CE-VE(IV))
C      WRITE(6,510)IL,IP,IV,PV(IL,IP,IV)
C 510  FORMAT(1H ,4HIL =,I4,2X,4HIP =,I4,2X,4HIV =,I4,2X,
C      14HPV =,E12.5)
C      COMPUTE THE INTERNAL CONVERSION COEFFICIENTS
C      INITIALIZE THE VALUE OF THE TOTAL ICC.
C      THE VALUE FOR NS WILL BE LOOPEED FROM 1 TO 3, THE NUMBER
C      OF ATOMIC SHELLS FOR CONVERSION (I.E. K,L,M)
      DO 415 NS=1,3
      NP=1
      ETT=(CE-VE(IV))*1000.0
      IF(ETT.EQ.0.0)GO TO 107
C      WRITE(6,413)IL,NS,ETT
C 413  FORMAT(1H ,5HIL = ,I4,3X,8HSHELL = ,I4,3X,7HT.E. = ,E12.5)
C      NV(NS) IS THE NUMBER OF VALUES IN TABLE FOR A GIVEN NS,IP,IL.
      NA=NV(NS)
      ALV(NS)=0.0
      CALL FIT

```

```

      IF(ALV(NS).LT.O.)GO TO 415
      ALT=ALT+ALV(NS)
C      IF(IC.GT.3)GO TO 415
C      WRITE(6,414)IP,IL,NS,ETT,ALV(NS)
C 414 FORMAT(1H ,2(I3,1X),4HNS =,I3,2X,4HE =
C      1,E12.5,3X,6HICC = ,E12.5)
      GO TO 415
C 417 WRITE(6,418)ETT
C 418 FORMAT(1H ,2X,4HE = ,E12.5,1X,4HMEV ,5X,12HOUT OF RANGE)
      415 CONTINUE
C      WRITE(6,419)ETT,ALT
C 419 FORMAT(1H ,2X,4HE = ,E12.5,1X,4HMEV ,5X,12HICC TOTAL = ,E12.5)
C COMPUTE THE TRANSITION PROBABILITY FOR AN
C INTERNAL CONVERSION EVENT.
      410 PE(IL,IP,IV)=PV(IL,IP,IV)*ALT
C COMPUTE THE TOTAL TRANSITION PROBABILITY (SUM THE
C GAMMA AND THE ICC PROBABILITIES).
      TT(IL,IP,IV)=PV(IL,IP,IV)+PE(IL,IP,IV)
C ACCUMULATE THE TOTAL TRANSITION PROBABILITY
      T1=T1+TT(IL,IP,IV)
      107 CONTINUE
C      IF(IC.EQ.1) WRITE(6,511) IL,IP,IV,I1,I2,LA
C 511 FORMAT(1H ,4HIL =,I4,2X,4HIP =,I4,2X,4HIV =I4,2X,
C      14HI1 =,I4,2X,4HI2 =,I4,5X,I4)
C      IF(IC.EQ.1) WRITE(6,512) PV(IL,IP,IV),PE(IL,IP,IV),
C      1ALT,TT(IL,IP,IV),T1
C 512 FORMAT(1H ,4HPV =,E12.5,2X,4HPE =,E12.5,2X,5HALT =,
C      1E12.5,
C      12X,4HTT =,E12.5,2X,4HT1 =,E12.5)

```

```

110 CONTINUE
C CONTINUUM LEVELS
C TRANSITION RATES TO CONTINUUM LEVELS

DO 120 IE=1,NE
DO 120 IJ=1,NJ
PT(IL,IP,IJ,IE)=0.
PC(IL,IP,IJ,IE)=0.
ALT=0.0
ETT=0.0
TU(IL,IP,IJ,IE)=0.
IF(CE.LE.CD) GO TO 128
DE=(CE-CD)/NE
EE=CD+(IE-.5)*DE
RJ=IJ-.5
I1=ABS(CJ-RJ)
I2=CJ+RJ
122 IF(IL.EQ.I1) GO TO 124
I1=I1+1
IF(I1.GT.I2) GO TO 128
GO TO 122
124 PT(IL,IP,IJ,IE)=RP(IP)*RL(IL)*(CE-EE)**(2.*IL+1)
1*DE*(2.*RJ+1.)*EXP(-RJ*(RJ+1)/SJ)
2*.00010091*EXP(9.7494*SQRT(EE+.58))/(EE+.58)**1.86000
PT(IL,IP,IJ,IE)=PT(IL,IP,IJ,IE)*HF(IL,IP)
IF(IL.EQ.1) PT(IL,IP,IJ,IE)=PT(IL,IP,IJ,IE)*(CE-EE)
C WRITE(6,520)IL,IP,IJ,IE,PT(IL,IP,IJ,IE)
C 520 FORMAT(1H ,4HIL =,I4,2X,4HIP =,I4,2X,4HIJ =,I4,2X,
C 14HIE =,I4,2X,4HPT =,E12.5)
C COMPUTE THE INTERNAL CONVERSION COEFFICIENTS

```

```

C INITIALIZE THE VALUE OF THE TOTAL ICC.
C THE VALUE FOR NS WILL BE LOOPEO FROM 1 TO 3, THE NUMBER
C OF ATOMIC SHELLS FOR CONVERSION (I.E. K,L,M)

      DO 15 NS=1,3
      NP=1
      ETT=ABS((CE-EE))*1000.0
      IF(ETT.EQ.0.0)GO TO 15
C      WRITE(6,13)IL,NS,ETT
C 13 FORMAT(1H ,5HIL = ,I4,3X,8HSHELL = ,I4,3X,7HT.E. = ,E12.5)
C NV(NS) IS THE NUMBER OF VALUES IN TABLE FOR A GIVEN NS,IP,IL.
      NA=NV(NS)
      ALV(NS)=0.0

      CALL FIT
      IF(ALV(NS).LT.0.)GO TO 15
      ALT=ALT+ALV(NS)
C      IF(IC.GT.3)GO TO 15
C      WRITE(6,14)IP,IL,NS,ETT,ALV(NS)
C 14 FORMAT(1H ,2(I3,1X),4HNS =,I3,2X,4HE =
C      1,E12.5,3X,6HICC = ,E12.5)
      GO TO 15
C 17 WRITE(6,18)ETT
C 18 FORMAT(1H ,2X,4HE = ,E12.5,1X,4HMEV ,5X,12HOUT OF RANGE)
      15 CONTINUE
C      WRITE(6,19)ETT,ALT
C 19 FORMAT(1H ,2X,4HE = ,E12.5,1X,4HMEV ,5X,12HICC TOTAL = ,E12.5)
C COMPUTE THE TRANSITION PROBABILITY FOR AN
C INTERNAL CONVERSION EVENT.
      PC(IL,IP,IJ,IE)=PT(IL,IP,IJ,IE)*ALT
C      WRITE(6,530)ALT,PT(IL,IP,IJ,IE),PC(IL,IP,IJ,IE)

```

```

C 530 FORMAT(1H ,SHALT =,E12.5,2X,4HPT =,E12.5,2X,4HPC
C      1=,E12.5)
C COMPUTE THE TOTAL TRANSITION PROBABILITY (SUM THE
C GAMMA AND THE ICC PROBABILITIES).
      TU(IL,IP,IJ,IE)=PT(IL,IP,IJ,IE)+PC(IL,IP,IJ,IE)
C ACCUMULATE THE TOTAL TRANSITION PROBABILITY
      T1=T1+TU(IL,IP,IJ,IE)
128 CONTINUE
C      IF(IC.EQ.1) WRITE(6,22) IL,IP,IE,IJ,I1,I2,LB
C      IF(IC.EQ.1) WRITE(6,21) PT(IL,IP,IJ,IE),PC(IL,IP,IJ,IE),
C      1ALT,TU(IL,IP,IJ,IE),T1
120 CONTINUE
140 CONTINUE
C NORMALIZE AND SELECT TRANSITION
C T1 IS SUM OF RATES. T2 IS CUMULATIVE PROBABILITY
      CALL GGUBS(DSEED,1,RN)
      T2=0.
      DO 150 IL=1,NL
      DO 150 IP=1,2
      DO 152 IV=1,NVD
      TT(IL,IP,IV)=TT(IL,IP,IV)/T1
      T2=T2+TT(IL,IP,IV)
C      WRITE(6,540)TT(IL,IP,IV),T1,T2,RN(1),IL,IP,IV
C 540 FORMAT(4HTT =,E12.5,2X,4HT1 =,E12.5,2X,4HT2 =,E12.5,2X,
C      17HRN(1) =,E12.4,3X,3(I4,2X))
      IF(RN(1).LT.T2) GO TO 164
152 CONTINUE
      DO 154 IE=1,NE
      DO 154 IJ=1,NJ

```



```

      TU(IL,IP,IJ,IE)=TU(IL,IP,IJ,IE)/T1
      T2=T2+TU(IL,IP,IJ,IE)
C      WRITE(6,541)TU(IL,IP,IJ,IE),T1,T2,RN(1),IL,IP,IJ,IE
C 541  FORMAT(4HTU =,E12.5,2X,4HT1 =,E12.5,2X,4HT2 =,E12.5,2X,
C      17HRN(1) =,E12.5,3X,4(I4,2X))
      IF(RN(1).LE.T2) GO TO 162
154  CONTINUE
150  CONTINUE
C  TRANSITION TO DISCRETE LEVEL
164  ET=CE-VE(IV)
      IT=IT+1
      CE=VE(IV)
      CJ=VJ(IV)
      CP=VP(IV)
C  COMPUTE PROBABILITY OF GAMMA TRANSITION GIVEN
C  A TRANSITION OCCURS.
      IF(TT(IL,IP,IV).EQ.0.) GO TO 220
      PG=PV(IL,IP,IV)/(PV(IL,IP,IV)+PE(IL,IP,IV))
C  COMPUTE PROBABILITY OF INTERNAL CONVERSION
C  GIVEN A TRANSITION OCCURS.
      PI=PE(IL,IP,IV)/(PV(IL,IP,IV)+PE(IL,IP,IV))
C      IF(IC.GT.5)GO TO 222
C      WRITE(6,550)RN(1),PG,PI,IL,IP,IV
C 550  FORMAT(1H ,E12.5,1X,4HPG =,E12.5,2X,4HPI
C      1=,E12.5,3X,3(I4,2X))
      GO TO 222
220  PG=0.
      PI=0.
222  CALL GGUBS(DSEED,1,RN)

```

```

C      IF(IC.EQ.1) WRITE(6,22) IC,IT,IL,IP,IV,LC
C      IF(IC.EQ.1) WRITE(6,21) ET,CE,CJ,CP
C      IF(IC.EQ.1) WRITE(6,21) PV(IL,IP,IV),PE(IL,IP,IV),
C      1TT(IL,IP,IV)
C      IF(IC.EQ.1) WRITE(6,21) PG,PI,RN(1)
C      IF(PG.GT.RN(1)) GO TO 165
C      IZ=2
C      GO TO 166
165 IZ=1
C      GO TO 166
C TRANSITION TO CONTINUUM LEVEL
162 ET=CE-(CD+(IE-.5)*DE)
C      IT=IT+1
C      CE=CE-ET
C      CJ=IJ-.5
C      CP=CP*(-1.)**(IP+IL+1)
C COMPUTE PROBABILITY OF GAMMA TRANSITION GIVEN
C A TRANSITION OCCURS.
C      IF(TU(IL,IP,IJ,IE).EQ.0.)GO TO 320
C      PH=PT(IL,IP,IJ,IE)/(PT(IL,IP,IJ,IE)+PC(IL,IP,IJ,IE))
C COMPUTE PROBABILITY OF INTERNAL CONVERSION
C GIVEN A TRANSITION OCCURS.
C      PJ=PC(IL,IP,IJ,IE)/(PT(IL,IP,IJ,IE)+PC(IL,IP,IJ,IE))
C      IF(1C.GT.5)GO TO 330
C      WRITE(6,560)RN(1),PH,PJ,IL,IP,IJ,IE
C 560 FORMAT(1H ,E12.5,1X,4HPH =,E12.5,2X,4HPJ
C      1=,E12.5,3X,4(I4,2X))
C      GO TO 330
320 PH=0.

```

```

      PJ=0.
330 CALL GGUBS(DSEED,1,RN)
C     IF(IC.LE.10) WRITE(6,21) PH,PJ,RN(1),ZA
      IF(PH.GT.RN(1)) GO TO 161
      IZ=2
      GO TO 169
161 IZ=1
169 IF(IC.EQ.1) WRITE(6,22) IC,IT,IL,IP,IJ,IE,LD
C     IF(IC.EQ.1) WRITE(6,21) ET,CE,CJ,CP
C     IF(IC.EQ.1) WRITE(6,21) PT(IL,IP,IJ,IE),PC(IL,IP,IJ,IE),
C     1TU(IL,IP,IJ,IE)
C     IF(IC.EQ.1) WRITE(6,21) PH,PJ,RN(1)
C     IF(IC.EQ.1) WRITE(6,22) IZ
166 CONTINUE
C TALLIES
C DETERMINE THE ENERGY GROUP OF THE TRANSITION.
      DO 170 I1=1,NG
      IG=NG-I1+1
C     WRITE(6,570)I1,IG,ET,EG(IG)
C 570 FORMAT(1H ,4HI1 =,I4,2X,4HIG =,I4,2X,4HET =,E12.5,2X,
C     14HEG =,E12.5)
      IF (ET.LT.EG(IG)) GO TO 172
170 CONTINUE
      IG=1
C SEPERATE THE GAMMA TRANSITIONS FROM THE INTERNAL
C CONVERSION TRANSITIONS.
172 IF(IZ.EQ.2) GO TO 176
      SG(IG)=SG(IG)+1.
      EO(IC,I1)=ET

```

```

      TL(IC,II)=IL
      TP(IC,II)=IP
C SUM THE GAMMAS FOR EACH INDIVIDUAL MULTIPOLARITY
      CM(IG,IP,IL)=CM(IG,IP,IL)+1.0
C DETERMINE THE TOTAL GAMMA ENERGY FOR EACH BIN
      IF(IZ.EQ.2) GO TO 184
      DO 182 INT=1,NG
      IGT=NG-INT+1
      IF(ET.LE.EG(IGT)) GO TO 183
182 CONTINUE
183 EINT(IGT)=EINT(IGT)+ET
      ETS(IC)=ETS(IC)+EO(IC,II)
      ETH(IC)=ETH(IC)+EO(IC,II)*PGE(IG)
      WRITE(6,333)IG,EO(IC,II),PGE(IG)
333 FORMAT(1H ,4HIG =,I4,2X,4HEO =,E12.5,2X,5HPGE =,E12.5)
184 CONTINUE
      CG(IG)=CG(IG)+1.
      TG(IC,IG)=TG(IC,IG)+1
      GN(II,IG)=GN(II,IG)+1
      II=II+1
      TET=TET+ET
C   WRITE(6,900)IZ,IG,SG(IG),SE(IG),ET,TET
      GO TO 177
176 SE(IG)=SE(IG)+1.
      CI(IG)=CI(IG)+1.
      TI(IC,IG)=TI(IC,IG)+1
      TET=TET+ET
C   WRITE(6,900)IZ,IG,SG(IG),SE(IG),ET,TET
C 900 FORMAT(1H ,4HIZ =,I4,2X,4HIG =,I4,2X,4HSG =,E12.5,2X

```

```

C      1,4HSE =,E12.5,2X
C      2,19HTRANSITION ENERGY =,E12.5,2X,14HTOTAL ENERGY =,E12.5)
      GO TO 199
177 CALL GGUBS(DSEED,2,RN)
      EU=ET-ET*ET/24.
      DU=EU/5.
      DO 171 IU=1,5
      IF(RN(1).LT.PF(IU)) GO TO 173
171 CONTINUE
      IU=5
173 EH=DU*(IU-1)+RN(2)*DU
      EH=EH*(.95+.006*ET)
      CR=DP(IG)
      IF(ET.GT.1.01) CR=CR+.0215*(1.-1./ET)
      EH=EH*CR
      ED=ED+EH
      IF(IC.LE.100) WRITE(6,27) IC,ED,ET,EU,EH,ZB
199 IF(CE.GT.VE(1)) GO TO 112
C END CASCADE AT GROUND STATE
      DO 174 ID=1,25
      IF(ED.LT..2*ID) GO TO 175
174 CONTINUE
      ID=25
175 PS(ID)=PS(ID)+1.
      EF=EF+ED
160 CONTINUE
C DETERMINE THE ORDER OF GAMMAS EMITTED
C      DO 724 II=1,10
C      DO 724 I3=1,NG

```

```

C      IG=NG-I3+1
C      GNX=GNX+GN(II,IG)
C      WRITE(6,726)II,IG,GN(II,IG),GNX
C 726 FORMAT(1H ,15HORDER OF GAMMA:,1X,I4,2X,
C      16HGROUP:,1X,I4,2X,17HNUMBER OF
C      1GAMMAS:,E12.5,4X,E12.5)
C 724 CONTINUE
      DO 728 II=1,7
      DO 728 I4=1,NG
      IG=NG-I4+1
      GN(II,IG)=GN(II,IG)/NC
      WRITE(6,727)II,EG(IG),GN(II,IG)
727 FORMAT(1H ,I4,2X,E12.5,2X,E12.5)
728 CONTINUE
C PRINT OUT THE GAMMAS EMITTED IN GIVEN CASCADE
      DO 820 IC=1,NC
      WRITE(6,826)IC
826 FORMAT(I4)
      DO 820 II=1,7
      WRITE(6,827)II,E0(IC,II),TP(IC,II),TL(IC,II)
827 FORMAT(I4,2X,E12.5,2X,E12.5,2X,E12.5)
820 CONTINUE
C PRINT OUT THE FRACTION OF GAMMA ENERGY IN EACH BIN
      DO 284 INT=1,NG
      IGT=NG-INT+1
      EINTN(IGT)=EINT(IGT)/TET
284 WRITE(6,901)IGT,EINTN(IGT),EG(IGT)
901 FORMAT(I4,2X,E12.5,2X,E12.5)
C PRINT OUT THE INDIVIDUAL MULTIPOLARITY OUTPUT

```

```

DO 950 IP=1,2
DO 950 IL=1,NL
DO 950 IG=1,NG
950 WRITE(6,952)EG(IG),CM(IG,IP,IL)
952 FORMAT(E12.5,2X,E12.5)
C CASCADE AVERAGES
C THE STANDARD DEVIATION AND FRACTIONAL UNCERTAITY IN
C THE GAMMA MULTIPLICITY ARE DETERMINED.
TE=0.
TY=0.
TZ=0.
YT=0.
ZT=0.
DO 180 IG=1,NG
SD=0.
SI=0.
RD=0.
RI=0.
WRITE(6,21) SG(IG),SD,SE(IG),SI,ZC
IF(SG(IG).GT.0.) SD=1./SQRT(SG(IG))
IF(SG(IG).GT.0.) RD=SD/SG(IG)
SG(IG)=SG(IG)/NC
TY=TY+SG(IG)
IF(SE(IG).GT.0.) SI=1./SQRT(SE(IG))
IF(SE(IG).GT.0.) RI=SI/SE(IG)
SE(IG)=SE(IG)/NC
TZ=TZ+SE(IG)
IF(IG.LT.NG) DE=EG(IG)-EG(IG+1)
IF(IG.EQ.NG) DE=EG(NG)

```

```

WRITE(6,21) DE,SD,RP SI,RI,ZD
SA(IG)=SG(IG)/DE
SB(IG)=SE(IG)/DE
IF (IG.LT.NG) EA=(EG(IG)+EG(IG+1))* .5
IF (IG.EQ.NG) EA=EG(NG)* .5
EY=EA*SG(IG)
EZ=EA*SE(IG)
YT=YT+EY

ZT=ZT+EZ
WRITE(6,28) EG(IG),SG(IG),SD,SA(IG),EY,YT,ZE
WRITE(6,28) EG(IG),SE(IG),SI,SB(IG),EZ,TET,ZT
180 CONTINUE
EF=EF/NC
TM=TY+TZ
WRITE(6,21) EF,TY,TZ,TM
DO 185 IG=1,NG
SG(IG)=SG(IG)/TM
SA(IG)=SA(IG)/TM
SE(IG)=SE(IG)/TM
SB(IG)=SB(IG)/TM
185 WRITE(6,21) EG(IG),SG(IG),SA(IG),SE(IG),SB(IG)
DO 190 ID=1,25
SP=0.
IF(PS(ID).GT.0.) SP=1./SQRT(PS(ID))
PS(ID)=PS(ID)/NC
T4=.2*ID
190 WRITE(6,21) T4,PS(ID),SP
C PRINT OUT THE NUMBER OF GAMMAS AND INTERNAL CONVERSIONS PER
C ENERGY GROUP

```



```

      DO 992 IG=1,NG
      WRITE(6,21)EG(IG),CG(IG),CI(IG)
992  CONTINUE

      DO 986 IC=1,NC
986  WRITE(6,987)IC,ETS(IC),ETH(IC)
987  FORMAT(I4,2X,E12.5,2X,E12.5)
C FORMATS
10  FORMAT(20A4)
11  FORMAT(5E12.5)
12  FORMAT(10I4)
20  FORMAT(1H ,20A4)
22  FORMAT(1H ,10I4)
21  FORMAT(1H ,6E12.5)
24  FORMAT(1H ,3I4,3E12.5)
25  FORMAT(1H ,4I3,3E12.5)
26  FORMAT(1H )
27  FORMAT(1H ,I4,5E12.5)
28  FORMAT(1H ,7E12.5)

      STOP
      END
C
C THIS SUBROUTINE FITS THE POINTS TO A CUBIC SPLINE FIT.
      SUBROUTINE FIT
      REAL A(23),B(4),C(23),D(4,23),E(23),F(23),H(23),S(23),
1T(23),X(23),Y(23),ST(23)
      COMMON/C1/A,B,C,D,E,F,H,S,T,X,Y,ST
      REAL E1(3),E2(3),AL(3,2,4,23),ALV(3),ALT,CG(40),CI(40)
1,TJ(20),PV(3,2,25),PT(3,2,40,1000),SG(40),E0(1000,10)
2,VJ(30),VP(30),VE(30),EG(40),DP(20),SL(3),CD

```

```

3,RP(2),AW,AE,SJ,GE,HF(3,2),RL(3),PS(50),PF(5),SA(40)
4,PE(3,2,25),TT(3,2,25),PC(3,2,40,1000),GN(10,40)
5,TU(3,2,40,1000),SE(40),SB(40),ETM(3),TL(1000,10)
6,TP(1000,10),EINT(40),EINTN(40),ETS(1000),PGE(40)
7,TH(1000),ETH(1000),TG(1000,40),TI(1000,40),CM(40,2,3)
    INTEGER NS,IP,IC,NA,NP,NV(3),NG,NVD,II
    COMMON/PASS/TJ,PV,PT,SG,ED
1,E1,E2,NS,IP,IL,IC,NA,AL,NP,ETT,ALV,ALT,CG,CI
2,VJ,VP,VE,EG,DP,SL,NG,NV,CD,NVD
3,RP,AW,AE,SJ,GE,HF,RL,PS,PF,SA
4,PE,TT,PC,GN,II,PGE
5,TU,SE,SB,ETM,TL,TP
6,EINT,EINTN,ETS,TH,ETH,TG,TI,CM
    DIMENSION ERG(23,3),EN(23)

```

C THE FOLLOWING ENERGY VALUES SPAN THE RANGE OF THE TABLES.

```

    DATA ERG/1.,1.7,3.0,6.2,10.,14.,20.,28.,40.,53.,70.
1,83.,100.,123.,150.,215.,300.,390.,500.,730.,1000.,1250.,1500.
2,1.,1.7,3.0,6.2,10.,14.,20.,28.,40.,53.,70.,83.,100.
3,123.,150.,215.,300.,390.,500.,730.,1000.,1500.,0.0
4,1.,2.,4.,8.,15.,25.,40.,52.,70.,103.,150.,280.,500.
5,10*0./

```

```

C    WRITE(6,29)
    E1(1)=116.0
    E1(2)=-1.0
    E1(3)=-1.0
    E2(1)=116.0
    E2(2)=35.0
    E2(3)=29.0
    ES=E1(NS)

```

```
ETM(1)=1600.0
ETM(2)=1500.0
ETM(3)=500.0
C  WRITE(6,335)NS,E1(NS),ETT
C  WRITE(6,337)E2(NS),ETM(NS)
  IF(ETT.GT.ETM(NS))GO TO 51
  IF(ETT.LT.E2(NS))GO TO 50
  IF(NS.EQ.1)E2(NS)=E1(NS)
  E1(NS)=-E1(NS)+1.
  E2(NS)=-E2(NS)+1.
  NE2=-E2(NS)+.501
  NN=NA
C  WRITE(6,338)E1(NS),E2(NS),NE2,NN
  IF(ES.LT.0.)NN=NA+5
  DO 15 I=6,NN
  M=ERG(I,NS)+.01
  J=M+NE2
  IJ=9
C  WRITE(6,339)IJ
C  WRITE(6,336)J,M,I,NS,ERG(I,NS)
  IF(M.LT.150)GO TO 13
  IF(M.GE.390)GO TO 11
  J=5*((10*J+25)/50)
  IJ=10
C  WRITE(6,339)IJ
  GO TO 14
11 IF(M.GE.1000)GO TO 112
  IJ=11
C  WRITE(6,339)IJ
```

```

      J=10*((J+5)/10)
      GO TO 14
112 J=50*((J+25)/50)
      IJ=12
C      WRITE(6,339)IJ
      GO TO 14
13 J=(10*J+5)/10
      IJ=13
C      WRITE(6,339)IJ
14 EN(I)=J
15 C(I)=EN(I)+E1(NS)
C      WRITE(6,340)C(I),ES
      IF(ES.LT.0.)GO TO 30
      DO 16 I=1,5
      C(I)=ERG(I,NS)
C      WRITE(6,341)I,NS,ERG(I,NS)
16 EN(I)=ERG(I,NS)-E1(NS)
      DO 17 I=1,NA
      IZZ=17
C      WRITE(6,330)I,NA,C(I),EN(I),IZZ
17 C(I)=ALOG(SQRT((1021.952+C(I))*C(I)))
      DO 18 I=1,NP
      IZZ=18
      W=ETT+E1(NS)
C      WRITE(6,331)I,W,IZZ
18 X(I)=ALOG(SQRT((1021.952+W)*W))
      M=2*IL+1
      DO 19 I=1,NA
      IZZ=19

```

```

      Z=AL(NS,IP,IL,I)*EN(I)**M
C      WRITE(6,332)I,M,EN(I),Z,IZZ
19  A(I)=ALOG(AL(NS,IP,IL,I)*EN(I)**M)
      CALL SPLINE(NA,NP)
      DO 20 I=1,NP
      ZZ=EXP(Y(I))/ETT**M
C      WRITE(6,342)ZZ,NS
20  ALV(NS)=EXP(Y(I))/ETT**M
      GO TO 33
30  DO 31 I=1,NA
C      WRITE(6,333)I,EN(I+5),AL(NS,IP,IL,I),ETT,ES,EN(I)
      C(I)=ALOG(EN(I+5))
31  A(I)=ALOG(AL(NS,IP,IL,I))
      DO 35 I=1,NP
C      WRITE(6,343)I,ETT
35  X(I)=ALOG(ETT)
C      WRITE(6,334)
      CALL SPLINE(NA,NP)
      ALV(NS)=EXP(Y(I))
C      WRITE(6,344)Y(I)
33  CONTINUE
      L1=0
      IF(ES.LT.0.)L1=5
      M1=NA+L1
C      WRITE(6,345)ES,NA,L1,M1
      DO 37 I=1,NP
C      WRITE(6,346)ETT,EN(L1+1),EN(M1)
      IF(ETT.LT.EN(L1+1))ALV(NS)=-1.
37  IF(ETT.GT.EN(M1))ALV(NS)=-1.

```

```

      GO TO 47
C 50 WRITE(6,347)
      50 ALV(NS)=AL(NS,IP,IL,1)
      GO TO 47
C 51 WRITE(6,348)
      51 ALV(NS)=AL(NS,IP,IL,NV(NS))
C 29 FORMAT(1H ,24HBEGINNING OF FIT ROUTINE)
C 330 FORMAT(1H ,3HI =,I4,2X,4HNA =,I4,2X,6HC(I) =,E12.5
C 1,2X,7HEN(I) =,E12.5,2X,12HLOOP NUMBER ,I4)
C 331 FORMAT(1H ,3HI =,I4,3X,3HW =,E12.5,2X,12HLOOP NUMBER ,I4)
C 332 FORMAT(1H ,3HI =,I4,2X,3HM =,I4,2X,7HEN(I) =,E12.5,
C 12X,3HZ =,E12.5,2X,12HLOOP NUMBER ,I4)
C 333 FORMAT(1H ,3HI =,I4,2X,4HEN =,E12.5,2X,4HAL =,E12.5,
C 12X,5HETT =,E12.5,2X,4HES =,E12.5,2X,4HEN =,E12.5,2X,7HLOOP 31)
C 334 FORMAT(1H ,14HCALLING SPLINE)
C 335 FORMAT(1H ,4HNS =,I4,2X,8HE1(NS) =,E12.5,2X,5HETT =,E12.5)
C 336 FORMAT(1H ,3HJ =,I4,2X,3HM =,I4,2X,3HI =,I4,2X,4HNS =,I4,
C 12X,11HERG(I,NS) =,E12.5)
C 337 FORMAT(1H ,8HE2(NS) =,E12.5,2X,9HETM(NS) =,E12.5)
C 338 FORMAT(1H ,8HE1(NS) =,E12.5,2X,8HE2(NS) =,E12.5,2X,5HNE2 =
C 1,I4,2X,4HWN =,I4)
C 339 FORMAT(1H ,19HUSED THE J IN LINE ,I4)
C 340 FORMAT(1H ,6HC(I) =,E12.5,2X,4HES =,E12.5)
C 341 FORMAT(1H ,3HI =,I4,2X,4HNS =,I4,2X,11HERG(I,NS) =,E12.5,
C 12OHAND IS SET = TO C(I))
C 342 FORMAT(1H ,7HLOOP 20,2X,4HZZ =,E12.5,2X,9H= ALV(NS),
C 12X,4HNS =,I4)
C 343 FORMAT(1H ,7HLOOP 35,2X,3HI =,I4,2X,5HETT =,E12.5)
C 344 FORMAT(1H ,6HY(I) =,E12.5)

```

```

C 345 FORMAT(1H ,4HES =,E12.5,2X,4HNA =,I4,2X,4HL1 =,I4,2X,
C    14HM1 =,I4)
C 346 FORMAT(1H ,5HETT =,E12.5,2X,10HEN(L1+1) =,E12.5,2X,
C    18HEN(M1) =,E12.5)
C 347 FORMAT(1H ,5HAT 50)
C 348 FORMAT(1H ,5HAT 51)
C    WRITE(6,349)NS,ALV(NS)
C 349 FORMAT(1H ,15HEND OF FIT LOOP,2X,4HNS =,I4,2X,9HALV(NS) =,
C    1E12.5)
      47 RETURN
      END
C THIS IS THE CUBIC SPLINE SURROUTINE
      SUBROUTINE SPLINE(NA,NP)
      REAL A(23),B(4),C(23),D(4,23),E(23),F(23),H(23),S(23),
      1T(23),X(23),Y(23),ST(23)
      COMMON/C1/A,B,C,D,E,F,H,S,T,X,Y,ST
C    WRITE(6,338)
      338 FORMAT(1H ,27HBEGINNING OF SPLINE ROUTINE)

      M=NA-1
      DO 7 I=1,M
      E(I)=C(I+1)-C(I)
      7 F(I)=A(I+1)-A(I)
      MS=NA-2
      DO 8 I=1,MS
      D(1,I)=E(I+1)
      D(2,I)=2.*(E(I)+E(I+1))
      D(3,I)=E(I)
      8 D(4,I)=3.*(E(I+1)*F(I)/E(I)+E(I)*F(I+1)/E(I+1))
      S(1)=-1.

```

```

T(1)=2.*F(1)/E(1)
DO 9 I=2,M
L=I-1
S(I)=- (D(1,L)+D(2,L)*S(L))/(D(3,L)*S(L))
9 T(I)=(-T(L)*(D(2,L)+D(3,L)*S(I))+D(4,L))/D(3,L)
AA=2.*F(M)/E(M)
H(NA)=(T(M)+AA*S(M))/(S(M)+1.)
DO 10 I=1,M
K=NA-I
10 H(K)=(H(K+1)-T(K))/S(K)
DO 12 I=1,NP
DO 13 K=1,M
IF(X(I).LT.C(K+1)) GO TO 14
13 CONTINUE
14 K1=K
Z=(C(K1+1)-C(K1))/2.
B(3)=(H(K1+1)-H(K1))/(4.*Z)
B(4)=.25*((H(K1+1)+H(K1))*Z-A(K1+1)+A(K1))/Z**3
B(1)=(A(K1+1)+A(K1)-2.*B(3)*Z**2)/2.
B(2)=(H(K1+1)+H(K1)-6.*B(4)*Z**2)/2.
ZP=X(I)-(C(K1+1)+C(K1))/2.
Y(I)=B(1)+ZP*(B(2)+ZP*(B(3)+ZP*B(4)))
12 CONTINUE
RETURN
END
BLOCK DATA
REAL E1(3),E2(3),AL(3,2,4,23),ALV(3),ALT,CG(40),CI(40)
1,TJ(20),PV(3,2,25),PT(3,2,40,1000),SG(40),EO(1000,10)
2,VJ(30),VP(30),VE(30),EG(40),DP(20),SL(3),CD

```



```

3,RP(2),AW,AE,SJ,GE,HF(3,2),RL(3),PS(50),PF(5),SA(40)
4,PE(3,2,25),TT(3,2,25),PC(3,2,40,1000),GN(10,40)
5,TU(3,2,40,1000),SE(40),SB(40),ETM(3),TL(1000,10)
6,TP(1000,10),EINT(40),EINTN(40),ETS(1000),PGE(40)
7,TH(1000),ETH(1000),TG(1000,40),TI(1000,40),CM(40,2,3)

INTEGER NS,IP,IC,NA,NP,NV(3),NG,NVD,II

COMMON/PASS/TJ,PV,PT,SG,E0

1,E1,E2,NS,IP,IL,IC,NA,AL,NP,ETT,ALV,ALT,CG,CI
2,VJ,VP,VE,EG,DP,SL,NG,NV,CD,NVD
3,RP,AW,AE,SJ,GE,HF,RL,PS,PF,SA
4,PE,TT,PC,GN,II,PGE
5,TU,SE,SB,ETM,TL,TP
6,EINT,EINTN,ETS,TH,ETH,TG,TI,CM

DATA AW,AE,SJ,GE,CD/239.2,9.302,3.702,.04948,.95/
DATA NG,NVD/40,25/
DATA NV(1),NV(2),NV(3)/23,17,8/
DATA EG(1),EG(2),EG(3)/10.,9.75,9.50/
DATA EG(4),EG(5),EG(6)/9.25,9.0,8.75/
DATA EG(7),EG(8),EG(9)/8.5,8.25,8.0/
DATA EG(10),EG(11),EG(12)/7.75,7.5,7.25/
DATA EG(13),EG(14),EG(15)/7.0,6.75,6.50/
DATA EG(16),EG(17),EG(18)/6.25,6.0,5.75/
DATA EG(19),EG(20),EG(21)/5.5,5.25,5.0/
DATA EG(22),EG(23),EG(24)/4.75,4.5,4.25/
DATA EG(25),EG(26),EG(27)/4.,3.75,3.50/
DATA EG(28),EG(29),EG(30)/3.25,3.0,2.75/
DATA EG(31),EG(32),EG(33)/2.5,2.25,2.0/
DATA EG(34),EG(35),EG(36)/1.75,1.5,1.25/
DATA EG(37),EG(38),EG(39)/1.,0.75,0.5/

```

```
DATA EG(40)/0.25/
DATA DP(1),DP(2),DP(3)/.533,.565,.602/
DATA DP(4),DP(5),DP(6)/.646,.697,.746/
DATA DP(7),DP(8),DP(9)/.782,.801,.808/
DATA DP(10),DP(11),DP(12)/.800,.780,.752/
DATA DP(13),DP(14),DP(15)/.677,.549,.341/
DATA DP(16),DP(17),DP(18)/.122,.004,.000/
DATA HF(1,1),HF(2,1),HF(3,1)/.000001,1.,1./
DATA HF(1,2),HF(2,2),HF(3,2)/10.,1.,1./
DATA SL(1),SL(2),SL(3)/.25,.0048,.000060469/
DATA VJ(1),VP(1),VE(1)/2.5,1.,.0/
DATA VJ(2),VP(2),VE(2)/3.5,1.,.043/
DATA VJ(3),VP(3),VE(3)/4.5,1.,.097/
DATA VJ(4),VP(4),VE(4)/.5,1.,.133/
DATA VJ(5),VP(5),VE(5)/1.5,1.,.144/
DATA VJ(6),VP(6),VE(6)/5.5,1.,.165/
DATA VJ(7),VP(7),VE(7)/3.5,1.,.173/
DATA VJ(8),VP(8),VE(8)/2.5,1.,.191/
DATA VJ(9),VP(9),VE(9)/3.5,1.,.220/
DATA VJ(10),VP(10),VE(10)/4.5,1.,.229/
DATA VJ(11),VP(11),VE(11)/5.5,1.,.300/
DATA VJ(12),VP(12),VE(12)/4.5,1.,.307/
DATA VJ(13),VP(13),VE(13)/6.5,1.,.373/
DATA VJ(14),VP(14),VE(14)/.5,1.,.696/
DATA VJ(15),VP(15),VE(15)/1.5,1.,.715/
DATA VJ(16),VP(16),VE(16)/1.5,1.,.735/
DATA VJ(17),VP(17),VE(17)/1.5,-1.,.742/
DATA VJ(18),VP(18),VE(18)/.5,-1.,.754/
DATA VJ(19),VP(19),VE(19)/3.5,-1.,.799/
```

```

DATA VJ(20),VP(20),VE(20)/.5,-1.,.812/
DATA VJ(21),VP(21),VE(21)/1.5,-1.,.821/
DATA VJ(22),VP(22),VE(22)/2.5,-1.,.854/
DATA VJ(23),VP(23),VE(23)/5.5,-1.,.894/
DATA VJ(24),VP(24),VE(24)/2.5,-1.,.930/
DATA VJ(25),VP(25),VE(25)/4.5,-1.,.943/
DATA PF(1),PF(2),PF(3)/.01,.04,.1/
DATA PF(4),PF(5)/.25,1./
DATA ETM(1),ETM(2),ETM(3)/1600.0,1500.0,500.0/
DATA AL(1,1,1,1),AL(1,1,1,2)/.273,.269/
DATA AL(1,1,1,3),AL(1,1,1,4),AL(1,1,1,5)/.262,.247,.230/
DATA AL(1,1,1,6),AL(1,1,1,7),AL(1,1,1,8)/.212,.191,.167/
DATA AL(1,1,1,9),AL(1,1,1,10),AL(1,1,1,11)/.139,.115,.0923/
DATA AL(1,1,1,12),AL(1,1,1,13),AL(1,1,1,14)/.0792,.0655,.0521/
DATA AL(1,1,1,15),AL(1,1,1,16),AL(1,1,1,17)/.0413,.0256,.0159/
DATA AL(1,1,1,18),AL(1,1,1,19),AL(1,1,1,20)/.0105,.00725,.0040
18/
DATA AL(1,1,1,21),AL(1,1,1,22),AL(1,1,1,23)/.00260,.00184,.001
139/
DATA AL(1,1,2,1),AL(1,1,2,2)/.188,.191/
DATA AL(1,1,2,3),AL(1,1,2,4),AL(1,1,2,5)/.198,.210,.220/
DATA AL(1,1,2,6),AL(1,1,2,7),AL(1,1,2,8)/.228,.231,.229/
DATA AL(1,1,2,9),AL(1,1,2,10),AL(1,1,2,11)/.217,.200,.176/
DATA AL(1,1,2,12),AL(1,1,2,13),AL(1,1,2,14)/.158,.138,.116/
DATA AL(1,1,2,15),AL(1,1,2,16),AL(1,1,2,17)/.096,.0636,.0413/
DATA AL(1,1,2,18),AL(1,1,2,19),AL(1,1,2,20)/.0282,.0198,.0113/
DATA AL(1,1,2,21),AL(1,1,2,22),AL(1,1,2,23)/.00717,.00501,
1.00317/
DATA AL(1,1,3,1),AL(1,1,3,2)/.0369,.0441/

```

DATA AL(1,1,3,3),AL(1,1,3,4),AL(1,1,3,5)/.058,.0927,.133/
 DATA AL(1,1,3,6),AL(1,1,3,7),AL(1,1,3,8)/.177,.229,.282/
 DATA AL(1,1,3,9),AL(1,1,3,10),AL(1,1,3,11)/.332,.354,.353/
 DATA AL(1,1,3,12),AL(1,1,3,13),AL(1,1,3,14)/.340,.316,.279/
 DATA AL(1,1,3,15),AL(1,1,3,16),AL(1,1,3,17)/.240,.164,.106/
 DATA AL(1,1,3,18),AL(1,1,3,19),AL(1,1,3,20)/.0708,.0480,.0257/
 DATA AL(1,1,3,21),AL(1,1,3,22),AL(1,1,3,23)/.0156,.0105,.00759

1/

DATA AL(1,1,4,1),AL(1,1,4,2)/.00166,.00352/
 DATA AL(1,1,4,3),AL(1,1,4,4),AL(1,1,4,5)/.00847,.0289,.0668/
 DATA AL(1,1,4,6),AL(1,1,4,7),AL(1,1,4,8)/.125,.218,.348/
 DATA AL(1,1,4,9),AL(1,1,4,10),AL(1,1,4,11)/.519,.649,.736/
 DATA AL(1,1,4,12),AL(1,1,4,13),AL(1,1,4,14)/.755,.741,.685/
 DATA AL(1,1,4,15),AL(1,1,4,16),AL(1,1,4,17)/.603,.418,.262/
 DATA AL(1,1,4,18),AL(1,1,4,19),AL(1,1,4,20)/.166,.107,.0526/
 DATA AL(1,1,4,21),AL(1,1,4,22),AL(1,1,4,23)/.0298,.0191,.0134/
 DATA AL(1,2,1,1),AL(1,2,1,2)/12.1,11.9/
 DATA AL(1,2,1,3),AL(1,2,1,4),AL(1,2,1,5)/11.6,10.7,9.8/
 DATA AL(1,2,1,6),AL(1,2,1,7),AL(1,2,1,8)/8.88,7.80,6.63/
 DATA AL(1,2,1,9),AL(1,2,1,10),AL(1,2,1,11)/5.28,4.21,3.21/
 DATA AL(1,2,1,12),AL(1,2,1,13),AL(1,2,1,14)/2.66,2.11,1.59/
 DATA AL(1,2,1,15),AL(1,2,1,16),AL(1,2,1,17)/1.19,.653,.350/
 DATA AL(1,2,1,18),AL(1,2,1,19),AL(1,2,1,20)/.201,.119,.0519/
 DATA AL(1,2,1,21),AL(1,2,1,22),AL(1,2,1,23)/.0264,.0154,.0098

14/

DATA AL(1,2,2,1),AL(1,2,2,2)/55.9,54.7/
 DATA AL(1,2,2,3),AL(1,2,2,4),AL(1,2,2,5)/52.8,48.3,43.5/
 DATA AL(1,2,2,6),AL(1,2,2,7),AL(1,2,2,8)/38.8,33.4,27.6/
 DATA AL(1,2,2,9),AL(1,2,2,10),AL(1,2,2,11)/21.1,16.1,11.7/

DATA AL(1,2,2,12),AL(1,2,2,13),AL(1,2,2,14)/9.39,7.17,5.15/
DATA AL(1,2,2,15),AL(1,2,2,16),AL(1,2,2,17)/3.96,1.84,.907/
DATA AL(1,2,2,18),AL(1,2,2,19),AL(1,2,2,20)/.490,.278,.115/
DATA AL(1,2,2,21),AL(1,2,2,22),AL(1,2,2,23)/.0576,.0338,.0219/
DATA AL(1,2,3,1),AL(1,2,3,2)/52.7,53.2/
DATA AL(1,2,3,3),AL(1,2,3,4),AL(1,2,3,5)/54.2,55.5,55.7/
DATA AL(1,2,3,6),AL(1,2,3,7),AL(1,2,3,8)/54.7,52.2,47.7/
DATA AL(1,2,3,9),AL(1,2,3,10),AL(1,2,3,11)/40.5,33.3,25.6/
DATA AL(1,2,3,12),AL(1,2,3,13),AL(1,2,3,14)/21.0,16.3,11.9/
DATA AL(1,2,3,15),AL(1,2,3,16),AL(1,2,3,17)/8.49,4.12,1.93/
DATA AL(1,2,3,18),AL(1,2,3,19),AL(1,2,3,20)/.989,.533,.205/
DATA AL(1,2,3,21),AL(1,2,3,22),AL(1,2,3,23)/.0974,.0553,.0351/
DATA AL(1,2,4,1),AL(1,2,4,2)/11.5,13.6/
DATA AL(1,2,4,3),AL(1,2,4,4),AL(1,2,4,5)/17.6,26.9,36.8/
DATA AL(1,2,4,6),AL(1,2,4,7),AL(1,2,4,8)/46.1,55.2,61.8/
DATA AL(1,2,4,9),AL(1,2,4,10),AL(1,2,4,11)/63.5,59.3,50.4/
DATA AL(1,2,4,12),AL(1,2,4,13),AL(1,2,4,14)/43.3,35.1,26.2/
DATA AL(1,2,4,15),AL(1,2,4,16),AL(1,2,4,17)/19.0,9.09,4.08/
DATA AL(1,2,4,18),AL(1,2,4,19),AL(1,2,4,20)/1.98,1.01,.355/
DATA AL(1,2,4,21),AL(1,2,4,22),AL(1,2,4,23)/.158,.0862,.0530/
DATA AL(2,1,1,1),AL(2,1,1,2)/1.51,.997/
DATA AL(2,1,1,3),AL(2,1,1,4),AL(2,1,1,5)/.624,.350,.210/
DATA AL(2,1,1,6),AL(2,1,1,7),AL(2,1,1,8)/.122,.0859,.0579/
DATA AL(2,1,1,9),AL(2,1,1,10),AL(2,1,1,11)/.0369,.0242,.0109/
DATA AL(2,1,1,12),AL(2,1,1,13),AL(2,1,1,14)/.00525,.00302,.00
1182/
DATA AL(2,1,1,15),AL(2,1,1,16),AL(2,1,1,17)/.000885,.000519,
1.000255/
DATA AL(2,1,2,1),AL(2,1,2,2)/1530.0,706.0/

DATA AL(2,1,2,3),AL(2,1,2,4),AL(2,1,2,5)/296.0,103.0,40.8/
DATA AL(2,1,2,6),AL(2,1,2,7),AL(2,1,2,8)/15.3,8.22,4.09/
DATA AL(2,1,2,9),AL(2,1,2,10),AL(2,1,2,11)/1.86,.890,.224/
DATA AL(2,1,2,12),AL(2,1,2,13),AL(2,1,2,14)/.0661,.0269,.0123/
DATA AL(2,1,2,15),AL(2,1,2,16),AL(2,1,2,17)/.00428,.00290,
1.000851/
DATA AL(2,1,3,1),AL(2,1,3,2)/95600.0,38500.0/
DATA AL(2,1,3,3),AL(2,1,3,4),AL(2,1,3,5)/13900.0,3980.0,1330.
10/
DATA AL(2,1,3,6),AL(2,1,3,7),AL(2,1,3,8)/418.0,199.0,86.6/
DATA AL(2,1,3,9),AL(2,1,3,10),AL(2,1,3,11)/33.7,13.9,2.62/
DATA AL(2,1,3,12),AL(2,1,3,13),AL(2,1,3,14)/.580,.188,.0690/
DATA AL(2,1,3,15),AL(2,1,3,16),AL(2,1,3,17)/.0175,.00691,.002
125/
DATA AL(2,1,4,1),AL(2,1,4,2)/2120000.0,839000.0/
DATA AL(2,1,4,3),AL(2,1,4,4),AL(2,1,4,5)/286000.0,74500.0,
122500.0/
DATA AL(2,1,4,6),AL(2,1,4,7),AL(2,1,4,8)/6220.0,2720.0,1070.0/
DATA AL(2,1,4,9),AL(2,1,4,10),AL(2,1,4,11)/368.0,135.0,20.2/
DATA AL(2,1,4,12),AL(2,1,4,13),AL(2,1,4,14)/3.85,.968,.300/
DATA AL(2,1,4,15),AL(2,1,4,16),AL(2,1,4,17)/.0588,.0193,.00504
1/
DATA AL(2,2,1,1),AL(2,2,1,2)/80.5,50.4/
DATA AL(2,2,1,3),AL(2,2,1,4),AL(2,2,1,5)/29.8,15.7,8.90/
DATA AL(2,2,1,6),AL(2,2,1,7),AL(2,2,1,8)/4.88,3.31,2.14/
DATA AL(2,2,1,9),AL(2,2,1,10),AL(2,2,1,11)/1.30,.810,.325/
DATA AL(2,2,1,12),AL(2,2,1,13),AL(2,2,1,14)/.138,.0697,.0366/
DATA AL(2,2,1,15),AL(2,2,1,16),AL(2,2,1,17)/.0137,.00639,
1.00219/

DATA AL(2,2,2,1),AL(2,2,2,2)/6090.0,2930.0/
DATA AL(2,2,2,3),AL(2,2,2,4),AL(2,2,2,5)/1290.0,483.0,205.0/
DATA AL(2,2,2,6),AL(2,2,2,7),AL(2,2,2,8)/83.9,47.6,25.3/
DATA AL(2,2,2,9),AL(2,2,2,10),AL(2,2,2,11)/12.4,6.41,1.85/
DATA AL(2,2,2,12),AL(2,2,2,13),AL(2,2,2,14)/.603,.256,.117/
DATA AL(2,2,2,15),AL(2,2,2,16),AL(2,2,2,17)/.0375,.0162,.00527

1/

DATA AL(2,2,3,1),AL(2,2,3,2)/547000.0,200000.0/
DATA AL(2,2,3,3),AL(2,2,3,4),AL(2,2,3,5)/65600.0,17100.0,5390

1.0/

DATA AL(2,2,3,6),AL(2,2,3,7),AL(2,2,3,8)/1620.0,759.0,328.0/
DATA AL(2,2,3,9),AL(2,2,3,10),AL(2,2,3,11)/128.0,54.1,10.9/
DATA AL(2,2,3,12),AL(2,2,3,13),AL(2,2,3,14)/2.63,.910,.349/
DATA AL(2,2,3,15),AL(2,2,3,16),AL(2,2,3,17)/.0897,.0339,.00

1966/

DATA AL(2,2,4,1),AL(2,2,4,2)/100000000.0,23700000.0/
DATA AL(2,2,4,3),AL(2,2,4,4),AL(2,2,4,5)/2040000.0,426000.0

1,110000.0/

DATA AL(2,2,4,6),AL(2,2,4,7),AL(2,2,4,8)/26600.0,10900.0,4010

1.0/

DATA AL(2,2,4,9),AL(2,2,4,10),AL(2,2,4,11)/1310.0,466.0,67.9/
DATA AL(2,2,4,12),AL(2,2,4,13),AL(2,2,4,14)/12.3,3.42,1.09/
DATA AL(2,2,4,15),AL(2,2,4,16),AL(2,2,4,17)/.219,.0707,.0170/

DATA AL(3,1,1,1),AL(3,1,1,2)/.630,.206/

DATA AL(3,1,1,3),AL(3,1,1,4),AL(3,1,1,5)/.108,.0515,.0194/

DATA AL(3,1,1,6),AL(3,1,1,7),AL(3,1,1,8)/.00743,.00165,.00047

13/

DATA AL(3,1,2,1),AL(3,1,2,2)/1060.0,138.0/

DATA AL(3,1,2,3),AL(3,1,2,4),AL(3,1,2,5)/42.9,11.3,2.0/

```

DATA AL(3,1,2,6),AL(3,1,2,7),AL(3,1,2,8)/.370,.0280,.00365/
DATA AL(3,1,3,1),AL(3,1,3,2)/120000.0,9380.0/
DATA AL(3,1,3,3),AL(3,1,3,4),AL(3,1,3,5)/2220.0,432.0,52.4/
DATA AL(3,1,3,6),AL(3,1,3,7),AL(3,1,3,8)/6.75,.288,.0222/
DATA AL(3,1,4,1),AL(3,1,4,2)/10400000.0,444000.0/
DATA AL(3,1,4,3),AL(3,1,4,4),AL(3,1,4,5)/76900.0,10800.0,887.
10/
DATA AL(3,1,4,6),AL(3,1,4,7),AL(3,1,4,8)/80.6,2.06,.103/
DATA AL(3,2,1,1),AL(3,2,1,2)/34.0,9.92/
DATA AL(3,2,1,3),AL(3,2,1,4),AL(3,2,1,5)/4.88,2.16,.739/
DATA AL(3,2,1,6),AL(3,2,1,7),AL(3,2,1,8)/.255,.0458,.00981/
DATA AL(3,2,2,1),AL(3,2,2,2)/4290.0,608.0/
DATA AL(3,2,2,3),AL(3,2,2,4),AL(3,2,2,5)/201.0,57.4,11.5/
DATA AL(3,2,2,6),AL(3,2,2,7),AL(3,2,2,8)/2.47,.236,.0335/
DATA AL(3,2,3,1),AL(3,2,3,2)/667000.0,45300.0/
DATA AL(3,2,3,3),AL(3,2,3,4),AL(3,2,3,5)/9960.0,1810.0,208.0/
DATA AL(3,2,3,6),AL(3,2,3,7),AL(3,2,3,8)/26.7,1.26,.109/
DATA AL(3,2,4,1),AL(3,2,4,2)/61100000.0,2330000.0/
DATA AL(3,2,4,3),AL(3,2,4,4),AL(3,2,4,5)/374000.0,47700.0,350
10.0/
DATA AL(3,2,4,6),AL(3,2,4,7),AL(3,2,4,8)/292.0,7.16,.372/
END

```

C VARIABLES

```

C   AE=LEVEL DENSITY ENERGY PARAMETER
C   AL(IL,IV)=INTERNAL CONVERSION COEFFICIENT
C   AW=ATOMIC WEIGHT
C   CJ,CP,CE=CURRENT LEVEL SPIN, PARITY, AND ENERGY
C   DP(IG)=FOIL ESCAPE PROBABILITY FOR GAMMA OF GROUP IG
C   E1(NS) = LOWEST TABULATED ENERGY OF SUBSHELL TO BE

```


C INTERP. EXCEPT FOR L AND M SHELL WHICH HAVE $E1(NS) = -1.0$
C $E2(NS) =$ LOWEST VALUE OF THE NS SUBSHELL
C ED=ENERGY DEPOSITED IN TANK BY CASCADE
C EF=AVERAGE ENERGY DEPOSITED IN DETECTOR BY CASCADES
C $EO(IC,II)$ =ENERGY OF II-TH GAMMA IN IC-TH CASCADE
C ET=TRANSITION ENERGY
C EU=MAX ENERGY DEPOSITED IN TANK BY GAMMA
C $EG(IG)$ =UPPER ENERGY OF GROUP IG
C $GN(II,IG)$ =GROUP NUMBER OF II-TH GAMMA IN CASCADE
C $HF(IL,IP)$ =HINDRANCE FACTOR FOR IL,IP
C $HG(IL,IP)$ =HINDRANCE FACTOR FOR IL,IP TRANSITIONS
C IC=CASCADE INDEX
C IE=EXCITATION ENERGY INDEX
C IJ=FINAL LEVEL SPIN PLUS 1/2
C IL=L FOR GAMMA TRANSITION

C IP=1 FOR ELECTRIC OR 2 FOR MAGNETIC TRANSITION
C IT=TRANSITION INDEX WITHIN CASCADE
C NC=NUMBER OF CASCADES
C NE=NUMBER OF INTERVALS IN ENERGY CONTINUUM
C NG=NUMBER TALLY ENERGY GROUPS
C NJ=LARGEST LEVEL SPIN USED IN CONTINUUM REGION
C NL=NUMBER OF MULTIPOLES USED IN CALCULATION
C NP = THE NUMBER OF INTERNAL CONVERSION COEFFICIENTS TO
C INTERPOLATED. THIS WILL BE 1, FOR THIS PROGRAM.
C NR=INTEGER PSEUDORANDOM NUMBER
C $NV(NS)$ =NUMBER OF VALUES IN TABLE FOR SHELL NS
C NVD=NUMBER OF DISCRETE LEVELS
C $PC(IL,IP,IJ,IE)$ =INTERNAL CONVERSION PROBABILITY IN
C CONTINUUM

C PE(IL,IP,IV)=INTERNAL CONVERSION COEFFICIENT IN
C DISCRETE LEVELS
C PF(IU)=PROBABILITY GAMMA DEPOSITS ENERGY IN TANK IN INTERVAL IU
C PS(ID)=PROBABILITY PULSE IS IN INTERVAL ID
C PT(IL,IP,IJ,IE)=TRANSITION PROBABILITY FOR CONTINUUM
C PV(IL,IP,IV)=TRANSITION PROBABILITY TO DISCRETE LEVEL IV
C RL(IL)=TRANSITION FACTOR FOR 2*IL POLE
C RJ=LJ-.5
C RN=PSEUDORANDOM NUMBER ON (0.,1.)
C RP(1)=WEISSKOPF FACTOR FOR ELECTRIC MULTIPOLE RADIATION
C RP(2)=WEISSKOPF FACTOR FOR MAGNETIC MULTIPOLE RADIATION
C SG(IG)=GAMMA MULTIPLICITY IN GROUP IG
C SL(IL)=COMBINATORIAL FACTOR FOR 2.*IL-POLE
C TE=TOTAL ENERGY RELEASE PER CASCADE
C TET=SUM OF ENERGIES IN A CASCADE
C SJ=LEVEL DENSITY PARAMETER FOR SPIN
C TT(IL,IP,IV)=TOTAL PROBABILITY OF TRANSITION IN
C DISCRETE LEVEL
C TU(IL,IP,IJ,IE)=TOTAL TRANSITION PROBABILITY IN THE
C CONTINUUM
C T1,T2,T3,I1,I2=TEMPORARIES
C TJ=ONE LINE JOB TITLE
C TL(IC,II)=L VALUE FOR THE II-TH GAMMA IN IC-TH CASCADE
C TP(IC,II)=IP VALUE FOR THE II-TH GAMMA IN IC-TH CASCADE
C TY=TOTAL GAMMA YIELD (MULTIPLICITY) PER CASCADE
C VJ(IV),VP(IV),VE(IV)=SPIN, PARITY, ENERGY OF DISCRETE LEVEL IV
C XE,XJ,XP=INITIAL NUCLEUS ENERGY, SPIN, PARITY

APPENDIX B

SAMPLE OF REPRESENTATIVE CASCADES

This appendix contains a listing of 100 cascades.

The gamma rays in each cascade are listed in order of emission and in units of MeV.

CASCADE 1	CASCADE 2	CASCADE 3	CASCADE 4
0.30631E+01	0.27934E+01	0.19843E+01	0.20228E+01
0.49367E+00	0.73640E+00	0.98107E+00	0.14184E+01
0.59800E+00	0.11402E+01	0.70567E+00	0.92989E+00
0.00000E+00	0.00000E+00	0.91196E+00	0.00000E+00
0.00000E+00	0.00000E+00	0.00000E+00	0.00000E+00

CASCADE 5	CASCADE 6	CASCADE 7	CASCADE 8
0.82840E+00	0.15605E+01	0.13678E+01	0.17146E+01
0.14972E+01	0.19830E+01	0.85739E+00	0.17642E+01
0.78662E+00	0.83426E+00	0.15383E+01	0.62822E+00
0.16478E+01	0.17300E+00	0.86653E+00	0.00000E+00
0.00000E+00	0.00000E+00	0.00000E+00	0.00000E+00

CASCADE 9	CASCADE 10	CASCADE 11	CASCADE 12
0.98252E+00	0.15605E+01	0.13293E+01	0.75134E+00
0.10797E+01	0.12265E+01	0.18045E+01	0.12872E+01
0.62081E+00	0.12087E+01	0.97326E+00	0.17328E+01
0.40736E+00	0.00000E+00	0.56300E+00	0.17300E+00
0.39146E+00	0.00000E+00	0.00000E+00	0.00000E+00

CASCADE 13	CASCADE 14	CASCADE 15	CASCADE 16
0.24081E+01	0.26778E+01	0.36604E+00	0.71281E+00
0.88860E+00	0.10988E+01	0.34347E+01	0.19312E+01
0.15063E+01	0.10264E+01	0.86930E+00	0.87651E+00
0.00000E+00	0.00000E+00	0.00000E+00	0.10915E+01
0.00000E+00	0.00000E+00	0.00000E+00	0.00000E+00

CASCADE 17	CASCADE 18	CASCADE 19	CASCADE 20
0.19075E+01	0.90546E+00	0.22155E+01	0.26008E+01
0.74634E+00	0.15475E+01	0.12527E+01	0.65742E+00
0.13978E+01	0.62304E+00	0.13348E+01	0.14008E+01
0.00000E+00	0.71877E+00	0.00000E+00	0.00000E+00
0.00000E+00	0.86428E+00	0.00000E+00	0.00000E+00

CASCADE 21	CASCADE 22	CASCADE 23	CASCADE 24
0.14449E+01	0.94399E+00	0.82840E+00	0.19072E+01
0.22757E+01	0.11200E+01	0.22231E+01	0.10410E+01
0.94945E+00	0.61722E+00	0.16075E+01	0.10693E+01
0.00000E+00	0.55662E+00	0.14400E+00	0.00000E+00
0.00000E+00	0.35374E+00	0.00000E+00	0.00000E+00

CASCADE 25	CASCADE 26	CASCADE 27	CASCADE 28
0.15605E+01	0.10596E+01	0.23696E+01	0.12137E+01
0.14328E+01	0.17459E+01	0.10755E+01	0.24677E+01
0.79522E+00	0.65830E+00	0.81575E+00	0.97755E+00
0.10145E+01	0.99634E+00	0.00000E+00	0.00000E+00
0.00000E+00	0.00000E+00	0.00000E+00	0.00000E+00

CASCADE 29	CASCADE 30	CASCADE 31	CASCADE 32
------------	------------	------------	------------

0.24852E+01	0.15990E+01	0.20614E+01	0.29090E+01
0.97799E+00	0.16567E+01	0.16214E+01	0.17030E+01
0.11958E+01	0.53459E+00	0.11202E+01	0.00000E+00
0.00000E+00	0.10127E+01	0.00000E+00	0.00000E+00
0.00000E+00	0.00000E+00	0.00000E+00	0.00000E+00

CASCADE 33	CASCADE 34	CASCADE 35	CASCADE 36
0.18302E+01	0.24081E+01	0.11366E+01	0.32173E+01
0.11631E+01	0.72966E+00	0.13446E+01	0.15857E+01
0.25361E+00	0.95021E+00	0.63787E+00	0.00000E+00
0.15131E+01	0.58200E+00	0.10008E+01	0.00000E+00
0.00000E+00	0.00000E+00	0.00000E+00	0.00000E+00

CASCADE 37	CASCADE 38	CASCADE 39	CASCADE 40
0.22155E+01	0.55869E+00	0.23311E+01	0.12522E+01
0.12200E+01	0.28825E+01	0.96643E+00	0.11313E+01
0.11946E+01	0.13618E+01	0.16411E+00	0.78615E+00
0.00000E+00	0.00000E+00	0.96688E+00	0.65372E+00
0.00000E+00	0.00000E+00	0.00000E+00	0.56300E+00

CASCADE 41	CASCADE 42	CASCADE 43	CASCADE 44
0.19458E+01	0.17531E+01	0.22925E+01	0.23696E+01
0.16688E+01	0.19844E+01	0.14746E+01	0.89746E+00
0.11205E+01	0.87449E+00	0.10358E+01	0.54200E+00
0.00000E+00	0.00000E+00	0.00000E+00	0.86095E+00
0.00000E+00	0.00000E+00	0.00000E+00	0.00000E+00

CASCADE 45	CASCADE 46	CASCADE 47	CASCADE 48
0.13678E+01	0.33328E+01	0.20999E+01	0.31787E+01

0.73313E+00	0.10917E+01	0.16742E+01	0.14913E+01
0.67454E+00	0.00000E+00	0.82585E+00	0.00000E+00
0.64112E+00	0.00000E+00	0.00000E+00	0.00000E+00
0.13864E+01	0.00000E+00	0.00000E+00	0.00000E+00

CASCADE 49	CASCADE 50	CASCADE 51	CASCADE 52
0.25622E+01	0.15990E+01	0.20999E+01	0.82840E+00
0.12198E+01	0.20624E+01	0.15866E+01	0.17391E+01
0.88799E+00	0.99759E+00	0.98355E+00	0.70057E+00
0.00000E+00	0.00000E+00	0.00000E+00	0.35970E+00
0.00000E+00	0.00000E+00	0.00000E+00	0.88143E+00

CASCADE 53	CASCADE 54	CASCADE 55	CASCADE 56
0.35640E+01	0.28705E+01	0.33714E+01	0.10210E+01
0.10950E+01	0.77396E+00	0.14316E+01	0.14868E+01
0.00000E+00	0.19100E+00	0.00000E+00	0.10291E+01
0.00000E+00	0.00000E+00	0.00000E+00	0.10751E+01
0.00000E+00	0.00000E+00	0.00000E+00	0.14800E+00

CASCADE 57	CASCADE 58	CASCADE 59	CASCADE 60
0.36796E+01	0.10596E+01	0.23696E+01	0.20228E+01
0.97938E+00	0.13548E+01	0.77068E+00	0.16929E+01
0.00000E+00	0.14026E+01	0.19100E+00	0.00000E+00
0.00000E+00	0.84197E+00	0.00000E+00	0.00000E+00
0.00000E+00	0.00000E+00	0.00000E+00	0.00000E+00

CASCADE 61	CASCADE 62	CASCADE 63	CASCADE 64
0.10596E+01	0.15605E+01	0.24852E+01	0.20228E+01
0.11313E+01	0.15245E+01	0.12379E+01	0.51561E+00

0.15374E+01	0.39972E+00	0.93594E+00	0.00000E+00
0.10747E+01	0.77784E+00	0.00000E+00	0.00000E+00
0.00000E+00	0.19100E+00	0.00000E+00	0.00000E+00

CASCADE 65	CASCADE 66	CASCADE 67	CASCADE 68
0.29090E+01	0.20999E+01	0.16375E+01	0.26393E+01
0.33512E+00	0.10080E+01	0.16284E+01	0.96489E+00
0.22000E+00	0.71154E+00	0.95571E+00	0.10658E+01
0.00000E+00	0.62100E+00	0.00000E+00	0.00000E+00
0.00000E+00	0.00000E+00	0.00000E+00	0.00000E+00

CASCADE 69	CASCADE 70	CASCADE 71	CASCADE 72
0.11752E+01	0.63575E+00	0.21384E+01	0.28320E+01
0.24502E+01	0.22038E+01	0.67726E+00	0.87299E+00
0.80566E+00	0.88676E+00	0.95952E+00	0.95405E+00
0.00000E+00	0.91650E+00	0.88380E+00	0.00000E+00
0.00000E+00	0.00000E+00	0.00000E+00	0.00000E+00

CASCADE 73	CASCADE 74	CASCADE 75	CASCADE 76
0.18302E+01	0.19843E+01	0.22155E+01	0.11366E+01
0.47536E+00	0.96238E+00	0.10398E+01	0.14533E+01
0.14778E+01	0.11449E+01	0.53494E+00	0.58735E+00
0.32364E+00	0.00000E+00	0.82176E+00	0.54399E+00
0.00000E+00	0.00000E+00	0.00000E+00	0.94877E+00

CASCADE 77	CASCADE 78	CASCADE 79	CASCADE 80
0.94399E+00	0.12522E+01	0.75134E+00	0.32943E+01
0.13818E+01	0.87126E+00	0.24658E+01	0.13177E+01
0.14585E+01	0.95988E+00	0.15858E+01	0.00000E+00

0.87472E+00	0.66573E+00	0.00000E+00	0.00000E+00
0.00000E+00	0.90990E+00	0.00000E+00	0.00000E+00

CASCADE 81	CASCADE 82	CASCADE 83	CASCADE 84
0.12522E+01	0.13293E+01	0.27549E+01	0.21384E+01
0.20416E+01	0.19306E+01	0.76318E+00	0.14145E+01
0.56300E+00	0.32916E+00	0.11409E+01	0.11061E+01
0.00000E+00	0.10229E+01	0.00000E+00	0.00000E+00
0.00000E+00	0.00000E+00	0.00000E+00	0.00000E+00

CASCADE 85	CASCADE 86	CASCADE 87	CASCADE 88
0.12908E+01	0.21769E+01	0.24852E+01	0.14449E+01
0.22420E+01	0.16174E+01	0.70442E+00	0.22757E+01
0.12273E+01	0.81766E+00	0.62027E+00	0.89145E+00
0.00000E+00	0.00000E+00	0.99312E+00	0.00000E+00
0.00000E+00	0.00000E+00	0.00000E+00	0.00000E+00

CASCADE 89	CASCADE 90	CASCADE 91	CASCADE 92
0.20614E+01	0.16375E+01	0.24852E+01	0.21769E+01
0.14781E+01	0.18278E+01	0.12516E+01	0.82965E+00
0.12635E+01	0.11937E+01	0.10663E+01	0.16054E+01
0.00000E+00	0.00000E+00	0.00000E+00	0.00000E+00
0.00000E+00	0.00000E+00	0.00000E+00	0.00000E+00

CASCADE 93	CASCADE 94	CASCADE 95	CASCADE 96
0.10520E+01	0.13678E+01	0.24467E+01	0.12137E+01
0.88750E+00	0.19260E+01	0.72427E+00	0.16232E+01
0.10626E+01	0.12392E+01	0.16321E+01	0.93992E+00
0.10881E+01	0.00000E+00	0.00000E+00	0.83521E+00

0.00000E+00 0.00000E+00 0.00000E+00 0.00000E+00

CASCADE 97 CASCADE 98 CASCADE 99 CASCADE 100

0.14449E+01 0.22925E+01 0.16375E+01 0.90546E+00

0.49367E+00 0.77243E+00 0.15841E+01 0.16654E+01

0.83279E+00 0.46100E+00 0.33149E+00 0.83983E+00

0.38399E+00 0.10860E+01 0.10769E+01 0.42687E+00

0.14567E+01 0.00000E+00 0.00000E+00 0.96548E+00